

Aus dem Bereich Experimentelle und Klinische Pharmakologie und Toxikologie

Theoretische Medizin und Biowissenschaften

der Medizinischen Fakultät

der Universität des Saarlandes, Homburg

Univ. Prof. Dr. Ulrich Boehm

***Funktionelle Rolle(n) der Gonadotropine im Leber-
und Knochenstoffwechsel***

Dissertation zur Erlangung des Grades eines MD/PhD

der Medizinischen Fakultät

der Universität des Saarlandes

vorgelegt von

Samer Alasmi

geboren am 22. Januar 1998

in Daraa, Syrien

2022

Department of Pharmacology and Toxicology
Saarland University
Medical School

***Functional role(s) of gonadotropins in liver and bone
metabolism***

Dissertation
in partial fulfillment of requirements for the degree of
MD/PhD

Submitted by
Samer Alasmi
born on the 22th of January 1998
in Daraa, Syria

2022

Tag der Promotion: 19. Dezember 2023

Dekan: Prof. Dr. M.D. Menger

1. Berichterstatter: Prof. Dr. Ulrich Boehm

2. Berichterstatter: Prof. Dr. Marcin Jan Krawczyk

3. Berichterstatter: Prof. Dr. Dirk Isbrandt

Widmung

Meinen beiden Familien in Dankbarkeit, besonders im Andenken an meinen Vater

Cooperations

Without the support of several colleagues, this work would not have been possible. I would like to take this opportunity to express my sincere gratitude for their cooperation. The following table lists the individual figures showing experimental results and provides information about my specific contribution and/or the names of the other colleagues involved. The experiments and subsequent analyses were supervised by Dr. Sen Qiao and Prof. Ulrich Boehm.

Chapter	Figures	Experiment	Main persons carrying out the experiments
2.2.2	Figure 15	Mouse generation	Amanda Wyatt
2.2.4.1	Figure 16	Vaginal cytology	Samer Alasmi
3.1	Figure 17	Gonadotrope ablation	Dr. Sen Qiao Samer Alasmi
3.2	Figure 18	Metabolic parameters	Dr. Sen Qiao Samer Alasmi
3.2	Figure 19	Acute gonadotrope ablation	Samer Alasmi
3.3	Figure 20	Microcomputed tomography (μ CT)	Dr. Sen Qiao Samer Alasmi
3.4	Figure 21	Metabolic parameters	Samer Alasmi
3.4	Figure 22	Oil Red O staining and quantification	Samer Alasmi
3.4	Figure 23	Microcomputed tomography (μ CT)	Samer Alasmi
3.5	Figure 24	Metabolic parameters	Samer Alasmi
3.5	Figure 25	Oil Red O staining and quantification	Samer Alasmi
3.5	Figure 26	Microcomputed tomography (μ CT)	Samer Alasmi
3.6	Figure 27	Chronic pharmacogenetic activation of gonadotropes	Debajyoti Das
3.7	Figure 28	Metabolic parameters in HFD-fed GRIC/eR26-DREADD mice	Samer Alasmi
3.8	Figure 29	Plasma hormone measurements	Samer Alasmi
3.8	Figure 30	Metabolic parameters in HFD-fed wildtype mice and H&E staining of the liver	Samer Alasmi
3.9	Figure 31	RT-qPCR analysis of <i>Fshr</i> expression	Dr. Sen Qiao Samer Alasmi
3.9	Figure 32	RNA-scope analysis of <i>Fshr</i> expression	Dr. Mari Aoki Dr. Sen Qiao Samer Alasmi

3.9	Figure 33	<i>In vitro</i> stimulation assay	Dr. Sen Qiao Samer Alasmi
3.9	Figure 34	RNA-seq data	Dr. Sen Qiao Dr. Kathrin Kattler
3.9	Figure 35	Corticosterone plasma levels and staining of gonadotropes and corticotrope cells	Dr. Sen Qiao Samer Alasmi
3.9	Figure 36	Virus generation, stereotaxic injection & Oil Red O staining and quantification	Amanda Wyatt Dr. Sen Qiao Samer Alasmi
4.1	Figure 37	Osteoclast analyses	Adapted from Zhou 2021, Thesis (MSc) McGill University, Montreal, Canada
4.2	Figure 38	Model of gonadotrope actions on the gonads and the pituitary	Dr. Sen Qiao Dr. Philipp Wartenberg Samer Alasmi

Table of Contents

<i>List of figures</i>	I
<i>List of tables</i>	III
<i>List of abbreviations</i>	IV
<i>Zusammenfassung</i>	VIII
<i>Abstract</i>	X
1. Introduction	1
1.1 Hypothalamic-pituitary-gonadal (HPG) axis.....	1
1.2 Hypothalamic-pituitary-adrenal (HPA) axis.....	3
1.3 Anatomy, histology, and physiology of the liver.....	4
1.4 Metabolic syndrome.....	8
1.5 Non-alcoholic fatty liver disease	9
1.5.1 Epidemiology, etiology, and classification of NAFLD	10
1.5.2 Diagnosis and therapy of NAFLD	12
1.6 Endocrine causes of NAFLD	12
1.6.1 The association between estrogen deficiency (menopause) and NAFLD.....	12
1.6.2 The association between testosterone and NAFLD	13
1.6.3 The association between glucocorticoids (Cushing syndrome) and NAFLD	13
1.7 The relationship between the bone and the reproductive axis	14
1.7.1 The histological structure of bone.....	15
1.7.2 Bone metabolism	16
1.7.3 Osteoporosis	19
1.8 Cellular mechanism of FSH signaling.....	20
1.9 Binary genetic approaches as powerful tools to decipher HPA- and HPG-axis pathology <i>in situ</i>	21
1.10 Aims of my study	22
2. Materials and Methods	23
2.1 General Materials	23
2.1.1 Ear lysis buffer.....	24
2.1.2 4% Paraformaldehyde (PFA).....	24
2.1.3 20X phosphate-buffered saline (PBS).....	24
2.1.4 50X Tris-acetate-EDTA (TAE)	24
2.2 General Methods	25
2.2.1 Mouse models.....	25
2.2.2 Generation of the Rosa26-NLSIRFP720-Gq (DREADD) knock-in mice.....	26
2.2.3 Genotyping	27
2.2.4 Tissue preparation and histology	27
2.2.5 Microscopy	31

2.2.6 Molecular biology techniques	32
2.2.7 Gene-expression analysis	32
2.2.8 Microcomputed tomography (μ CT).....	35
2.2.9 Quantification and data analysis	35
3. Results.....	36
3.1 Diphtheria toxin injection efficiently ablates gonadotropes	36
3.2 Acute gonadotrope ablation triggers metabolic disorders in a gender-specific manner	37
3.3 Acute gonadotrope ablation triggers bone loss in both male and female mice	40
3.4 Hepatic steatosis in gonadotrope-ablated females is independent of the gonads, however bone loss is due to gonadal sex steroids.....	40
3.5 Sex-steroid replacement abolishes metabolic disorders but does not improve hepatic steatosis .	43
3.6 Characterization of the GRIC/eR26-DREADD mouse model.....	45
3.7 Activation of gonadotropes improves metabolic disorders independently of the gonads in a female high fat diet mouse model.....	47
3.8 FSH administration improves metabolic disorders caused by ovariectomy and high fat diet	48
3.9 Disrupting FSH signaling in the pituitary induces a fatty liver phenotype	49
4. Discussion.....	56
4.1 The HPG-axis controls distinct aspects of the metabolic syndrome	56
4.2 Extra-gonadal FSH actions.....	62
4.3 FSH: a new therapeutic avenue?	64
Conclusions.....	66
5. Bibliography	67
6. Publication & Acknowledgements.....	79
7. Curriculum Vitae.....	81

List of figures

Figure 1: Regulation of the hypothalamic-pituitary-gonadal axis.....	2
Figure 2: Regulation of the hypothalamic-pituitary-adrenal axis.....	4
Figure 3: The macroscopic structure of the liver.	5
Figure 4: Cellular architecture of the liver.....	6
Figure 5: Hepatic lipid metabolism.	8
Figure 6: The spectrum of NAFLD progression.	10
Figure 7: Percentage of the most common liver diseases in the World in 2010.....	10
Figure 8: Prevalence of NAFLD according to BMI, age, and sex.	11
Figure 9: Sustained GC elevation leads to severe disturbances in different organs.	14
Figure 10: Summary of the direct effects of the reproductive axis on bone.....	15
Figure 11: The anatomical and histological structure of bone.	16
Figure 12: The effect of parathyroid hormone on osteoblasts.....	17
Figure 13: The regulation and action of FGF-23.....	18
Figure 14: Schematic illustration of FSH signaling.....	20
Figure 15: The Rosa26-NLSiRFP720-2A-Gq (DREADD) knock-in mouse line.	26
Figure 16: Estrous cycle in GRIC/eR26-DREADD mice.....	28
Figure 17: Ablation of gonadotropes results in profound hypogonadism.	37
Figure 18: Acute gonadotropes ablation leads to metabolic disorders in female mice.....	38
Figure 19: Gonadotrope ablation triggers a fatty liver phenotype in male and female mice.	39
Figure 20: Gonadotrope ablation induces bone loss in male and female mice.....	40
Figure 21: Gonadal loss mimics metabolic syndrome in female mice.....	41
Figure 22: Gonadotrope dysfunction triggers hepatic steatosis independently of the gonads in females.	42
Figure 23: Gonadal loss induces bone loss in male and female mice.	43
Figure 24: Replacement of sex steroids eliminates metabolic abnormalities.	44
Figure 25: Hepatic steatosis in females is independent of sex steroids.....	45
Figure 26: Gonadotropes regulate bone mass through both gonadal and non-gonadal ways in a sex specific manner.	45
Figure 27: CNO activates gonadotropes in GRIC/eR26-DREADD mice.....	46
Figure 28: Metabolic phenotype of HFD-fed GRIC/eR26-DREADD mice.	47
Figure 29: Plasma hormone measurements	48
Figure 30: Wildtype mice display improved body weight and glucose tolerance upon FSH treatment after ovariectomy.	49
Figure 31: Representative RT-PCR analysis of <i>Fshr</i> expression in major organs of adult female mice.	52

Figure 32: RT-qPCR and RNA-scope analysis of <i>Fshr</i> expression levels in the pituitary, ovary, and liver from adult female mice.	51
Figure 33: <i>In vitro</i> stimulation assay to analyze pituitary hormone secretion.....	52
Figure 34: Human corticotropes express the FSH receptor.	53
Figure 35: Increased corticosterone plasma levels after acute gonadotrope ablation.....	54
Figure 36: Paracrine FSH actions in the pituitary prevent hepatic steatosis in female mice.	55
Figure 37: FSH regulates bone metabolism independent of <i>Fshr</i> in osteoclasts.....	59
Figure 38: FSH receptor expression in the pituitary.	62

List of tables

Table 1: List of primers used for genotyping.....	23
Table 2: Kits.....	23
Table 3: List of antisera and antibodies	23
Table 4: List of primers used for qPCR.....	23
Table 5: List of primers used for CRISPR efficiency verification	24

List of abbreviations

11 β -HSD1	11 β -hydroxysteroid dehydrogenase type 1
AASLD	American Association for the Study of Liver Diseases
ACTH	Adrenocorticotrophic hormone
APOB	Apolipoprotein-B
AR	Androgen receptor
AVV	Adeno-associated virus
BMD	Bone mineral density
BMI	Body mass index
BV/TV	Fractional bone volume
CNO	Clozapine N-oxide dihydrochloride
CRH	Corticotropin-releasing hormone
DBD	DNA-binding domain
DHT	5 α -dihydrotestosterone
DREADD	Designer Receptor Exclusively Activated by Designer Drugs
DTR	Diphtheria toxin receptor
ER	Estrogen receptor
ERK1/2	Extracellular-regulated kinases
ES	Embryonic stem
FA	Fatty acid
FGF-23	Fibroblast growth factor-23
FOXO1	Fork head box protein O1
FSH	Follicle-stimulating hormone
FSHR	FSH receptor
GC	Glucocorticoid
GH	Growth hormone
GnRH	Gonadotropin-releasing hormone
GnRHR	GnRH receptor
GPCR	G protein-coupled receptor
GR	Glucocorticoid receptor
GRIC	GnRHR-IRES-CRE
H&E	Hematoxylin and eosin
HBV	Hepatitis B virus
HCC	Hepatocellular carcinoma
HCV	Hepatitis C virus
HFD	High fat diet
HPA-axis	Hypothalamic-pituitary-adrenal axis

HPG-axis	Hypothalamic-pituitary-gonadal axis
HSL	Hormone-sensitive lipase
IHC	Immunohistochemistry
IL-1	Interleukin-1
ipGTT	Intraperitoneal glucose tolerance test
ipITT	Intraperitoneal insulin tolerance test
IRS-1	Insulin receptor substrate-1
IRS-2	Insulin receptor substrate-2
KS	Klinefelter's syndrome
LBD	Ligand-binding domain
LCN-2	Lipocalin-2
LH	Luteinizing hormone
LPIN1	Lipin-1
MR	Mineralocorticoid receptor
MTPP	Microsomal triglycerides transfer protein
NAFLD	Nonalcoholic fatty liver disease
NASH	Nonalcoholic steatohepatitis
NTD	N-terminal transactivation domain
OPG	Osteoprotegerin
ORO	Oil red O
OVX	Ovariectomy
PO ₄ ³⁻	Phosphate
PBS	Phosphate-buffered saline
PCOS	Polycystic ovary syndrome
PFA	Paraformaldehyde
PHT	Parathyroid hormone
PI3K	Phosphatidylinositol 3-kinase
PKA	Protein kinase A
PKC	Protein kinase C
PLIN-5	Perilipin-5
POMC	Pro-opiomelanocortin
PPV	Positive predictive value
PR	Progesterone receptor
PVN	Paraventricular nucleus
PVT	Portal vein thrombosis
RT-qPCR	Real-time quantitative PCR
RANKL	Receptor activator of NF-κB ligand

rFSH	Recombinant FSH
TAE	Tris-acetate-EDTA
TgFSH	Transgenic female mice expressing human FSH
TGF- β	Transforming growth factor- β
TNF- α	Tumor necrosis factor- α
TRT	Testosterone replacement

Zusammenfassung

Die Gonadotropin-releasing hormone (GnRH) Neurone im Hypothalamus steuern die Reproduktionsachse der Säugetiere. Das GnRH wird pulsatil in das hypophysäre Pfortaderblut freigesetzt und stimuliert die Synthese und Sekretion der Gonadotropine, d.h. des Follikelstimulierenden Hormons (FSH) und des luteinisierenden Hormons (LH), in den gonadotropen Zellen des Hypophysenvorderlappens, um die Gonadenfunktion kontrollieren. Zahlreiche Studien in den letzten Jahrzehnten haben die funktionelle Rolle der Gonadotropine im Rahmen der Fortpflanzungsphysiologie untersucht. Jüngste Studien an Tiermodellen deuten allerdings darauf hin, dass FSH und LH auch physiologische Vorgänge außerhalb der Reproduktionsachse, wie z.B. den Leber- und Knochenstoffwechsel, beeinflussen. Wie genau die Gonadotropine auf extra-gonadale Organe wirken, ist bisher nur unzureichend untersucht.

Um die Rolle von FSH und LH systemisch zu analysieren haben wir ein neues Mausmodell generiert und die gonadotropen Zellen in adulten Tieren akut mittels Diphtherie-Toxin ablatiert. Neben einem tiefen Hypogonadismus führt der Verlust der gonadotropen Zellen bei weiblichen Mäusen zu Fettleibigkeit, Glukoseintoleranz, Lebersteatose und Knochenschwund. Wir zeigen, dass diese Phänotypen mit Ausnahme der Lebersteatose indirekt durch das Fehlen von Geschlechtshormonen verursacht werden. Eine erhöhte Gonadotropinfreisetzung durch gezielte pharmakogenetische Aktivierung der gonadotropen Zellen verbessert die hepatische Steatose.

Eine Verbesserung der hepatischen Steatose kann auch durch FSH-Injektion erreicht werden. Durch konditionalen Knock-out des FSH-Rezeptors in der Hypophyse mit Hilfe eines viralen CRISPR/Cas9-Ansatzes konnten wir schließlich nachweisen, dass eine parakrine Signalübertragung zu den kortikotropen Zellen des Hypophysenvorderlappens für die Verhinderung der Entwicklung von Lebersteatose unerlässlich ist. Zusammengefasst zeigen diese Ergebnisse, dass FSH neben seiner klassischen Rolle in der Reproduktionsphysiologie weitere wichtige Funktionen erfüllt. Die hier identifizierte parakrine Signalübertragung zwischen gonadotropen und kortikotropen Zellen dokumentiert zum ersten Mal eine Kommunikation unterschiedlicher Hormon-sezernierender Zelltypen in der adulten Hypophyse. Da die kortikotropen Zellen in der menschlichen Hypophyse ebenfalls den FSH-Rezeptor exprimieren, könnte dessen Aktivierung ein potenzielles therapeutisches Ziel darstellen.

Abstract

Gonadotropin-releasing hormone (GnRH) neurons in the hypothalamus regulate the mammalian reproductive axis. GnRH is released in pulses into the hypophyseal portal blood to stimulate both the synthesis and secretion of gonadotropins, follicle-stimulating hormone (FSH) and luteinizing hormone (LH), from gonadotrope cells in the anterior pituitary gland. FSH and LH in turn control gonadal function. Many efforts have been made over the past decades to dissect the functional aspects of gonadotropin signaling. However, these studies have almost exclusively focused on reproductive physiology. Interestingly, recent studies in animal models indicate that FSH and LH may also influence physiological processes outside of the reproductive axis, such as liver and bone metabolism. Exactly how the gonadotropins act on extragonadal organs is, however, not well understood.

To analyze the role of FSH and LH systemically, we generated a new mouse model and acutely ablated the gonadotrope cells in adult animals using diphtheria toxin. In addition to profound hypogonadism, the loss of gonadotrope cells in female mice leads to obesity, glucose intolerance, hepatic steatosis, and bone loss. We show that these phenotypes, with the exception of hepatic steatosis, are indirectly caused by the lack of sex hormones. We also demonstrate that increased gonadotropin release through targeted pharmacogenetic activation of gonadotrope cells improves hepatic steatosis.

An improvement in hepatic steatosis can also be achieved by FSH administration. Finally, by conditionally knocking out the FSH receptor in the pituitary gland using a viral CRISPR/Cas9 approach, we were able to demonstrate that paracrine signaling to the corticotrope cells of the anterior pituitary gland is essential for preventing the development of hepatic steatosis. Taken together, these results show that FSH exerts other important functions in addition to its classic role in reproductive physiology. The identified paracrine signaling between gonadotrope and corticotrope cells is the first to document communication between different hormone-secreting cell types in the adult pituitary gland. Since the corticotropes in the human pituitary also express the FSH receptor, its activation could represent a potential therapeutic target.

Introduction

1.1 Hypothalamic-pituitary-gonadal axis

Mammalian reproductive physiology is centrally regulated through the hypothalamic-pituitary-gonadal (HPG) axis. The gonads, pituitary gland, and hypothalamus work together and communicate via neuropeptides, neurotransmitters, and hormones to control gonadal development and fertility. In addition, this axis regulates the initiation of puberty and the maintenance of fertility in adulthood. The GnRH neurons are an essential neuronal population in the hypothalamus. These neurons produce GnRH: a decapeptide which is released in a pulsatile manner from axon terminals at the median eminence into the hypothalamic hypophysial-portal system (Gore *et al.*, 2002; Herbison *et al.*, 2016) resulting in GnRH binding to its receptor (GnRHR) on gonadotropes in the anterior pituitary. This regulates the production and secretion of the gonadotropins (FSH and LH), which are delivered, via circulation, to the gonads to regulate their activity (Figure 1).

GnRH neurons must correctly integrate a number of physiological stimuli, ranging from metabolic hormones to chemosensory signals, to ensure reproductive success. Although GnRH neuron activity reflects the integration of many factors, kisspeptin has been identified as an essential player in GnRH neurons regulation (Harter, Kavanagh & Smith, 2018), which has been shown to be the most potent stimulant of GnRH release discovered to date. Kisspeptin acts via the G-protein coupled receptor GPR54 (also known as Kiss1R) which is expressed in most GnRH neurons (Han *et al.*, 2005).

GnRH signaling subsequently controls the biosynthesis and release of LH and FSH from gonadotropes in the pituitary, and these hormones in turn regulate ovarian and testicular development and activity. FSH enhances follicular growth and development in females, as well as estrogen release in the mature Graafian follicle, in preparation for ovulation. LH increases progesterone secretion in the corpus luteum and causes ovulation. In males, FSH acts on Sertoli cells via its receptor (FSHR) and leads to spermatogenesis, while LH stimulates testosterone secretion by Leydig cells. In both sexes, these steroid hormones feed back onto the hypothalamus and gonadotrope cells to inhibit or stimulate the expression and release of GnRH and gonadotropins (Wintermantel *et al.*, 2006; Tsutsumi & Webster, 2009). A detailed understanding of this entire process across different hormonal conditions is particularly important as dysfunction in the control of these hormones leads to various pathologies and consequently infertility. One of the main hormonal disorders affecting female fecundity is polycystic ovary syndrome (PCOS) (Torchen *et al.*, 2017). PCOS is characterized by hyperandrogenism, often associated with ovarian cysts and anovulation and has been linked to metabolic disorders. In addition, increases in circulating LH, FSH, and GnRH secretion occur when the gonads are surgically removed or their normal secretion is pharmacologically suppressed (Tsutsumi & Webster, 2009). This is observed in men after castration when testosterone production decreases, or in menopausal women when follicular development in the ovaries decreases, and with it the production of large quantities of progesterone and estradiol in the ovaries.

However, recent studies have indicated that in addition to the gonads, other organs including bone, liver, and fat may also be directly regulated by gonadotropins, in particular by FSH (Sun *et al.*, 2006; Liu *et al.*, 2017; Guo *et al.*, 2019). Several clinical studies have reported an association of FSH with bone resorption as well as with metabolic disorders including obesity and hepatic steatosis, which occur independently of other hormones (Wang, Kuang, *et al.*, 2016; Wang, Li, *et al.*, 2016; Shieh *et al.*, 2019). Since gonadotropins tightly regulate gonadal function, which itself exerts multiple effects on body homeostasis throughout the whole lifespan of the organism, it has been difficult to experimentally disentangle direct gonadotropin effects on extra-gonadal tissues from indirect effects. Previous studies using either gonadotropin knock-out or overexpression mouse strains carrying global genetic modifications reported partially contradicting data in particular on FSH actions on extra-gonadal tissues (Sun *et al.*, 2006; Allan *et al.*, 2010). Novel genetic approaches in mice have set the stage to disentangle these effects.

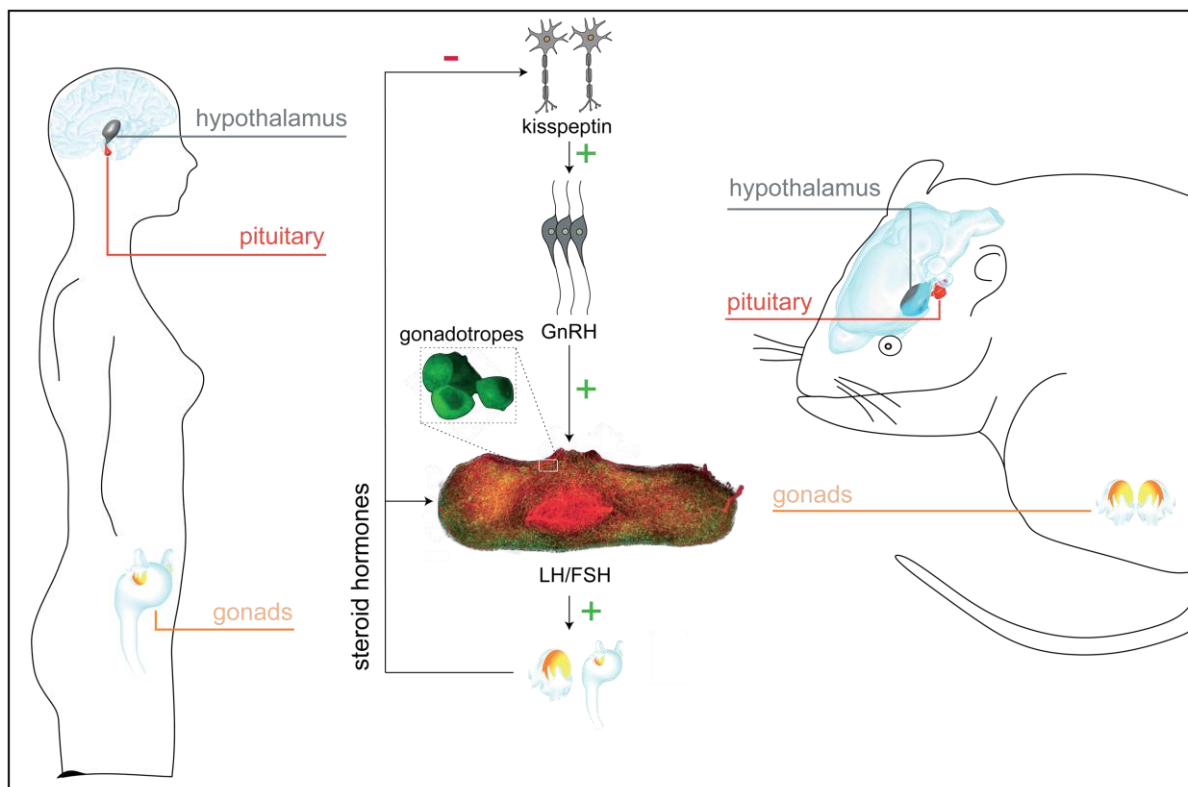


Figure 1: Regulation of the hypothalamic-pituitary-gonadal axis. GnRH secretion is regulated by kisspeptin neurons, and the gonads produce steroid hormones including estradiol which feed back onto the hypothalamus and the pituitary. Kisspeptin neurons in the hypothalamus release kisspeptin, which acts on the GPR54 receptor on the GnRH neuron. GnRH neurons release GnRH into the hypophyseal portal vasculature to act on the gonadotrope cells in the anterior pituitary gland to produce and secrete FSH and LH. FSH and LH activate the gonads to produce testosterone and estradiol. GnRH: gonadotropin-releasing hormone; LH: luteinizing hormone; FSH: follicle-stimulating hormone. Picture was modified from (Götz, Qiao, Beck & Boehm, 2017).

1.2 Hypothalamic-pituitary-adrenal axis

The hypothalamic-pituitary-adrenal (HPA) axis is also known as the stress axis and is responsible for integrating the current stress state of the animal with the appropriate physiological responses. A subset of hypothalamic neurons localized in the medial parvocellular subdivision of the paraventricular nucleus (PVN) synthesize and secrete corticotropin-releasing hormone (CRH), the principal regulator of the HPA-axis (Smith & Vale, 2006). In response to stress, CRH is secreted into hypophysial portal vessels to access the anterior pituitary gland (Figure 2). The release of adrenocorticotropic hormone (ACTH) into the systemic circulation is triggered by binding of CRH to CRH receptors within the pituitary. The adrenal cortex is the principal target for circulating ACTH, where it stimulates the zona fasciculata's glucocorticoid (GC) synthesis and secretion. ACTH consists of 39 amino acids but is synthesized as part of a much larger 241 amino acid precursor, pro-opiomelanocortin (POMC). Human POMC is synthesized in the anterior pituitary, the solitary tract of the medulla, the arcuate nucleus of the hypothalamus, and several peripheral tissues. The biological effects of GCs are normally adaptive; nevertheless, insufficient or excessive stimulation of the HPA-axis may contribute to the development of pathologies (Smith & Vale, 2006). Physical stress and the proinflammatory cytokines, including interleukins 1 and 6 (IL-1, IL-6), and tumor necrosis factor- α (TNF- α) increase both ACTH and cortisol secretion (Lenders *et al.*, 2002), which shows an important immune-endocrine interaction.

One important aspect of the regulation of ACTH and CRH secretion is the negative feedback which is controlled by GCs themselves. The transcription of the POMC gene in the anterior pituitary, as well as the synthesis and secretion of CRH in the hypothalamus, can be inhibited by GCs (Astuti *et al.*, 2001). Importantly, GCs interaction with their receptor (GR) influences multiple organ systems including the reproductive, cardiovascular, respiratory and nervous systems (Sapolsky, Romero & Munck, 2000). One physiological role of GCs in conditions of stress is to provide energy to the brain and peripheral tissues by stimulating hepatic gluconeogenesis. Indeed, long-term increase of GCs leads to severe disruptions of lipid and glucose metabolism (Rafacho, Ortsater, Nadal & Quesada, 2014).

A detailed understanding of the HPA-axis under various hormonal conditions is essential, as disruption of the control of these hormones leads to various pathologies such as Cushing's syndrome. The most common etiology of Cushing's syndrome is Cushing's disease. It is caused by a pituitary adenoma, which results in increased ACTH and cortisol release (Juszczak, Morris & Grossman, 2000). The excess circulating cortisol exerts negative feedback inhibition on ACTH and CRH secretion from the pituitary and hypothalamus and disrupts the normal physiological diurnal variation in cortisol levels (Juszczak, Morris & Grossman, 2000). Consequently, Cushing's disease is associated with elevated ACTH levels and suppressed CRH secretion (Juszczak, Morris & Grossman, 2000). Facial plethora, moon facies, hypertension, diabetes and obesity are the most common clinical attributes in adults. In prepubertal pediatric patients, the most common signs include decreased linear growth, rapid weight gain, and obesity. In postpubertal pediatric patients, clinical symptoms also include dorsal/sub-clavicular fat pads and amenorrhea in addition to rapid weight gain.

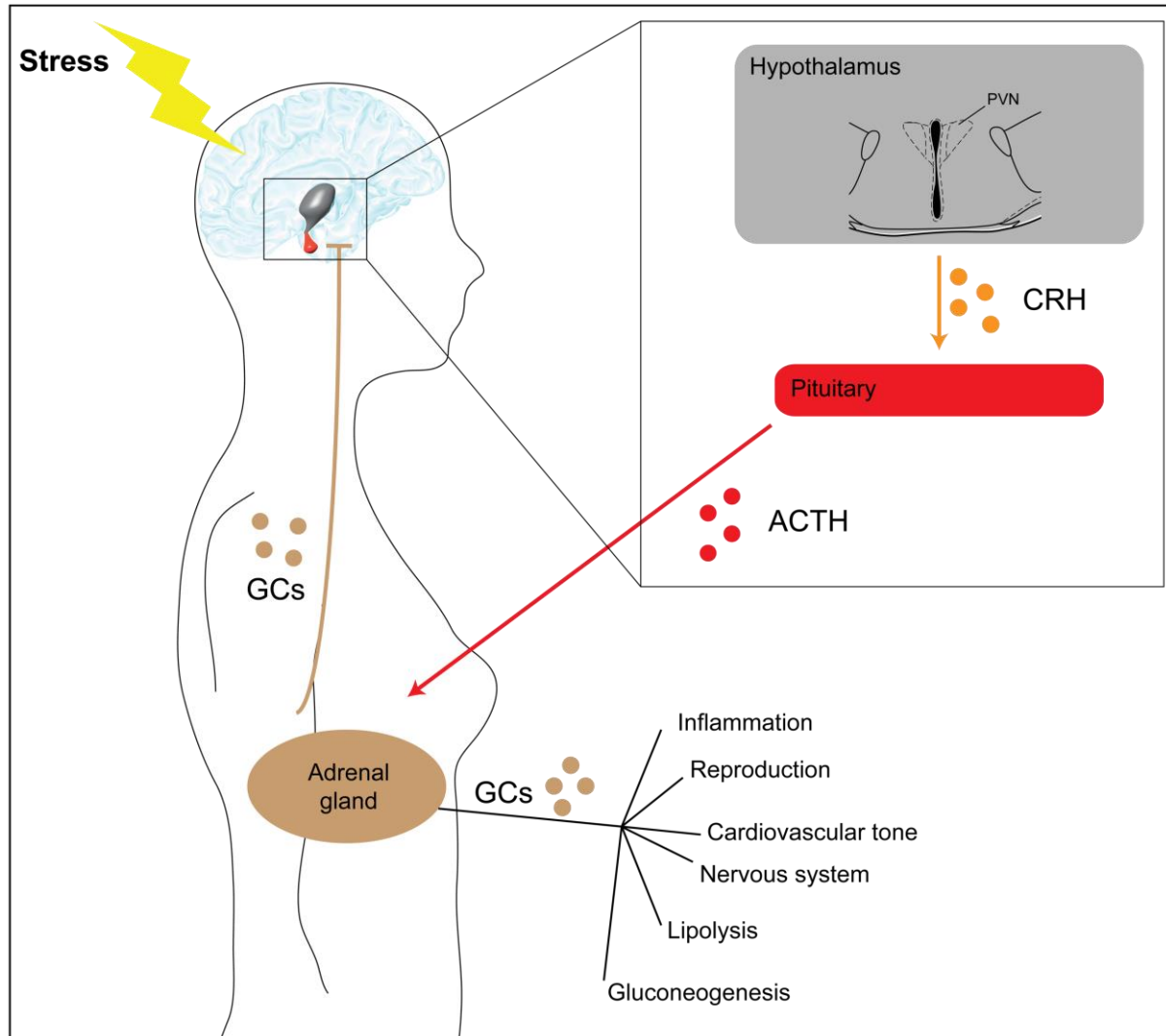


Figure 2: Regulation of the hypothalamic-pituitary-adrenal axis. The PVN of the hypothalamus is the main source of CRH that regulates the HPA-axis. The activation of CRH neurons depends on neural afferents from the brainstem and signals from the limbic system resulting in CRH synthesis and release in a sequential manner. The anterior pituitary gland produces ACTH in response to CRH. The adrenal gland releases GCs in response to ACTH. The diagram shows the feedback mechanism by corticosterone at the level of the pituitary and hypothalamus. GCs inhibitory feedback limits the extent and duration of neuronal CRH activation and ACTH release. ACTH: adrenocorticotrophic hormone; GCs: glucocorticoids; CRH: corticotropin-releasing hormone; PVN: paraventricular nucleus. Picture modified from (Melmed, Shlomo (2011) Williams Textbook of Endocrinology, 12th ed, Saunders, Philadelphia).

1.3 Anatomy, histology, and physiology of the liver

The liver weighs around 1.5 kg and makes up about 2.5% of an adult's body weight. The liver's surface is smooth, with a convex form such that it fits into the diaphragm's convex inferior surface (Figure 3). The liver is a metabolic workhouse that performs a diverse array of functions that are essential for maintaining metabolic homeostasis throughout the body (Kalra, Yetiskul, Wehrle & Tuma, 2021). The metabolic activities of the liver necessitate a sufficient blood supply for the delivery and export of hormones, substrates, and nutrients. It interacts with the endocrine and gastrointestinal systems by aiding in digestion and metabolism (Kalra, Yetiskul, Wehrle & Tuma, 2021). The liver acts as the storage

location for fat-soluble vitamins, controls cholesterol homeostasis and provides iron and copper (Kalra, Yetiskul, Wehrle & Tuma, 2021).

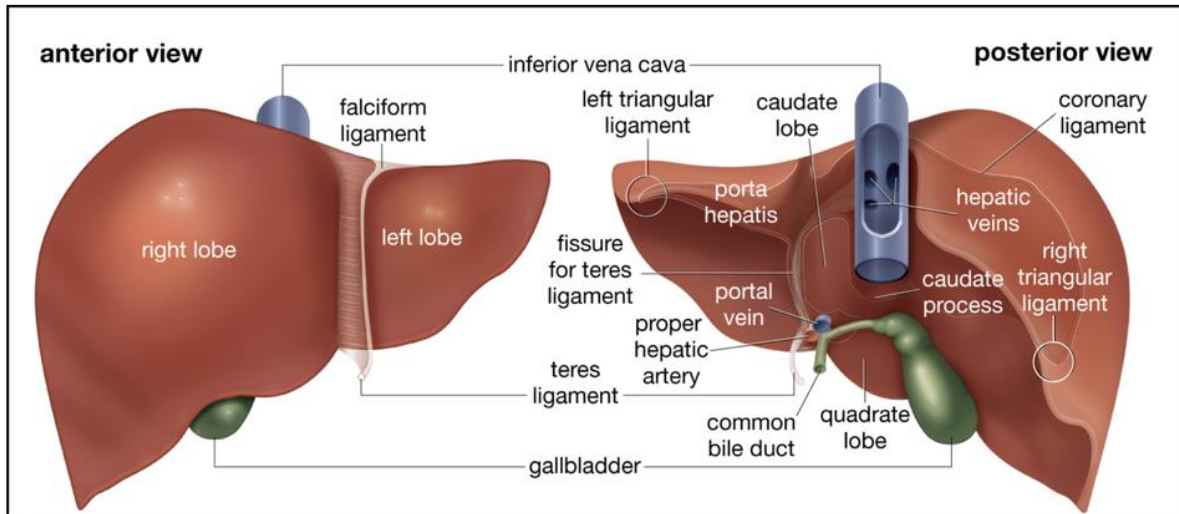


Figure 3: The macroscopic structure of the liver. Picture adapted from (Britannica, T. Editors of Encyclopaedia. "liver." *Encyclopedia Britannica*).

The liver is the largest gland in our body. Its histological structure basically consists of intertwined epithelial cell cords. The classic hepatic lobule is comprised of the blood supply and hepatic mass arrangement with the centrilobular vein in the center and the portal spaces at the periphery (Figure 4a). Surrounding each of the three liver lobules, small connective tissue islands, the portal triads, are found in the histological section. The portal triads consist of three vessels: a hepatic portal arteriole, a hepatic portal venule, and a bile duct (Figure 4c). This classic view is the most simple representation of the morpho-functional unit of the liver (Carotti *et al.*, 2020). The hepatocyte is the main hepatic cell type, making up 80% of the total cells in the liver. Between hepatocytes, there are vascular channels named sinusoids (Figure 4b). The hepatic sinusoids have a discontinuous epithelium due to the presence of fenestrae and gaps between endothelial cells, allowing blood plasma to move freely from the vessel to the perisinusoidal disse's space facing the hepatocytes. In the disse's space, situated between the layers of hepatocytes and the sinusoidal endothelial cells, are the hepatic stellate cells which are responsible for storing vitamin A. These cells are activated in response to chronic hepatic damage. Sinusoids also contain a specific macrophage cell type known as Kupffer cells as well as circulating monocytes, together with lymphocytic cells, such as natural killer cells. These cells play essential roles in the maintenance of the liver's immune tolerance or in the activation of the pro-inflammatory response.

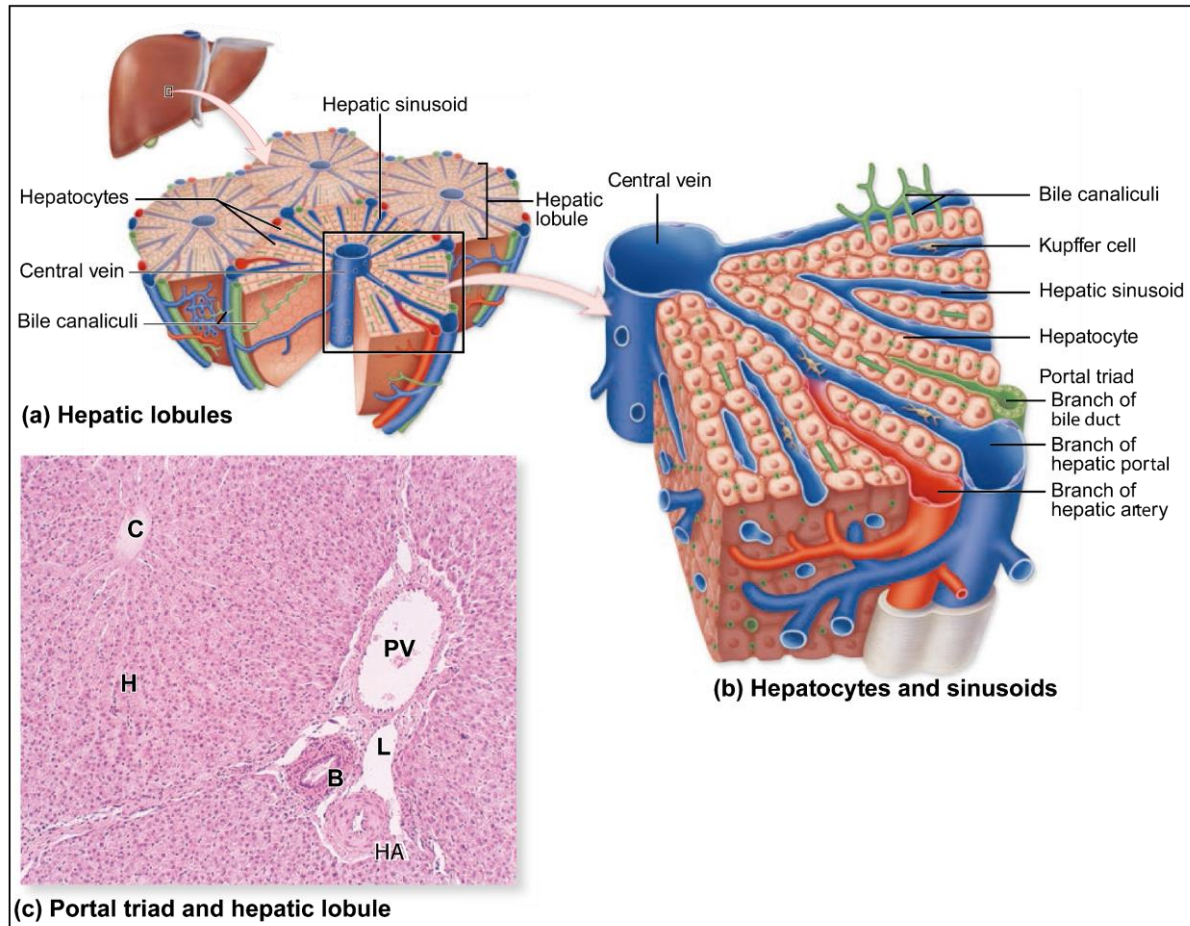


Figure 4: Cellular architecture of the liver. The schematic shows an adult liver. **(a)** Overview of histological components of the liver with the portal triad, central vein, and hepatic sinusoids. **(b)** A schematic of the cellular architecture of the liver showing the hepatocytes arranged in hepatic plates separated by sinusoid spaces radiating around a central vein. Bile canaliculi on the surface of adjoining hepatocytes drain bile into the bile ducts (green), which run parallel to portal veins (blue) and hepatic arteries (red) to form the portal triad. **(c)** Histological structure of a lobule showing the central vein (C), plates of hepatocytes (H) and in an adjacent portal area, a small lymphatic vessel (L) and components of the portal triad: a portal venule (PV), hepatic arteriole (HA), and bile duct (B)". Picture modified from (Mescher, Anthony L (2018) Junqueira's Basic Histology, 15th ed., McGraw-Hill Education, New York).

The liver plays a key role in energy metabolism by controlling the production of the critical energy molecule, glucose. It is able to store glucose during glycogen synthesis and lipogenesis and to synthesize glucose during glycogenolysis and gluconeogenesis (Kalra, Yetiskul, Wehrle & Tuma, 2021). These signaling pathways are regulated by hormones and transcription factors (Kalra, Yetiskul, Wehrle & Tuma, 2021). Genes controlling these processes are also transcriptionally regulated by hormones such as glucagon and insulin (Kalra, Yetiskul, Wehrle & Tuma, 2021).

The liver is also involved in the regulation of protein and amino acid metabolism (Kalra, Yetiskul, Wehrle & Tuma, 2021) and synthesizes the majority of plasma proteins. Of these proteins, albumin is the most abundant found within the plasma. In order to replace the degraded or lost albumin, the liver synthesizes it at a rate of about 12 g per day. This is equivalent to 3% of total body albumin (Kalra, Yetiskul, Wehrle & Tuma, 2021). The impaired albumin synthesis and the resulting low plasma albumin

concentration are considered as the hallmark of chronic liver disease (Kalra, Yetiskul, Wehrle & Tuma, 2021).

Liver cells are involved in many pathways of lipid metabolism (Kalra, Yetiskul, Wehrle & Tuma, 2021). It is the hub of fatty acid (FA) synthesis and lipid circulation through lipoprotein synthesis. FA is stored in lipid droplets principally in the liver and adipose tissue as triglycerides (TGs). The mobilization of FA from adipose tissue requires the activity of TG-lipases, which produce FA. FA is then released into the bloodstream, where it is taken up by hepatocytes (Mato, Alonso, Nouredin, & Lu, 2019) and re-incorporated into TGs (Figure 5). These re-esterified TGs form very-low-density lipoproteins (VLDL) when combined with apolipoprotein-B. As a result, VLDL are exported into the blood circulation. Microsomal triglycerides transfer protein (MTTP) regulates this process (Mato, Alonso, Nouredin, & Lu, 2019). Most of the TG in the circulation are associated with VLDL-TG during the post-absorptive phase. This process uncouples hepatic TG synthesis from its secretion resulting in low blood content of FAs, which are cytotoxic (Mato, Alonso, Nouredin, & Lu, 2019). However, the regulation of TG metabolism by other stimuli is still a subject of research.

De novo synthesis of FA or its influx from diet or adipose tissue increases the lipid content in the liver, whereas lipoprotein secretion and beta-oxidation decrease hepatic lipid content. Hormone-sensitive lipase (HSL) is the major enzyme involved in the regulation of lipolysis (Kalra, Yetiskul, Wehrle & Tuma, 2021). HSL activity is controlled by different hormones including insulin, glucagon, growth hormone (GH), catecholamines, and cortisol (Mato, Alonso, Nouredin, & Lu, 2019). Insulin levels are low during fasting and exercise, allowing growth hormone, cortisol, and norepinephrine to synergistically increase systemic fatty acid availability, stimulate lipolysis, and inhibit lipogenesis (Kalra, Yetiskul, Wehrle & Tuma, 2021). Conversely, hepatic lipid accumulation induces endocrine alterations that dysregulate adipose tissue lipolysis, including increased sympathetic tone, HPA-axis activity, and insulin resistance (Pratley, Coon, Rogus & Goldberg, 1995).

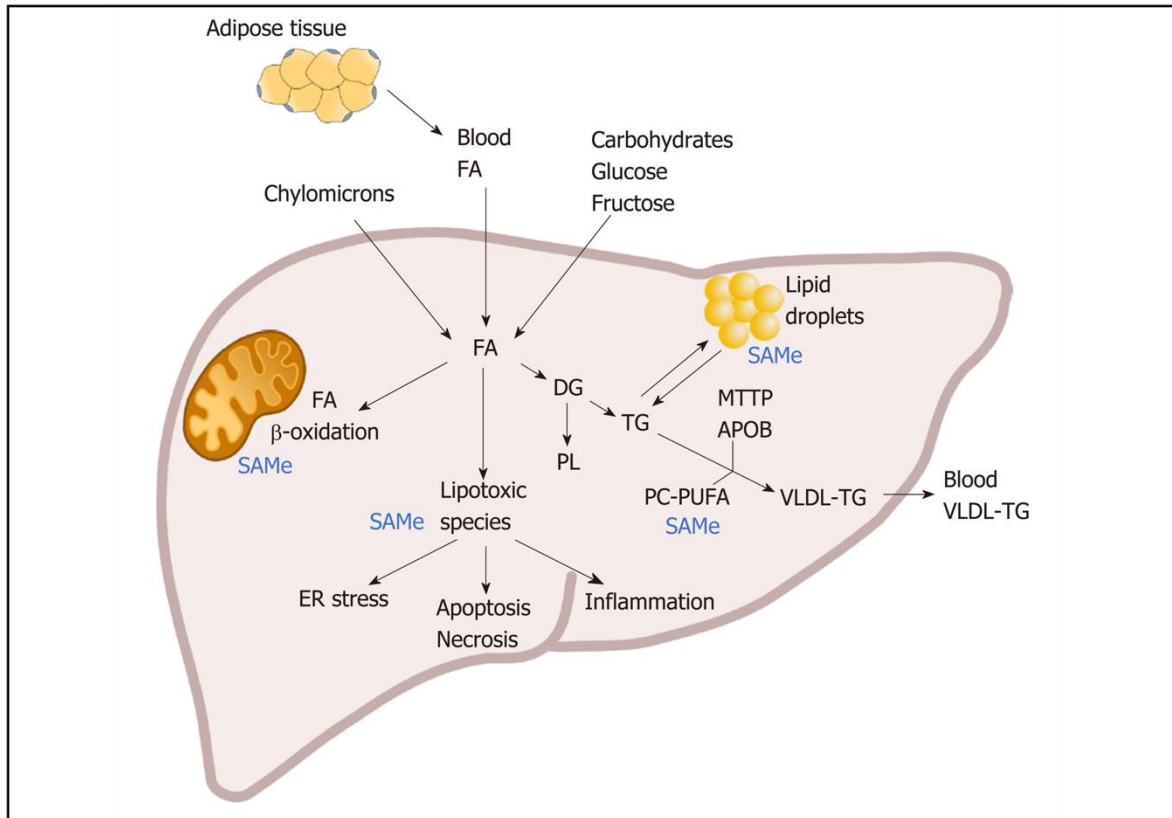


Figure 5: Hepatic lipid metabolism. HSL is involved in the mobilization of FA from their triglyceride stores in adipose tissue. The resultant FA released into the blood circulation is taken up by hepatocytes. Carbohydrates, on the other hand, are another source of hepatic FA-induced de novo lipogenesis. Chylomicrons are lipoprotein particles that are used to transport triglycerides, phospholipids, and cholesterol from the digestive tract to the liver. Subsequently, FA are metabolized by peroxisomal and mitochondrial β -oxidation, and the accumulation of FA in the cytoplasm induces lipotoxicity such as ER stress, apoptosis, necrosis, and inflammation. A number of re-esterified TG are packed, with the assistance of the MTP, into VLDL and exported into the circulation. HSL: Hormone-sensitive lipases; “APOB: Apolipoprotein-B; DG: Diglycerides; ER: Endoplasmic reticulum; FA: Fatty acids; MTP: Microsomal triglycerides transfer protein; PC-PUFA: Phosphatidylcholines containing polyunsaturated fatty acids; PL: Phospholipids; SAME: S-adenosylmethionine; TG: Triglycerides; VLDL: Very low-density lipoproteins”. Picture adapted from (Mato, Alonso, Noureddin, & Lu, 2019).

1.4 Metabolic syndrome

Metabolic syndrome is characterized by metabolic abnormalities including hypertension, insulin resistance, abdominal obesity, inflammation, and blood lipid disorders. People with metabolic syndrome are more likely to acquire diabetes and atherosclerotic cardiovascular disease. The development of metabolic syndrome is a result of both genetic and acquired factors and early diagnosis is important to achieve lifestyle changes. Metabolic syndrome has recently gained significant importance due to the exponential increase in obesity worldwide.

Insulin resistance is a key event in the pathophysiology of metabolic syndrome. A compensatory phenomenon of insulin resistance is hyperinsulinemia, which is caused by decreased insulin clearance by the liver and increased insulin secretion by pancreatic beta cells. Hyperinsulinemia is associated with increased concentrations of free FAs and leads to an increase in lipogenesis and fat mass. These changes are associated with an increase in lipid production and hepatic glucose and a further decrease in insulin

signaling (Bugianesi, McCullough & Marchesini, 2005). In addition to the role of the adipocyte as a reservoir of energy, it is also an active endocrine organ that produces and secretes several cytokines such as adipokines that contribute to the regulation of metabolic processes (Bugianesi, McCullough & Marchesini, 2005).

Hepatic lipid deposition is linked to various aspects of insulin resistance, including hypertriglyceridemia, hyperinsulinemia, and a low HDL content. Furthermore, higher liver adipose tissue composition is typically related to decreased hepatic insulin sensitivity. The molecular mechanisms underlying the development of hepatic insulin resistance have been studied and include a decrease in insulin-stimulated tyrosine phosphorylation of insulin receptor substrate 1 (IRS-1) and insulin receptor substrate 2 (IRS-2), which blocks the ability of insulin to activate glycogen synthase, reduces the ability to store glycogen and increases gluconeogenesis (Bugianesi, McCullough & Marchesini, 2005).

1.5 Non-alcoholic fatty liver disease

The pathomechanism of nonalcoholic fatty liver disease (NAFLD) and nonalcoholic steatohepatitis (NASH) is incompletely understood. It is, however, clear that patients with advanced fibrosis and steatohepatitis have a much higher risk of developing hepatocellular carcinoma (HCC) or liver-related mortality. Epidemiologic data suggest that steatohepatitis and steatosis constitute two distinct pathological entities, both of which can transition into one another. NASH is defined by the presence of inflammation and hepatic steatosis, as well as signs of hepatocyte injury, with or without fibrosis. The American Association for the Study of Liver Diseases (AASLD) defines NAFLD as a hepatic fat accumulation of more than 5-10% of the liver's weight (Figure 8). In all patients with NAFLD, hepatic fibrosis must be staged in order to identify those with severe fibrosis, who may develop liver-related complications including portal hypertension and hepatocellular dysfunction later. The end-stage of NAFLD, HCC, has the second highest mortality rate in the world (Torre *et al.*, 2015). HCC accounts for the majority of primary hepatic cancers and is one of the top causes of death in people with severe fibrosis or cirrhosis. It can produce complications such as portal vein thrombosis (PVT) (Quirk, Kim, Saab & Lee, 2015). PVT is present in 10-40% of HCC patients at the time of diagnosis (Llovet *et al.*, 1999).

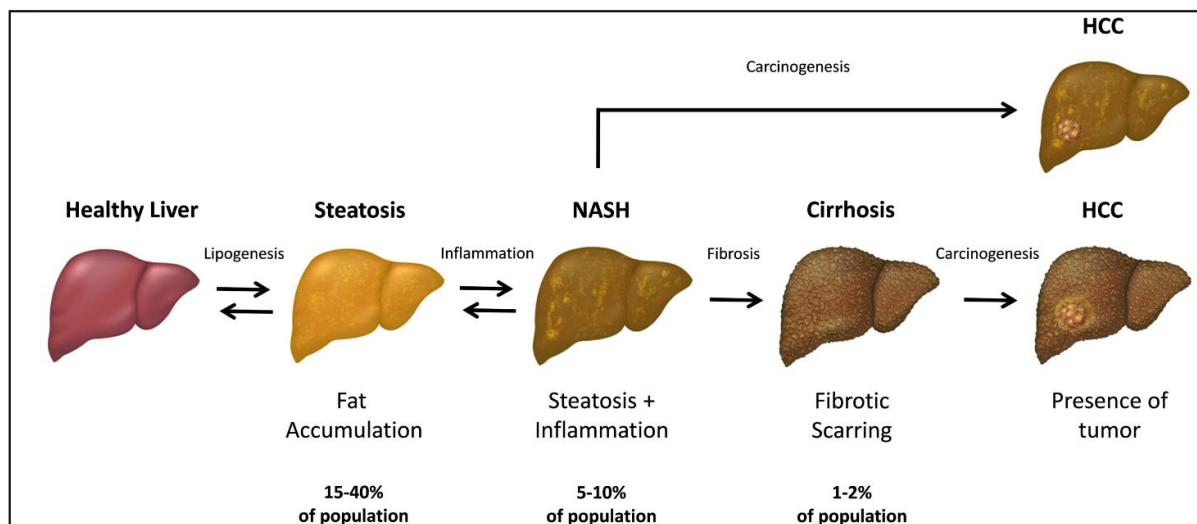


Figure 6: The spectrum of NAFLD progression. Steatosis is the first stage of NAFLD. It is defined by the buildup of fat in the hepatocytes. The advancement of NASH is accelerated by subsequent inflammatory diseases, that are followed by liver cirrhosis, which can lead to HCC. Furthermore, steatosis affects 15-40% of the population, while NASH affects 5-10% of the population, with 1-2% developing cirrhosis. Both NASH and steatosis can reverse to NAFLD. HCC: hepatocellular carcinoma; NASH: nonalcoholic steatohepatitis; NAFLD: nonalcoholic fatty liver disease. Picture adapted from (Turchinovich, Baranova, Drapkina & Tonevitsky, 2018).

1.5.1 Epidemiology, etiology, and classification of NAFLD

Liver disease is a major cause of illness and death worldwide. In 2010, the most common cause of liver disease was NAFLD with 44%, in second place was hepatitis B virus (HBV) with 30%, followed by hepatitis C virus (HCV) comprising 15%, and harmful alcohol consumption with 11% (Figure 7).

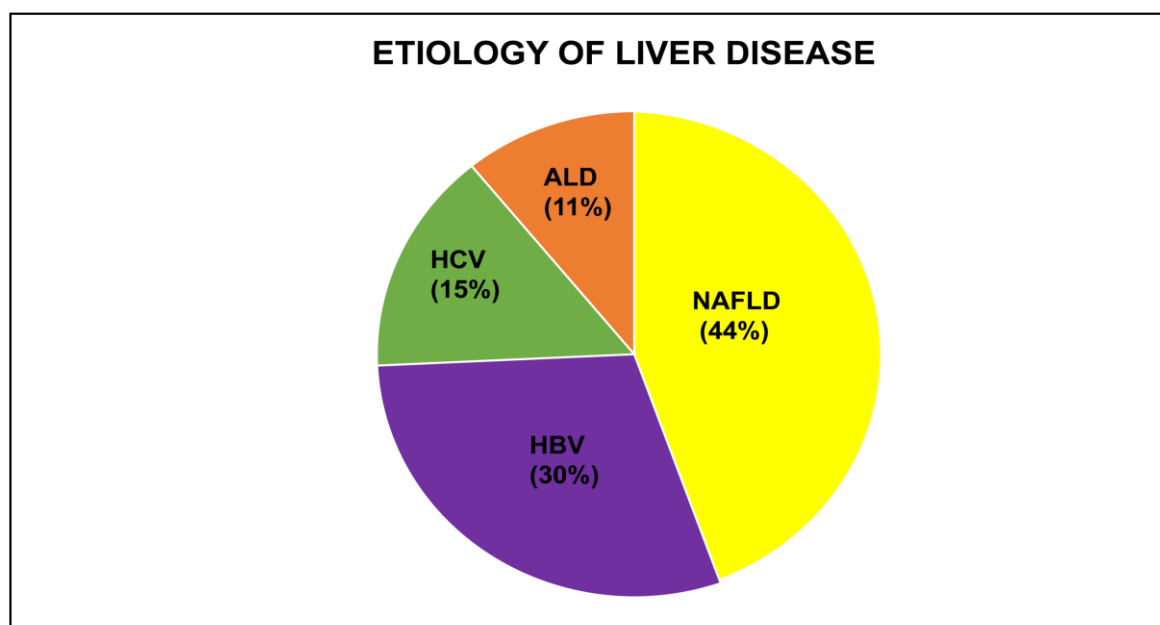


Figure 7: Percentage of the most common liver diseases in the World in 2010. HCV: hepatitis C virus; HBV: hepatitis B virus; ALD: alcoholic liver disease; NALFD: nonalcoholic fatty liver disease. Picture modified from (Muriel, Pablo (2017). Liver Pathophysiology Therapies and Antioxidants, 1th ed., Elsevier).

The global obesity epidemic has resulted in a significant increase in NAFLD prevalence. Obesity is defined as a body mass index (BMI) of more than 30 kg/m² in Caucasians and more than 25 kg/m² in Asian-Pacific people (Amedeo *et al.*, 2020). The estimated prevalence of NAFLD depends on the population studied and the procedures employed to determine the amount of fat in the liver. Recently, a sharp increase in NAFLD has been observed, particularly in adolescents and the elderly (Perumpail *et al.*, 2017). In the U.S., approximately 35% of adults are affected by this disease, and its increasing prevalence in young adults is a cause for concern (Hirode & Wong, 2020). In Germany, the estimated number of people affected by NAFLD was approximately 14 million in 2016. Studies predict that this number will increase to 20.9 million by 2030 (Estes *et al.*, 2018). In population-based studies, the disease occurred more frequently in men than in women, with the difference being even greater in overweight patients (Figure 8). NAFLD is also prevalent in developing countries (Estes *et al.*, 2018).

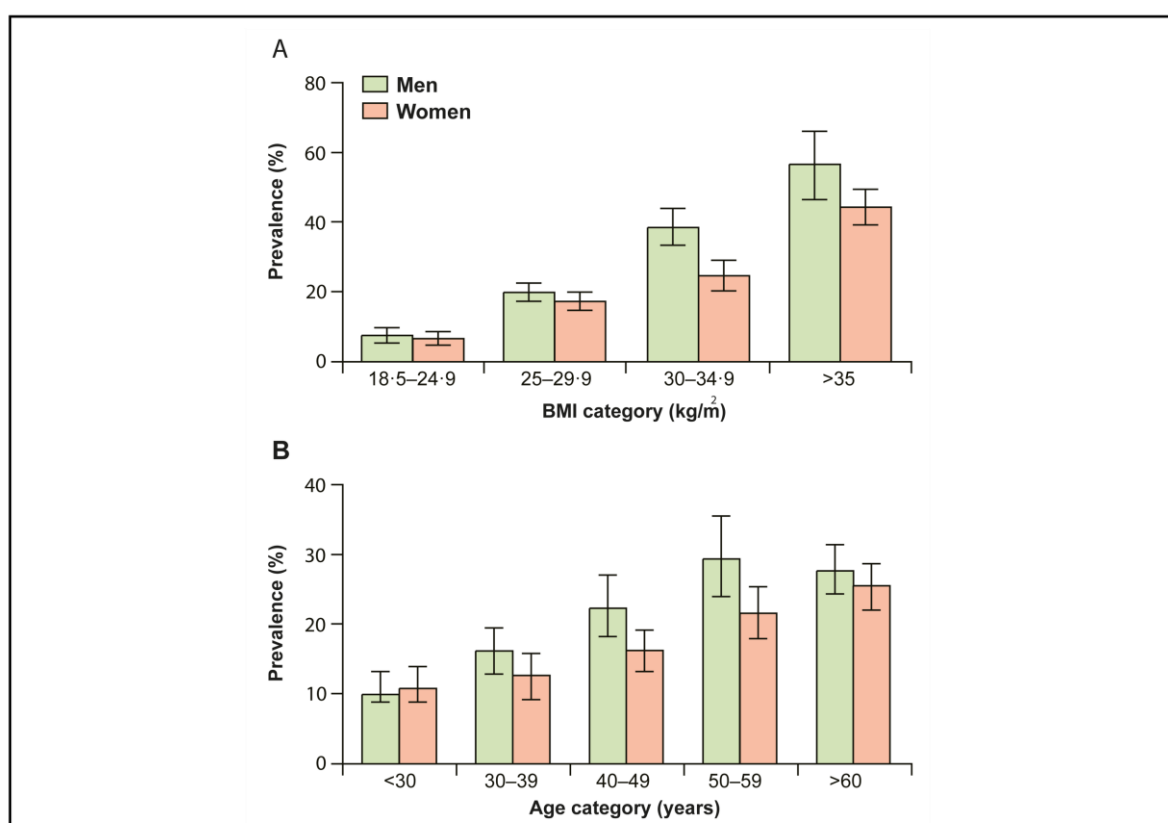


Figure 8: Prevalence of NAFLD according to BMI, age, and sex. “(A): Comparison of NAFLD prevalence diagnosed by ultrasound between normal weight (BMI 18.5-24.9 kg/m²), overweight (BMI 25.0-29.9 kg/m²), obese (BMI 30.0-34.9 kg/m²), and severely obese (BMI ≥35.0 kg/m²) men and women. (B): Prevalence of NAFLD by age in men and women in the same survey.” Picture modified from (Yki-Jarvinen *et al.*, 2014).

Over the past century, dramatic lifestyle changes have transformed health conditions in most regions of the world, leading to an increased incidence of metabolic syndrome. Associations have been found between metabolic syndrome and hepatic steatosis (Marchesini *et al.*, 2003). Patients with both NAFLD and metabolic syndrome have a higher risk of developing fibrosis of the liver and NASH compared to patients with a pure fatty liver (Dietrich & Hellerbrand, 2014).

1.5.2 Diagnosis and therapy of NAFLD

At the time of diagnosis, the majority of NAFLD patients have no symptoms or signs of liver disease, although many patients describe malaise or fatigue, as well as a feeling of fullness or discomfort on the right side of the upper abdomen (Weiss, Rau & Geier, 2014). In most patients, hepatomegaly is the only physical finding. Furthermore, in patients with NAFLD, increases in alanine and aspartate transaminase (ALT and AST respectively) serum levels are the most prevalent and often the only laboratory abnormalities identified (Weiss, Rau & Geier, 2014). The ratio of AST to ALT is normally < 1 , but as fibrosis progresses, this ratio increases, leading to a loss of its diagnostic accuracy in patients with cirrhotic NAFLD (Angulo *et al.*, 2002). In addition, many patients' serum levels of alkaline phosphatase and glutamyl transferase are also above the normal range. Moreover, there are other abnormalities that can be detected in patients with cirrhotic stage of NAFLD, including hypoalbuminemia, hyperbilirubinemia, and a prolonged prothrombin time. The majority of patients have elevated serum ferritin levels (Angulo, Keach, Batts & Lindor, 1999). The histologic involvement has the best predictive power over contrasting clinical diagnosis and liver tests. Although imaging studies can help to assess the presence and amount of fat infiltration in the liver, they can't reliably determine the severity of liver damage. A liver biopsy, which remains the best diagnostic technique as well as the most sensitive and specific way of delivering vital prognostic information, can only confirm a clinical suspicion of NAFLD (Weiss, Rau & Geier, 2014).

Patients with NAFLD have had no effective medical treatment options until now. There is currently no long-term treatment that can improve the course of fibrosis. The most successful treatment is weight loss along with a strict lifestyle change that includes more exercise, which has been demonstrated to improve histological findings. Nonetheless, liver transplantation remains a viable therapeutic option for people with decompensated cirrhosis.

1.6 Endocrine causes of NAFLD

1.6.1 The association between estrogen deficiency (menopause) and NAFLD

After 12 months of amenorrhea, menopause is diagnosed as the permanent cessation of menstruation caused by the decrease of ovarian follicular activity (Moe *et al.*, 2005). This estrogen reduction is accompanied by vasomotor responses, depression, and heat balance fluctuations in most women. Moreover, in the ensuing years, the loss of estrogen is followed by a high incidence of loss of bone mass, cardiovascular disease, and cognitive impairment. Menopause's average age (51.4 years) has remained constant and appears to be mostly driven by hereditary factors. NAFLD is becoming more common among women around the world. During reproductive age, the incidence of NAFLD is lower in women than in men, but this becomes more prominent after a woman reaches menopause. Postmenopausal women have a higher risk of NAFLD and a higher rate of severe hepatic fibrosis than premenopausal women, according to epidemiological, clinical, and experimental research. Older women with NAFLD have a higher mortality rate than men (Arshad, Golabi, Paik, Mishra & Younossi, 2019).

Several studies show that women with a lack of endogenous estrogen production like Turner's syndrome are at a higher risk for developing NAFLD (Quinn, Xu, Ronfani & Cidlowski, 2018). Women treated with tamoxifen, a selective estrogen receptor modulator (SERM), have an increased risk of obesity and NAFLD (Quinn *et al.*, 2018). The protective effect of estrogen depends on the estrogen receptor alpha (ER α). Estrogens act by binding to ER α or ER beta (ER β). In contrast to ER α knock-out mice, animals lacking functional ER β have protection mechanisms against metabolic syndrome and NAFLD (Quinn *et al.*, 2018). In addition, some studies suggest that the effect on ER α depends on gene transcription by binding genomic estrogen-responsive elements (Oftadeh, Perez-Viloria, Villa-Camacho, Vaziri & Nazarian, 2015; Quinn *et al.*, 2018). Furthermore, estrogen seems to exert protective roles against hepatic fat accumulation by suppressing glycogen storage, promoting lipolysis, gluconeogenesis, and lipogenesis (Hart-Unger *et al.*, 2017).

1.6.2 The association between testosterone and NAFLD

Male hypogonadism is defined by the International Society of Andrology by clinical and biochemical features including low sperm count and low testosterone, diminished libido, erectile dysfunction, increased visceral fat, and decreased lean body mass (Lunenfeld, Saad & Hoesl, 2005). Testosterone plays a key role in body composition, insulin sensitivity, and lipid metabolism (Kupelian *et al.*, 2006). Low testosterone levels and insulin resistance have a bidirectional relationship (Kupelian *et al.*, 2006). Different studies indicate that lower testosterone levels lead to a preferential deposition of abdominal fat and a higher accumulation of visceral adipose tissue (Couillard *et al.*, 2000), whereas higher testosterone levels are associated with a lower risk of central obesity. Furthermore, different studies demonstrated that mice with a conditional knock-out of the androgen receptor (AR) in the liver fed with a high-fat diet developed insulin resistance and hepatic steatosis (Livingstone *et al.*, 2015). Also, 5 α -reductase type 1 knock-out mice, fed on a high-fat diet, developed severe hyperinsulinemia and hepatic steatosis. 5 α -reductase catalyzes the conversion of testosterone to the more potent 5 α -dihydrotestosterone (DHT). In hypogonadal and eugonadal younger and older men, testosterone replacement treatment (TRT) reduced whole-body and visceral accumulation. Furthermore, TRT significantly decreased liver enzymes in hypogonadal men with NAFLD and metabolic syndrome (Haider, Gooren, Padungtod & Saad, 2010).

1.6.3 The association between glucocorticoids (Cushing syndrome) and NAFLD

The regulation of systemic metabolism relies heavily on GCs. Cushing's syndrome is associated with hepatic steatosis in 20% of patients (Rockall *et al.*, 2003). Insulin resistance, visceral obesity, hepatic steatosis, dyslipidemia, and hypertension all have metabolic features in common with hypercortisolism (Figure 9). Insulin sensitivity is affected by cortisol, either directly by interfering with the insulin receptor pathway or indirectly by activating proteolysis and lipolysis, resulting in an increase in free FA and amino acid release (Geer, Islam & Buettner, 2014). Enhanced activity of 11-hydroxysteroid

dehydrogenase type 1 (11-HSD1) leads to increased cortisone to cortisol activation in obese people, which stimulates metabolic alterations (Gathercole *et al.*, 2011). It is expressed in the brain, adipose tissue, and the liver. The increase of intracellular lipids in the liver is also linked to GC treatment. Increased expression of genes involved in triglyceride production and lipogenesis leads to the development of hepatic steatosis (Patel, Williams-Dautovich & Cummins, 2014). Some studies show that GC are able to trigger hepatic steatosis in ovariectomized mice via the glucocorticoid receptor (GR) in the liver (Quinn *et al.*, 2018). Vice versa, hepatocyte-specific GR knock-out mice are refractory to developing steatosis in hypogonadal females (Quinn *et al.*, 2018). These findings imply that estrogen deficiency causes GR transcriptional hypersensitivity in hypogonadism mice, which is coupled to enhanced GR recruitment to chromatin (Quinn *et al.*, 2018).

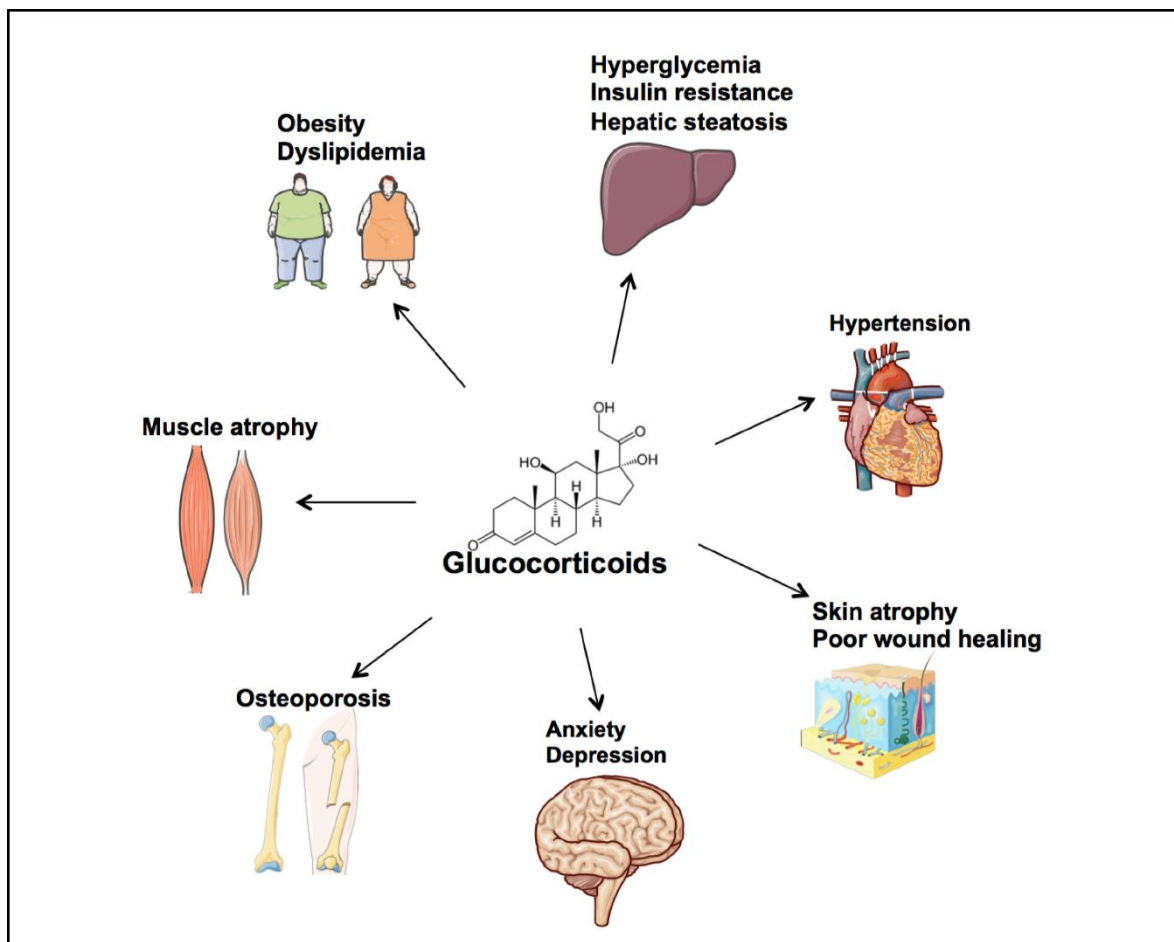


Figure 9: Sustained GC elevation leads to severe disturbances in different organs. Picture adapted from (Hemmer 2019, Thesis (PhD) Technical University of Munich, Munich, Germany).

1.7 The relationship between the bone and the reproductive axis

Previous studies have suggested a link between reproduction and bone metabolism (Mills *et al.*, 2021). Reproductive hormones have a critical function in bone metabolism development and maintenance. Common clinical reproductive disorders illustrate the physiological functions of hormonal regulation

including congenital hypogonadotropic hypogonadism, primary ovarian insufficiency, amenorrhea, and early menopause. Low bone mineral density (BMD) and an increased risk of fragility fracture are both clinical problems caused by these factors. The link between reproductive signals beyond sex steroid hormones including kisspeptin, GnRH, LH, and FSH and bone metabolism is not well understood (Figure 10) (Mills *et al.*, 2021).

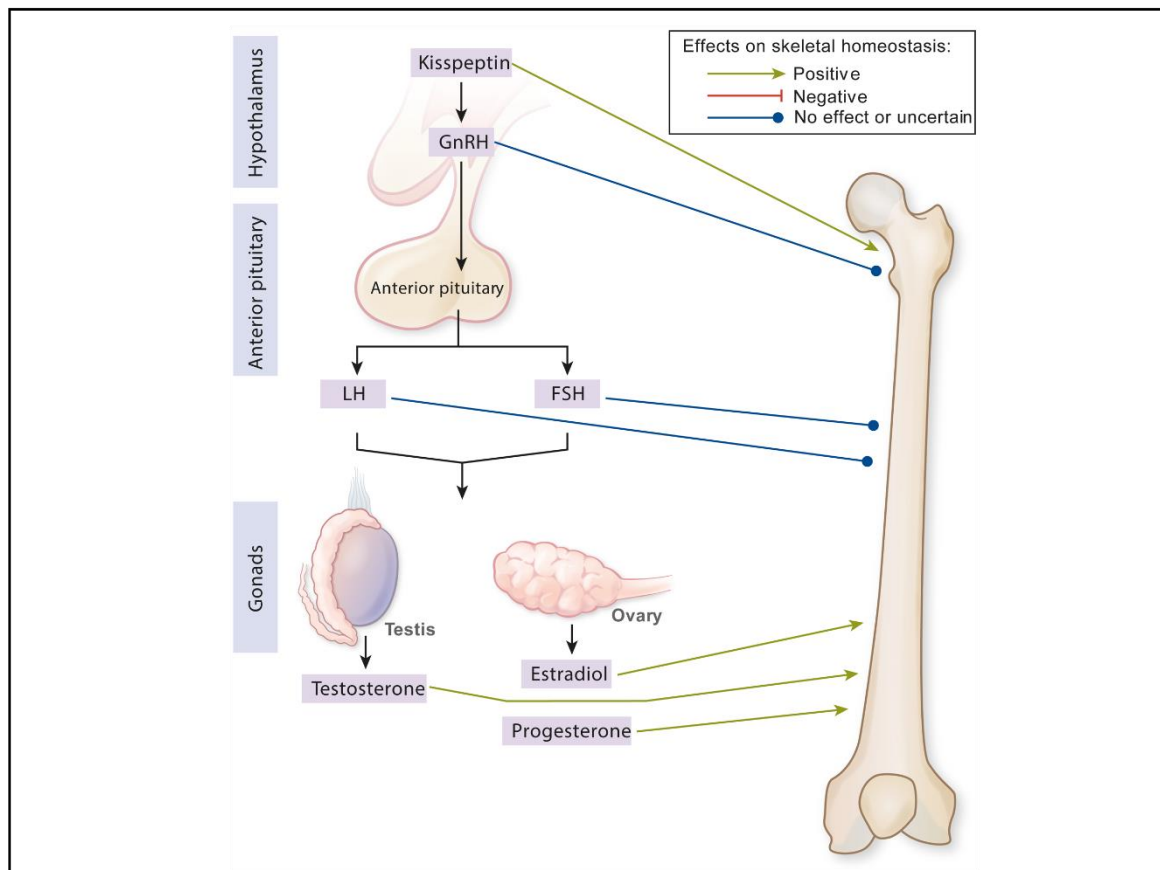


Figure 10: Summary of the direct effects of the reproductive axis on bone. Green arrow (positive effects) and red arrow (negative effects) on skeletal homeostasis. Gray arrows indicate no or uncertain effects on bone metabolism. Picture modified from (Mills *et al.*, 2021).

1.7.1 The histological structure of bone

Bone is a complex tissue that consists of different regions: diaphyseal, metaphyseal and epiphyseal, each with a periosteal and endosteal layer (Baig & Bacha, 2021). The human skeleton consists of 213 bones in total. Inorganic salts and type 1 collagen fibers are the main constituents of the bones (Baig & Bacha, 2021). Within the bone, osteoblasts form the main cellular component and are responsible for building up bone. Osteoblasts are derived from pleiotropic mesenchymal stem cells and are deposited on bones where they indirectly form the basis for new bone substances by excretion of predominantly type 1 collagen, calcium phosphates, and carbonates into the interstitial space (Baig & Bacha, 2021). During this process, osteoblasts transform into osteocytes that are no longer able to divide. Osteoclasts are large, multinucleated cells derived from hematopoietic stem cells. They are found on the bones' surface in pits called Howship lacunae. Proteolytic enzymes and hydrogen ions are secreted by osteoclasts to break-

down calcium hydroxyapatite crystals and remove calcium from bone (Baig & Bacha, 2021). Architecturally, bone can be categorized into two subtypes: cortical and trabecular bones (Figure 11). These two subtypes can be distinguished as follows:

1. Cortical bone makes up about 80% of the entire bones in the human body. It is much denser and stronger than trabecular bone and is resistant to compression, torsion, and bending. It's predominantly found in the diaphysis of long bones such as the tibia and femur, as well as the trabecular bone's outer shell.
2. Trabecular bone (cancellous bone): makes up only 20% of the skeletal mass but has 10 fold increased volume ratio and is metabolically four times more active than the cortical bone. It responds to variations in load eight times faster, making it significantly more dynamic. Trabecular bone is present primarily in compression-prone regions such as the pelvis, vertebral body, and metaphysis (Oftadeh *et al.*, 2015; Unal, Cingoz, Bagcioglu, Sozer & Akkus, 2018).

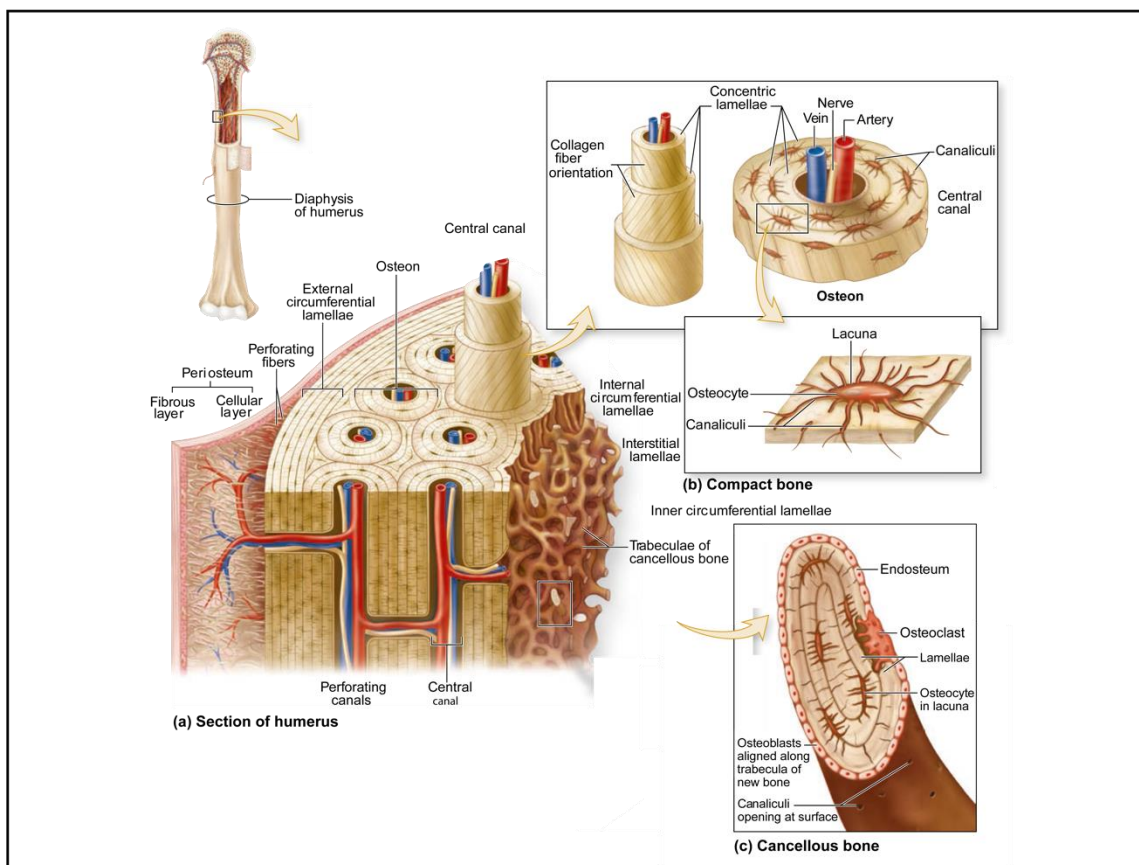


Figure 11: The anatomical and histological structure of bone. Microscopically, bone is divided into cortical and trabecular components. This diagram depicts the basic features of bone, as well as the three major cell types that make up bone: Osteocytes, Osteoblasts and Osteoclasts. Picture modified from (Mescher, Anthony L (2018) Junqueira's Basic Histology, 15th ed., McGraw-Hill Education, New York).

1.7.2 Bone metabolism

Calcium (Ca^{2+}) and phosphate (PO_4^{3-}) are the main components of bone, together accounting for 65% of its weight. Nearly all the Ca^{2+} and PO_4^{3-} and over half of the magnesium are contained in the human

body's bone (Kiela & Ghishan, 2009; M. Sun *et al.*, 2020). Bone growth and remodeling are influenced by a variety of systemic and local hormones. Parathyroid hormone (PTH) plays an essential role as a direct inhibitor of osteoblastic collagen synthesis and a potent stimulator of osteoclastic bone resorption (Kiela & Ghishan, 2009; M. Sun *et al.*, 2020) (Figure 12). PTH controls the level of ionized Ca^{2+} in the blood via binding to cell surface receptors in the kidneys and bones, thereby triggering responses that increase blood Ca^{2+} (Kiela & Ghishan, 2009; M. Sun *et al.*, 2020). PTH also enhances the synthesis of vitamin D₃, a hormonally active form of vitamin D, in the kidneys, which subsequently acts on the intestine to improve Ca^{2+} absorption (Kiela & Ghishan, 2009; M. Sun *et al.*, 2020). The resulting increase in 1,25[OH]2D₃ and in blood Ca^{2+} has a negative feedback effect on the parathyroid glands, causing PTH secretion to decrease. PTH-mediated Ca^{2+} homeostasis involves the bones, parathyroid glands, kidneys and intestines (Jeon *et al.*, 2008).

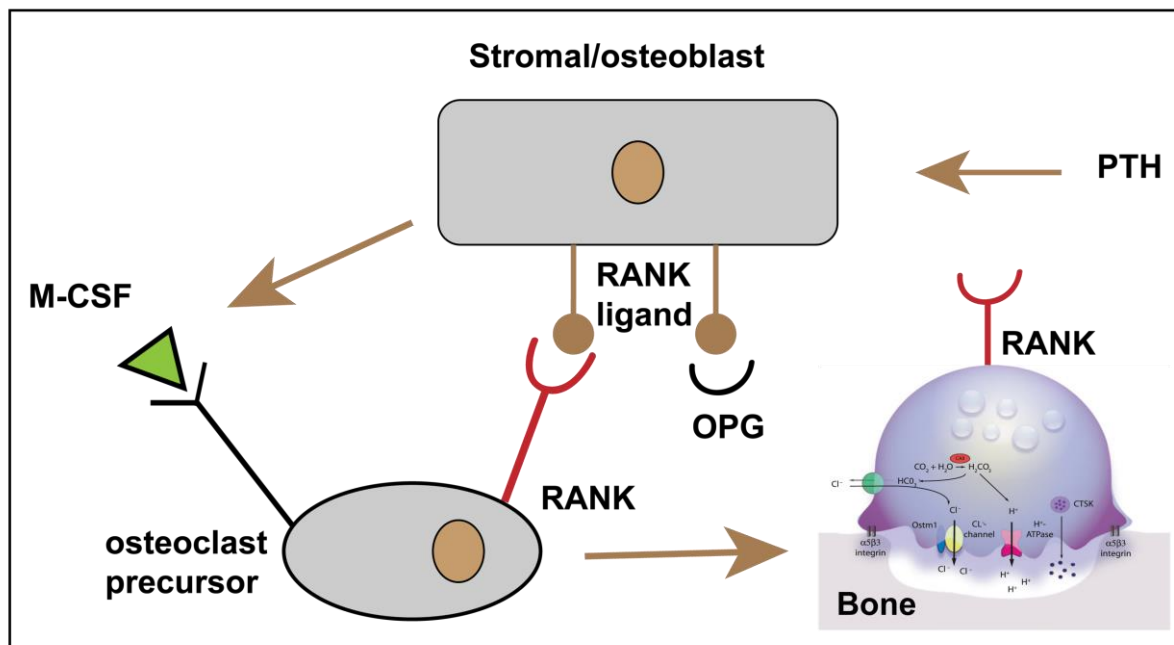


Figure 12: The effect of parathyroid hormone on osteoblasts. “Parathyroid hormone (PTH) acts on PTH-receptors on osteoblasts precursors to increase the production of macrophage colony-stimulating factor (M-CSF) and receptor activator for nuclear factor κB (RANK) ligand and to decrease the production of osteoprotegerin (OPG). M-CSF and RANK ligand stimulate the production of osteoclasts and increase the activity of mature osteoclasts by binding to RANK. OPG blocks the interaction between RANK ligand and RANK”. Picture modified from (Melmed, Shlomo (2011) Williams Textbook of Endocrinology, 12th ed, Saunders, Philadelphia).

Receptor activators of NF- κB ligand (RANKL) and osteoprotegerin (OPG) are the most important mediators in bone metabolism regulation. RANKL is an essential cytokine for the differentiation and activation of osteoclasts. A variety of cells produce RANKL, including B- and T-lymphocytes (Weitzmann & Ofotokun, 2016). RANKL interacts with RANK, that is expressed on the surface of osteoclasts. OPG is a soluble RANK which inhibits the interactions between RANKL and RANK and thereby osteoclastogenesis (Weitzmann & Ofotokun, 2016).

Calcitonin is also involved in the regulation of blood Ca^{2+} levels. It's a 32-amino-acid polypeptide with a disulfide connection between the cysteines in the chain (Kiela & Ghishan, 2009; M. Sun *et al.*, 2020).

The C-cells of the thyroid gland produce calcitonin. The release of calcitonin is stimulated by an acute rise in serum Ca^{2+} levels (Kiela & Ghishan, 2009; M. Sun *et al.*, 2020). The biological effect of calcitonin is to maintain Ca^{2+} homeostasis together with PTH and vitamin D.

Fibroblast growth factor 23 (FGF-23) is largely produced by osteocytes. It is a PO_4^{3-} -regulating substance (Ott *et al.*, 2015). Its main mechanism of action is to inhibit Na^+ -coupled inorganic PO_4^{3-} reabsorption in the renal proximal tubule. FGF-23 promotes the kidney's excretion of PO_4^{3-} . FGF-23 keeps the PO_4^{3-} level in the blood constant despite the different PO_4^{3-} intake with food. Increased FGF-23 blood levels lead to a decrease in the blood PO_4^{3-} level (hypophosphatasemia), reduced production of vitamin D and rickets, or bone softening (osteomalacia) (Figure 13).

Moreover, osteocytes secrete several important hormones such as sclerostin and prostaglandin (Ott *et al.*, 2015). These represent an important link to the cardiovascular system, mineral metabolism and bone physiology especially in bone disorder and chronic kidney disease. Furthermore, osteocytes precursors (osteoblasts) produce osteocalcin (Ott *et al.*, 2015) (Figure 13), which stimulates the secretion of insulin in the pancreas, increases insulin sensitivity in skeletal muscle and reduces fat accumulation in the liver (Ott *et al.*, 2015).

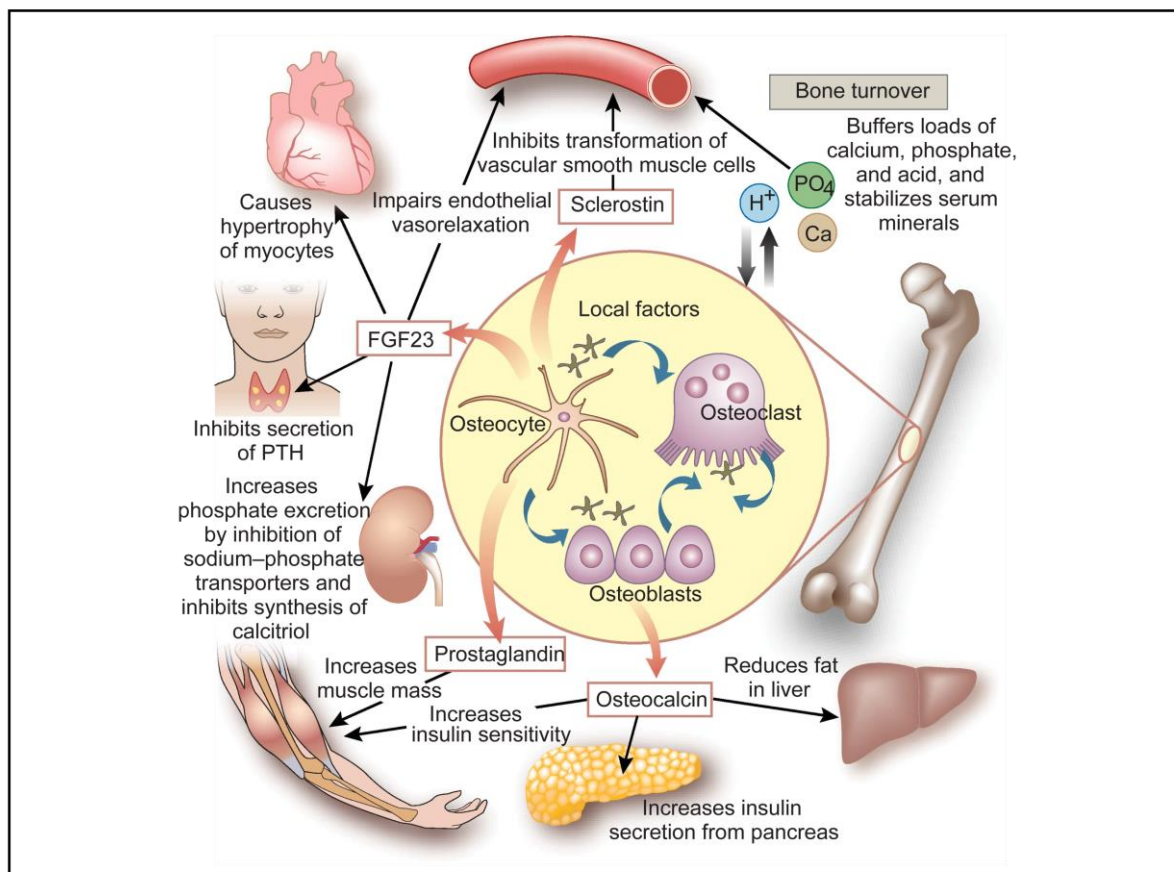


Figure 13: The regulation and action of FGF-23. FGF-23 is released by skeletal osteocytes and osteoblasts in response to hyperphosphatemia and inorganic PO_4^{3-} level. FGF-23 production is also stimulated by vitamin D3. FGF-23 has two main effects: it inhibits Na^+ - PO_4^{3-} cotransport in the kidney, resulting in phosphaturia, and it inhibits 1α -vitamin D₃ hydroxylase, lowering vitamin D3 levels. Reduced active vitamin D levels decrease gastrointestinal PO_4^{3-} and Ca^{2+} absorption. FGF-23 inhibits PTH secretion. By secreting hormones like sclerostin

and prostaglandin, osteocytes regulate important energy metabolism in the body. Osteoblasts, which are osteocytes progenitors, also produce osteocalcin, which plays an important function in metabolism. PTH: parathyroid hormone; PO_4^{3-} : phosphate; Ca^{2+} : calcium. Picture modified from (Ott *et al.*, 2015).

1.7.3 Osteoporosis

Since 1994, the World Health Organization (WHO) has defined osteoporosis as a condition marked by low bone mass and degeneration of bone microarchitecture, which leads to increased bone fragility and fracture risk (Kanis *et al.*, 1994). Bone loss in osteoporosis is caused by a high turnover rate, in which bone resorption outnumbers new bone creation. Bone loss is asymptomatic and progresses without pain or other symptoms until a fracture occurs. It is estimated that almost 30 million people in Europe suffer from osteoporosis (Hernlund *et al.*, 2013). The most common consequence of osteoporosis is fragility fractures. In Europe, the number of new fractures was predicted to be 3.5 million in 2010 (Hernlund *et al.*, 2013).

Different transcription factors and systemically active hormones directly or indirectly regulate the differentiation and proliferation of osteoclasts and osteoblasts in bone metabolism. Estrogen plays an important role in bone remodeling. Osteoporosis is a common side effect of estrogen deficiency in postmenopausal women (Vaananen & Harkonen, 1996). The estrogen biological functions are mediated via binding to $\text{ER}\alpha$ and $\text{ER}\beta$. Different studies show that conditional $\text{ER}\alpha$ knock-out in osteoblasts is linked to bone loss (Nakamura *et al.*, 2007). Similarly, in mice, ovariectomy (OVX) produces an osteoporotic bone phenotype. Furthermore, some experimental studies suggest that the $\text{ER}\alpha$ ablation in osteoclasts in OVX mice protects them against bone loss (Nakamura *et al.*, 2007). Other studies indicate that sex steroids regulate bone metabolism through the RANKL-OPG axis in osteoblasts (Nakamura *et al.*, 2007). Moreover, estrogen prevents bone loss by increasing the survival of osteoclasts through the secretion of transforming growth factor- β (TGF- β) (Hughes *et al.*, 1996) and via the induction of FAS ligand (Nakamura *et al.*, 2007).

Because estrogen deficiency and menopause are considered to be osteoporosis risk factors in women, the effectiveness of estrogen replacement therapy is well documented (Vaananen & Harkonen, 1996). Many studies show that estrogen slows bone loss and reduces the incidence of fractures (Vaananen & Harkonen, 1996), but the association between estrogen use and endometrial and breast cancer is of concern.

Secondary osteoporosis, which develops due to hypogonadism, is a common cause of overall bone loss (Golds, Houdek & Arnason, 2017). Low levels of bioavailable testosterone in elderly men, as well as lower estrogen levels after menopause in women, appear to be linked to a loss of BMD and an increased fracture risk (Golds *et al.*, 2017). However, testosterone can be converted to estrogens via aromatase. Many peripheral tissues, including bone, express this enzyme (Manolagas, O'Brien & Almeida, 2013). AR is expressed in bone cells specifically on osteoblasts (Chen, Lin, Tsai, Yang & Kang, 2019) as well as $\text{ER}\alpha$ (Manolagas, O'Brien, & Almeida, 2013). Furthermore, different studies show that AR knock-out mice display significant bone loss. These results indicate that osteoclastic function is predominantly

controlled by estrogens and ER. However, under conditions of estrogen and androgen excess, AR is upregulated in osteoblasts and stimulates proliferation and mineralization. Numerous studies with Klinefelter's syndrome (KS), the most frequent form of hypogonadism, report that KS patients display low BMD and impaired bone structure (Lin *et al.*, 2008).

GCs also exert direct as well as indirect effects on bone remodeling. Prednisone is used to treat a diversity of diseases, including inflammatory and respiratory diseases. There are a variety of studies showing that patients, who receive GCs as long-term therapy have a high risk of developing fractures (Buckley & Humphrey, 2018). GC suppress osteoclast proliferation and increase bone formation as well as a loss of BMD and bone resorption (Frenkel *et al.*, 2015).

1.8 Cellular mechanism of FSH signaling

FSHR belongs to the G protein-coupled receptor (GPCR) superfamily. The human FSHR is encoded by the *FSHR* gene located on chromosome 2q16.3 and comprises 10 exons (Casarini & Crepieux, 2019). The FSHR is predominantly expressed in the membrane of the gonads but also in specific extragonadal tissues (Kumar *et al.*, 2014). The molecular mechanisms of FSHR signaling are complex. The interaction between FSH and FSHR may involve several G Protein subtypes, including the G_i , G_s , and $G_{q/11}$ proteins (Casarini & Crepieux, 2019). The FSHR is also able to functionally interact with other membrane receptors and proteins including β -arrestins, epidermal growth factor receptor (EGFR), IGF-1 receptor (IGF-1R), phosphotyrosine binding domain, leucine zipper 1 (APPL1), and Forkhead box protein O1 (FOXO1) (Ulloa-Aguirre, Reiter & Crepieux, 2018).

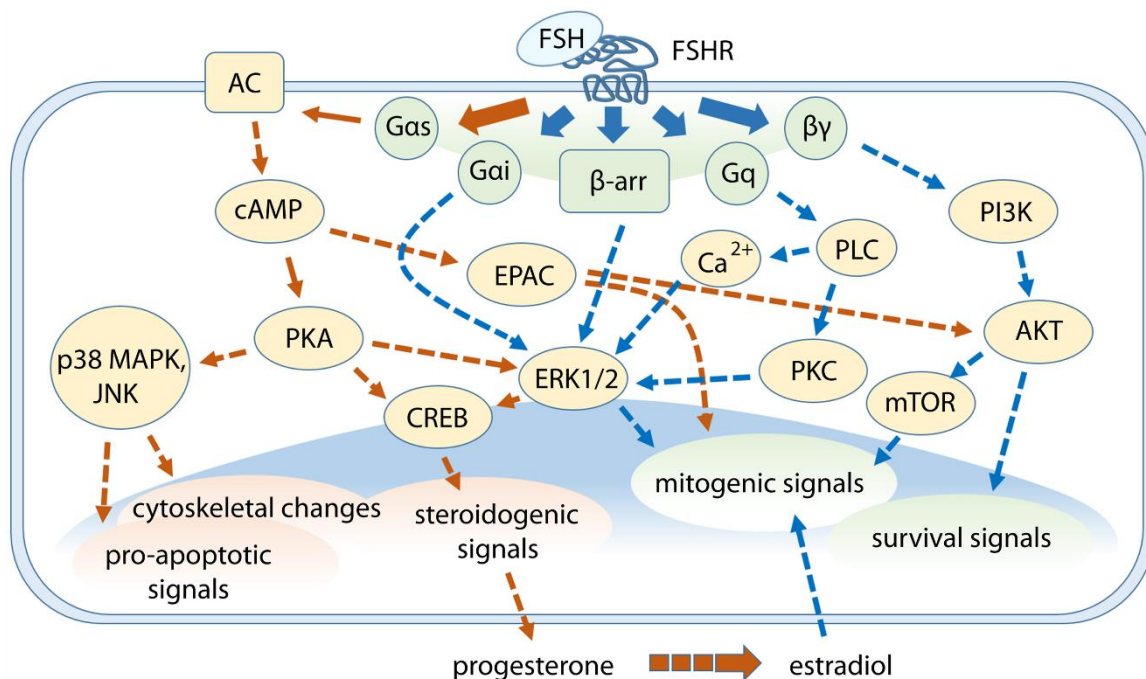


Figure 14: Schematic illustration of FSH signaling. Picture adapted from (Casarini & Crepieux, 2019).

1.9 Binary genetic approaches as powerful tools to decipher HPA- and HPG-axis pathology *in situ*

The Cre/loxP system is used in many different research areas to characterize genes of interest. This genetic tool allows the excision or inversion of genetically defined DNA sequences in a Cre-dependent manner. The approach is based on the ability of the Cre recombinase enzyme (from bacteriophage P1 (Hoess, Abremski & Sternberg, 1984)) to recognize *loxP* sites in the genome. For example, two *loxP* sites (when aligned in the same direction) flanking a particular DNA sequence are recombined by Cre (when Cre is expressed in the same cell), leading to excision of the flanked sequence. In 1987, Sauer *et al.* showed that Cre recombinase is able to recognize inserted *loxP* sites in yeast (*S. cerevisiae*). In parallel, the Cre/loxP strategy was successfully used in mouse cell lines (Sauer & Henderson, 1988) and in mouse embryonic cells (Thomas & Capecchi, 1987), followed by the development of the first conditional knock-out mouse model by (Gu, Marth, Orban, Mossmann & Rajewsky, 1994). Shortly thereafter, the Cre/loxP system was used not only to introduce cell-specific knock-outs but also to express transgenes in specific cells. A widely used approach to achieve reporter gene expression in Cre-expressing cells is to insert a floxed transcriptional stop signal followed by a transgene into the ubiquitously expressed *Rosa26* (R26) locus (Friedrich & Soriano, 1991; Soriano, 1999). This ensures transcriptional arrest of reporter gene expression in all Cre- cells, whereas the stop cassette is removed by Cre-mediated recombination in Cre+ cells. In the GnRHR-IRES-Cre (GRIC) mouse model (Wen *et al.*, 2008; Wen, Ai, Alim & Boehm, 2010; Hirdes, Dinu, Bauer, Boehm & Schwarz, 2010), Cre expression is coupled to that of GnRHR. By crossing this mouse line with any R26 reporter mouse line, gonadotropes express the desired reporter gene. Expression of the reporter gene into the *R26* locus can be further increased by inserting a β -actin promoter and a CMV enhancer element (CAGS) (eR26). The present work utilizes this approach and involves the generation of a novel mouse model that leads to the expression of genetically encoded DTR (diphtheria toxin receptor) (Buch *et al.*, 2005) and DREADD (Designer Receptor Exclusively Activated by Designer Drugs) specifically in gonadotropes.

Global knock-out animals (i.e. animals that lack a particular gene in each cell) are frequently used to discover the function of a gene, but it can be challenging to interpret the phenotype to determine the function of a gene in a specific cell type. In 1994, Gu *et al.* used conditional knock-out mice to silence a gene only in a genetically determined cell group. These mice are extremely useful for studying gene function in individual cell populations. This is crucial because the phenotype of global knock-out mice could be the result of several gene knock-outs in different cell types and organs. It is possible to explain gene function in a cell type-specific manner using conditional knock-out mice. Multiple genetic approaches and surgical methodologies in mice allow us to decipher the complex relationship between NAFLD, osteoporosis, HPG- and the HPA-axis.

1.10 Aims of my study

Reproduction is tightly controlled by the HPG-axis; however, this axis has also been implicated to interact with extragonadal tissues. Recent experiments have suggested that in particular FSH may modulate tissue function outside of the classic HPG-axis. Exactly how the gonadotropins act on extragonadal organs is, however, not well understood. We therefore decided to systemically investigate gonadotropin signaling capitalizing on different genetically modified mouse strains.

Aim 1:

To analyze the functional role(s) of FSH and LH systemically, after acutely ablating the gonadotrope cells in adult mice using diphtheria toxin.

Aim 2:

To analyze the functional role(s) of FSH and LH systemically, through targeted pharmacogenetic activation of gonadotrope cells in mice.

Materials and Methods

2.1 General Materials

Table 1: List of primers used for genotyping

Primer name	Sequence
<i>R26 Rev</i>	5'AACCACTGGAAAGACCGCGAAG3'
<i>Cre Fwd1</i>	5'GCGGTCTGGCAGTAAAACTATC3'
<i>Cre Rev2</i>	5'GTGAAACAGCATTGCTGTCACTT3'
<i>eROSA Rev</i>	5'GGGCGTACTTGGCATATGATACAC3'
<i>ROSA For</i>	5'GGAAGCACTTGCTCTCCCAAAG3'
<i>ROSA WT Rev</i>	5'CTTTAAGCCTGCCCAGAAGACTC3'

Table 2: Kits

Kit name	Product reference
RNeasy Mini Kit	(Qiagen, 74104)
SensiFAST SYBR No-ROX one-step kit	(Bioline, BIO-72005)
Follitropin alfa	(Merck, GONAL-f)
Corticosterone ELISA Kit	(Life Sciences Farmingdale, 108821)

Table 3: List of antisera and antibodies

Antiserum	Dilution	Species
anti-LH	1:5000	Rabbit
anti-FSH	1:5000	Guinea pig
anti-cFOS	1:500	Rabbit
anti-ACTH	1:10000	Mouse
anti-chicken Alexa Fluor 488	1:500	Goat
anti-guinea pig Cy5	1:500	Goat
anti-rabbit Cy3	1:500	Goat
anti-GFP	1:1000	Chicken

Table 4: List of primers used for qPCR

Primer name	Sequence
FSHR 2f	5'GGT CTA TTC CCT GCC CAA CC3'
FSHR 2r	5'GTT CAG AGG TTT GCC GCC T3'
<i>Actb</i> /β-actin (sense primer)	5'AAG GAG ATT ACT GCT CTG GCT CCT A3'
<i>Actb</i> /β-actin (antisense primer)	5'ACT CAT CGT ACT CCT GCT TGC TGA T3'

Table 5: List of primers used for CRISPR efficiency verification

Primer name	Sequence
FSHR f	5'GCT ATG ATC CTT GTT CAT CTC TCC3'
FSHR r	5'GAC TCT TGA GAA GGA TAG ACATCT G3'

2.1.1 Ear lysis buffer

50 mM Tris-HCl (pH 7.5-8.0), 100 mM NaCl, 0.2% NP-40, 0.2% Tween 20 and 1 mM EDTA. Before use, proteinase K was added to a final concentration of 100 µg/ml.

2.1.2 4% paraformaldehyde (PFA)

800 ml of dH₂O were heated to 60°C, placed on a magnetic stirrer and 40 g of paraformaldehyde were added. Two to three drops of 10 M NaOH were added in order to depolymerize the PFA. Once visibly clear, the solution was then cooled to room temperature, 50 ml of 20X PBS added and dH₂O were added to reach a final volume of one liter. pH was adjusted to 7.4. The solution was then cooled to 4°C and used within 12 hours.

2.1.3 20X phosphate-buffered saline (PBS)

3 M NaCl, 161 mM Na₂HPO₄ and 39 mM KH₂PO₄. pH was adjusted to 7.4.

2.1.4 50X Tris-acetate-EDTA (TAE)

2 M Tris, 1 M acetate, 1 mM EDTA.

2.2 General Methods

This project capitalizes on an interdisciplinary approach in which different genetically modified mouse strains, Cre-dependent viruses and high-resolution imaging techniques are used and integrated at organ and body scales. The following methods used in this thesis would have been extremely difficult to do without the cooperation with different scientists in our and other labs during my MD/PhD. In particular, I would like to thank Dr. Sen Qiao who supported and guided me in learning all the techniques in our laboratory. Please see the table above for a detailed description of the contribution of individual people to the different experiments.

2.2.1 Mouse models

Animal care and experimental procedures were approved by the Animal Welfare Committee of Saarland University and performed in accordance with their established guidelines. All mice were housed on a typical light/dark cycle with free access to water and food. To label and ablate gonadotropes or chemogenetically activate GnRHR-expressing cells, we used the GnRHR-IRES-CRE (GRIC) knock-in mouse strain (Wen *et al.*, 2008) crossed with enhanced *ROSA26*- τ GFP (*eR26*- τ GFP) (Wen *et al.*, 2011) and *ROSA26*-DTR (*R26*-DTR) (Buch *et al.*, 2005) animals, or with *eROSA26*- τ GFP (*eR26*- τ GFP) and *eROSA26*-DREADD (*eR26*-DREADD) animals. In the resulting GRIC/*eR26*- τ GFP/*R26*-DTR and GRIC/*eR26*- τ GFP/*eR26*-DREADD mice, Cre recombinase is bicistronically expressed under the control of the *GnRHR* promoter. In these animals, Cre-mediated recombination results in the removal of a strong transcriptional stop cassette from the *ROSA26* locus and subsequent constitutive expression of τ GFP (GRIC/*eR26*- τ GFP) exclusively in GnRHR cells. All mice are on a mixed 129 \times C57BL/6 genetic background. Importantly, this binary genetic approach allows for unbiased sampling of the gonadotrope population because, after initial Cre-mediated recombination, the expression of the fluorescent reporter is independent of the heavily regulated *GnRHR* promoter.

The GRIC/*eR26*- τ GFP/*R26*-DTR mouse line expresses the DTR specifically in GnRHR cells, enabling us to selectively ablate gonadotropes upon DT injection. For ablation experiments, 8-10 weeks old females or 14-16 weeks old males were intraperitoneally injected with 20 ng/g bodyweight DT (322326, EMD Millipore) twice with a 3-day interval between injections. Injecting the mice with DT after they had already reached adulthood and had therefore already undergone normal reproductive development, allowed us to focus on the function of gonadotropes specifically in adults.

The GRIC/*eR26*- τ GFP/*eR26*-DREADD mice express DREADD (Designer Receptor Exclusively Activated by Designer Drugs) specifically in GnRHR cells. We used Gq-coupled DREADD in this study, as GnRHR signaling normally occurs through the Gq protein. This mouse line enables us to chronically activate gonadotropes in adults upon administration of Clozapine N-Oxide dihydrochloride (CNO) drug. 2.5 mg of CNO (CNO, 6329, Tocris Bioscience) in 200 ml of drinking water were administered to the mice while kept on a high fat diet.

2.2.2 Generation of the Rosa26-NLSiRFP720-2A-Gq (DREADD) knock-in mice

The DREADD mouse line was generated by homologous recombination in mouse embryonic stem (ES) cells using a targeting construct designed to insert a CAGS promoter (CMV enhancer plus chicken β -actin promoter)-driven NLSiRFP720-2A-Gq receptor (DREADD receptor) within the first intron of the *Rosa26*. This encodes both a red fluorescent protein which is directed to the nucleus and a Gq receptor which can be specifically activated by CNO administration. To ensure that this expression is Cre-dependent, floxed strong transcriptional stop signals (three SV40 polyA signals) are present in such a way that the CAGS promoter can only drive expression following Cre-dependent removal of the stop signals. Correct insertion of the NLSiRFP720-2A-Gq receptor construct was verified using Southern blot analysis as follows. DNA was extracted from tail tip biopsies using lysis buffer containing 0.1 mg mL⁻¹ proteinase K (1 mg mL⁻¹ was used for extraction from ES cells). Following extraction, genomic DNA was digested overnight with EcoRI and run on a 0.7% agarose gel, then transferred to a nylon membrane by capillary transfer and screened by hybridization of a 491 bp 32P-labeled probe complementary to sequences located 5' to the 5' homology arm of the targeting construct. Probe hybridization produces a 15.6 kb band from the wild-type allele, whereas the correctly targeted allele generates a 5.8 kb band. Correctly targeted ES cells were injected into C57BL/6J blastocysts to generate male chimeras that were backcrossed to C57BL/6J females to produce heterozygous Rosa26-NLSiRFP720-2A-Gq mice. Mice were then further crossed to produce a homozygous colony. Homozygous Rosa26-NLSiRFP720-2A-Gq mice were crossed with appropriate Cre-expressing lines to generate offspring in which specific cell populations can be activated by CNO. Mice were maintained on a mixed genetic background of 129S \times C57BL/6J. The genotypes of the Rosa26-NLSiRFP720-2A-Gq mice were confirmed by PCR using the primer sequences: 5-GGAAGCACTTGCTCTCCCAAAG-3' (common forward primer); 5'-GGGCGTACTTGGCATATGATACAC-3' (DREADD allele reverse primer) and 5'-CTTTAAGCCTGCCAGAAGACTC-3' (wildtype allele reverse primer). Wild-type offspring were confirmed by the presence of a single band of 256 bp. For the Rosa26-NLSiRFP720-2A-Gq allele, heterozygous offspring gave two products of 256 and 495 bp, whereas homozygous offspring was identified by the presence of one band at 495 bp (Figure 15). This knock-in mouse line was generated in our lab by Amanda Wyatt.

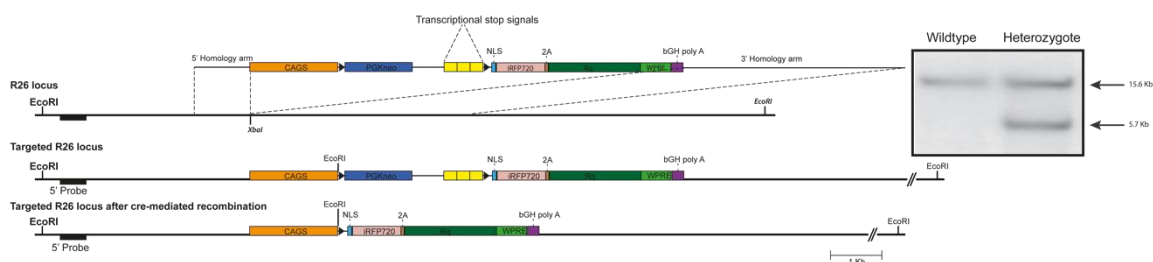


Figure 15: The Rosa26-NLSiRFP720-2A-Gq (DREADD) knock-in mouse line. The targeting strategy used to express a Cre-dependent DREADD allele in the *ROSA26* locus under the control of CAGS is depicted in this

diagram. After digestion with *EcoRI*, Southern blot analysis of genomic DNA from a wildtype and a heterozygous mutant mouse.

2.2.3 Genotyping

Routine genotyping was performed by technical staff within the laboratory. Crude genomic DNA was extracted from biopsies using 100 μ l of ear lysis buffer containing 100 μ g/ml proteinase K by incubating at 55°C overnight under agitation. After incubation, 1 μ l of extracted DNA was combined with 6.25 μ l of MyTaq HS Red Mix (Boline (BIO-25047)), 2 μ M each of the appropriate primers (see Table 2) and dH₂O to a total volume of 12.5 μ l. The samples were then placed in a Bio-Rad T100 thermal cycler and the appropriate program initiated. After amplification of the target gene, a 2% agarose/TAE gel was prepared with the addition of 4 μ l of ethidium bromide per 100 ml of agarose/TAE. Each sample was loaded into separate wells alongside a molecular weight ladder (HyperLadder 100 bp, Boline) and run at 130 V for 45 minutes. Bands were visualized using a Herolab E.A.S.Y Doc Plus gel documentation system.

2.2.4 Tissue preparation and histology

2.2.4.1 Vaginal cytology

Vaginal smears were taken and examined. Briefly, ~50 μ l of saline were used to wash out the vagina and the resulting sample was taken for cytological analysis. The proportion of nucleated epithelial cells, nucleated cornified cells, and leukocytes was used to determine the stage of the estrus cycle. This was performed daily, at the same time, for four weeks in the GRIC/ROSA26-DREADD mouse line after gonadotrope activation (Figure 16).

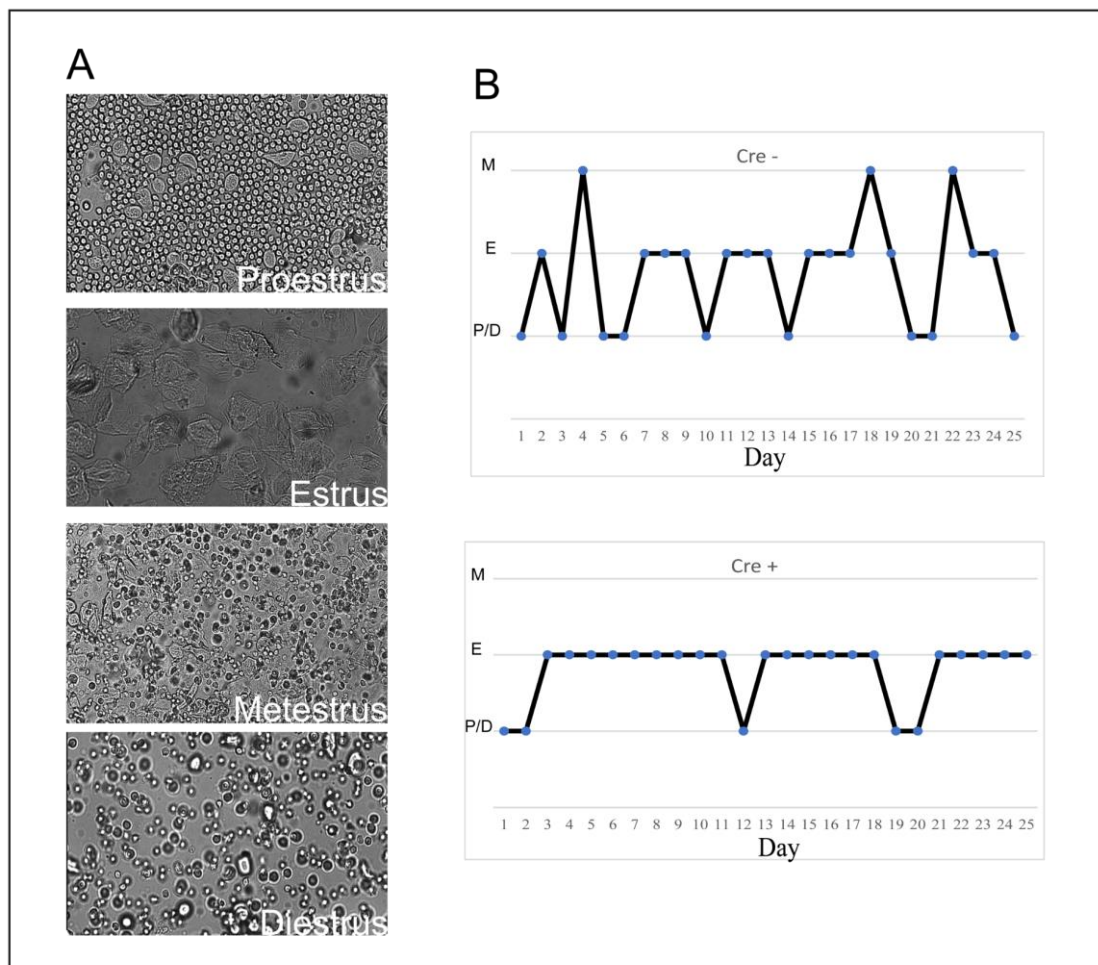


Figure 16: Estrous cycle in GRIC/eR26-DREADD mice. (A) The estrous cycle stage in mice was determined by vaginal cytology. Proestrus stage (1), mainly round and nucleated cells. Estrus stage (2), mainly cornified cells. Metestrus (3), a mix of nucleated, cornified cells and small leukocytes. Diestrus (4), mainly small leukocytes and nucleated cells. (B) Estrous cycle stage of two individual female mice. Cre+, an experimental mouse after being treated with CNO for 4 weeks. The Cre- control mouse was treated with water. M, metestrus; E, estrus; P, proestrus; D, diestrus.

2.2.4.2 Ovariectomy and hormone supplementation

Unless otherwise stated, females were ovariectomized in adulthood (8-12 weeks old female mice) under general anesthesia, which was performed after administration of 5% isoflurane. After the respiratory rate slowed, the mouse was removed from the desiccator and placed on a surgical board. The mouse continued to receive 2% isoflurane during the procedure. The region to be operated was sterilized, and ovaries were typically approached by two separate flank skin incisions measuring approximately 5 mm. The skin was separated from the underlying muscle before incising the muscle. A sharp scissor was inserted just through the muscle layer to separate the muscle fibers by opening the scissors in a dorso-ventral direction. The ovary was gently pulled through the incision with blunt forceps by grasping the fat pad surrounding it. A micro cross-action bulldog clamp was placed at the boundary between the ovary and oviduct, a ligature was placed just below the clamp and a cut was made just above the clamp. After that, the fat tissue and the oviduct were returned into the abdominal cavity. Muscle and skin layers

were closed with surgical sutures. At the same time, all females received a 2 cm-long silastic capsule (inner diameter: 1.57 mm; outer diameter: 3.18 mm) containing 17 β -estradiol dissolved in sesame oil (36 μ g 17 β -estradiol/mL sesame oil) (Ingberg, Theodorsson, Theodorsson & Strom, 2012) subcutaneously in the neck. The subcutaneous silastic capsules are convenient and produce the most stable serum concentrations (Ingberg, Theodorsson, Theodorsson & Strom, 2012). The dose of 17 β -estradiol/ml (E2758, sigma) was based on a previous study showing that this treatment leads to estradiol levels similar to mice in estrus (Ingberg, Theodorsson, Theodorsson & Strom, 2012).

2.2.4.3 Castration and hormone supplementation

Males were castrated in adulthood (14-16 weeks old male mice) under general anesthesia, which was performed after administration of 5% isoflurane. After the respiratory rate slowed, the mouse was removed from the desiccator and placed on a surgical board. The mouse continued to receive 2% isoflurane during the procedure. After sterilizing the caudal abdomen, testes were approached by a single midline incision on the scrotal sac. Skin was separated from the muscle layer, then a similar sagittal incision was made through the muscle. Both testes were reached through the same incision. The testicular fat pad on the inside was pulled through the incision using blunt forceps. Then a cross-action bulldog clamp was placed below the testes and testes were removed with scissors. After that, the fat tissue was returned into the abdominal cavity. Muscle and skin layers were closed with a surgical suture. At the same time, all males received a 2-cm-long silastic capsule (inner diameter: 1.57 mm; outer diameter: 3.18 mm) containing 100% testosterone (T1500, Sigma) subcutaneously in the neck.

2.2.4.4 Diets

8-11 weeks old female mice were randomly selected in two groups for receiving high fat diet (HFD; 60 kJ % fat (Lard) and 34% cholesterol [E15742347; SSNIFF SPEZIALDIATEN]) for five weeks. Daily, at 2:00 pm, the two groups were intraperitoneally injected with either FSH (GONAL-f, Merck) solution having a concentration of approximately 30 IU/kg bodyweight, or with 0.9% NaCl. Body weight was measured weekly.

2.2.4.5 Insulin Tolerance Tests (ITT)

Mice were tested 3 weeks after treatment with estradiol and testosterone. For the intraperitoneal insulin tolerance test (ipITT), mice were placed in an empty cage with water and fasted for 6 hours during the day. Mice were intraperitoneally injected with 1g/kg (0.5 U/Kg body weight, dissolved in sterile physiological saline) insulin (883732, Pharma Gerke Arzneimittelvertriebs GmbH). The exact injection volume was estimated based on each mouse's body weight. Blood glucose levels were determined from the tail vein using the OneTouch Ultra Digital Glucometer (Accu-Check performa) per manufacturer's instructions. After intraperitoneal injection, blood glucose levels were measured at 0 (basal level before injection) and at 30, 60 and 90 minutes.

2.2.4.6 Glucose Tolerance Tests (GTT)

For the intraperitoneal glucose tolerance test (ipGTT), mice were placed in an empty cage with water and fasted for 16 hours. Mice were intraperitoneally injected with 1g/kg (0.5 U/Kg body weight, dissolved in sterile physiological saline) Glucose (20% D- (+) -Glucose; Sigma Aldrich). The volume of the injection was estimated based on the individual mouse's body weight. According to the manufacturer's recommendations, blood glucose levels were taken from the tail vein using the OneTouch Ultra Digital Glucometer (Accu-Check performa). After intraperitoneal injection, blood glucose levels were measured at 0 (basal level before injection) and at 30, 60, 90 and 120 minutes.

2.2.4.7 Transcardial Perfusion

Mice were anesthetized using ketamine and xylazine (solution of 10 ml sterile 0,9% NaCl and 2.8 ml of ketamin and 2.8 ml of xylazine). Once under general anesthesia, the thoracic cavity was exposed and an incision was made in the right atrium. Then, approximately 600 µl of blood were removed from the heart and transferred to EDTA. 20 ml of room temperature PBS was injected into the left ventricle. After this, 40 ml of ice-cold 4% paraformaldehyde (PFA) were injected into the left ventricle. Tissues were then dissected and post-fixed in 4% PFA. Liver, kidney, pituitary, and fat tissue were then transferred to 30% sucrose overnight at 4°C. The protocol was performed as previously described (Hellier *et al.*, 2018).

2.2.4.8 OCT Embedding and Cryosectioning

Fixed tissue was embedded in optimal cutting temperature compound (OCT, Leica Microsystem). A glass box was partially immersed in a bath of ethanol and dry ice. After that, the glass box was filled partially with isopentane (2-methylbutane). The tissue was frozen quickly in isopentane after being inserted in a plastic cuvette filled with tissue freezing media. The embedded samples were then stored at -80°C. For subsequent cryosectioning tissues were cut in 14 µm serial sections using a Leica cryostat.

2.2.4.9 Hematoxylin and Eosin (H & E)

Slides were washed three times with ddH₂O and then incubated for 10 minutes with 0.1% Mayer's Hematoxylin (Sigma; MHS -16) in a 50 ml conical tube. They were then rinsed with tap water for six minutes, incubated for five minutes with 0.5% eosin and dehydrated through an alcohol gradient (50%, 70%, 95%, 100%) followed by xylene. Slides were then covered with a coverslip with DePex (18243; SERVA).

2.2.4.10 Immunohistochemistry (IHC)

Immunohistochemistry was performed as previously described (Hellier *et al.*, 2018). The appropriate protocol was selected based on the level of sensitivity required in order to detect a particular protein. Slides were removed from -80°C and left for 15 minutes to allow the samples to reach room temperature.

A hydrophobic barrier was applied to the slide's edges using a PAP pen. The slides were then washed three times with PBS for 10 minutes, followed by a 1.5-hour incubation with blocking buffer (0.1 M PBS containing 5% normal donkey serum, 0.2% Triton X-100, and 0.02% sodium acid). After that, slides were incubated with the appropriate primary antiserum solution in the following concentrations: rabbit anti-LH (1:5000; National Institute of Diabetes and Digestive and Kidney Diseases [NIDDK]), guinea pig anti-FSH (1:5000; [NIDDK]), rabbit anti-cFos (1:500; 2250, Cell signaling Technology), mouse anti-ACTH (1:10000; [NIDDK]), chicken anti-GFP (1:1000; A10262 ThermoFisher) after covering the pituitary with parafilm over two nights at 4°C in a humidified chamber. After this incubation, the slides were washed three times with PBS for 5 minutes. Then, an appropriate secondary antiserum from the following list was diluted in blocking buffer and applied to the slides for two hours: goat anti-rabbit Cy3 (1:500; Invitrogen), goat anti-guinea pig Cy5 pig (1:500; Invitrogen) and goat anti-chicken Alexa Fluor 488 (1:500; Invitrogen). The slides were then washed three times in PBS for 5 minutes. For nuclear staining, sections were incubated with 5 µg/mL Hoechst 33258 dye (Sigma) in 0.1 M PBS solution for 10 minutes. Slides were then washed three times with PBS for 5 minutes at room temperature. Slides were then covered with a coverslip with Fluoromount-G (Southern Biotech).

2.2.4.11 Oil Red O

Oil red O is used to stain neural triglycerides and lipids on cryosections. First, slides were taken from -80°C and allowed to reach room temperature for 30 minutes. 300 mg Oil Red O (ORO, O0625-100G, Sigma) were dissolved in 100 ml 100% isopropanol as a stock. The slides were washed in 60% (v/v) isopropanol for 10 minutes. After washing, slides were incubated with ORO solution (7:5 140 ml ORO stock mix with 100 ml dH₂O) for another 10 minutes. The slides were then washed in 60% isopropanol twice for three minutes. During the first washing step, the slides were placed on a shaker with a speed of 50 rpm (Edmund Buehler). The section was then washed in dH₂O twice for one minute each. Slides were then covered with Fluoromount-G (SouthernBiotech) and coverslipped. For visualization, slides were scanned using a Zeiss Axio Scan.Z1. We noticed that the ORO signals were not evenly distributed within the sections. Therefore at least three complete sections per mouse liver were stained and the ORO units (ORO area/tissue area * 100) were calculated by Image J as previously described (Mehlem, Hagberg, Muhl, Eriksson & Falkevall, 2013).

2.2.5 Microscopy

Epifluorescence photomicrographs were taken using either a Zeiss Axioskop2 equipped with the Zeiss AxioVision software or a Zeiss Axio Scan.Z1 equipped with the Zeiss Zen 2 software. Confocal microscopy was performed with either a Zeiss LSM 710 or a Zeiss ELYRA PS.1 combined with an LSM 780 and equipped with Zeiss Zen software. For Z-stack images, 0.3 µm optical sections with the pinhole adjusted to one airy unit were taken using a 20X objective.

2.2.6 Molecular biology techniques

2.2.6.1 RNA purification

To analyze *Fshr* expression in different tissues, total RNA was purified using the RNeasy Plus Micro kit (Qiagen) according to the manufacturer's instructions. Purified RNA was stored at -80°C until further use.

2.2.6.2 Real-time quantitative PCR (qPCR) and reverse transcription

Real-time PCR was performed using the SensiFAST SYBR No-ROX one-step kit (Bioline) with a CFX-96 real-time PCR detection system (Bio-Rad Laboratories) as described previously (Qiao *et al.*, 2016). For reverse transcription PCR, genomic DNA removal and cDNA synthesis were performed using a maximum H Minus First Strand cDNA-Synthesis kit (Thermo Fisher). PCR was performed using MYTaq Red Mix kit (Bioline). The reaction conditions were as follows: 10 minutes at 45°C, followed by 2 minutes at 95°C and then 40 cycles of 5 seconds at 95°C and 20 seconds at 60°C. β -actin was used as an endogenous control. Quantified results represent the fold induction of target gene expression using the $-2\Delta\Delta$ -cycle threshold method (Livak & Schmittgen, 2001). No-template control (reagent alone without template) was included in each assay to detect possible contamination of the PCR reagents.

2.2.6.3 ELISA (corticosterone)

The enzyme-linked immunosorbent assay (ELISA) is an immunological, plate-based assay used for detecting and quantifying the presence of a specific protein in a complex mixture. Blood was harvested from hearts of euthanized mice and collected in EDTA-coated microvette tubes on ice. Plasma was obtained after centrifugation at 2,000 g for 15 minutes at 4°C. An enzyme immunoassay kit was used to measure plasma corticosterone levels (corticosterone, Arbor Assays, Ann Arbor, MI; FSH, Enzo Life Sciences Farmingdale, NY) according to the manufacturer's instructions.

2.2.6.4 Luminex Assay

Pituitary hormone measurements were performed with a Milliplex MAP mice pituitary magnetic bead panel (RPTMAG-86K; Millipore, Billerica, MA) on a Luminex Magpix (Austin, TX) with Milliplex Analyst software according to the manufacturer's protocol.

2.2.7 Gene expression analysis

2.2.7.1 RNAscope *in situ* hybridization

Detection of *Fshr* mRNA was undertaken in the pituitary, liver and ovary from adult female mice using RNAscope 2.5 High-definition Assay-RED (Advanced Cell Diagnostics, Hayward, CA), according to manufacturer's instruction and as previously described (Aoki *et al.*, 2019). The *Fshr* probe was designed to target transcript NM_013523.3 which has a target sequence that spans nucleotides 554 to 1487. Probes targeting the DapB gene from *Bacillus subtilis* were used as a negative control. In brief, the activity of

endogenous peroxidase was inhibited using RNAscope hydrogen peroxide solution. Tissues were permeabilized with RNAscope protease plus. The *Fshr* or the negative control probe were then used to hybridize the sections. Following that, a series of amplification incubation steps was performed. Finally, the hybridization signals were detected using detection reagents. Bisbenzimidazole was used to stain the nuclei. A Zeiss Axio Scan Z1 was used to capture the images. The RNAscope scoring parameters from Advanced Cell Diagnostics were used to determine positive hybridization. To determine the colocalization of *Fshr* mRNA and ACTH, immunolabeling of ACTH was performed on the same pituitary sections after RNAscope *in situ* hybridization.

2.2.7.2 *In vitro* pituitary assay

Intact pituitaries were removed from adult females at diestrus and incubated with 1 ml DMEM in a 12-well-plate at 37°C, 5% CO₂ with constant shaking for 1 hour. After resting, pituitaries were incubated with new 1 ml DMEM with either mouse monoclonal anti-FSH antibody (10 µg/ml; MIF2709, Invitrogen) or mouse IgG (10 µg/ml; MAB002, R&D Systems) for 1 hour. 50 µl of culture medium were measured as the 0-time point. Then pituitaries were stimulated with 100 nM GnRH (L7134, Sigma-Aldrich). 50 µl of culture medium were removed at 30, 60, and 90 minutes, respectively separately.

2.2.7.3 Cloning and guideRNA selection

Potential guideRNA (gRNA) sequences for the *Fshr* gene were identified using Chopchop (Labun *et al.*, 2019). From the identified gRNAs, an optimal sequence was selected to have the lowest possibility of off-target events whilst having a high predicted efficiency and frameshift likelihood at the targeting site after analysis with Cas-OFFinder (Bae, Park & Kim, 2014) and CRISPOR (Concordet & Haeussler, 2018). The following gRNA was selected for targeting; *Fshr*: 5'-GAGATTTGTGCTCACCAAGCT. This gRNA was generated as a primer dimer and then independently cloned into pX601-AAV-CMV (a gift from Feng Zang (Makarova *et al.*, 2015); Addgene plasmid #61591) using the *BsaI* sites present within this plasmid. This inserted the gRNA sequence subsequent to a U6 promoter and immediately upstream of the gRNA scaffold sequence required for correct interaction with the Cas9 protein. The saCas9 sequence was also present within this plasmid under the control of the strong CMV enhancer and promoter. Following cloning, all elements were verified by sequencing of the entire region contained between the 2 ITR sites. For the production of a control virus, the unmodified pX601-AAV-CMV plasmid without gRNA was used.

2.2.7.4 AVV (Adeno-associated virus) vector production

Both the gRNA and control viruses were produced using the triple transfection helper-free method. This involved transfecting HEK293T cells in culture with 3 plasmids in a 1:1:1 ratio, the first containing essential viral genes such as E2 and E4 (pAdDeltaF6 was a gift from James M. Wilson; Addgene plasmid # 112867), the second which facilitates the generation of serotype 5 AAV vectors (pAAV2/5 was a gift

from Melina Fan; Addgene plasmid # 104964) and the third, which dictates the packaged contents of the virus particles, as previously described. Cells were transfected when they reached 60-70% confluency using a 4:1 (v:w) ratio of polyethylenimine (PEI) to plasmid DNA. 60-72 hours after transfection, cells were pelleted and processed to recover the virus. Virus samples were then subjected to purification through an iodixanol gradient before desalting and concentrating using a centrifugal filter (MWCO 100). Viral titer was detected by qPCR analysis with primers specific to the ITR region of the packaging plasmid (fwd ITR primer: 5'-GGAACCCCTAGTGATGGAGTT, rev ITR primer: 5'-CGGCCTCAGTGAGCGA). Both of the gRNA and control viruses were generated in our lab by Amanda Wyatt, and Vanessa Wahl.

2.2.7.5 Stereotaxic injection

The stereotaxic injection was performed as previously described (Hellier *et al.*, 2018). Mice were anesthetized with 5% isoflurane and placed in a motorized stereotaxic frame (Neurostar, Germany). A midline scalp incision revealed the skull, and the stereotaxic frame was positioned at Bregma using visual markers. After the mouse head was aligned, a drill was put above the skull at coordinates corresponding to the pituitary, and a hole was drilled through the skull bone to reveal the brain (according to the Paxinos Brain Atlas). A 33-gauge steel needle loaded with 2 μ l of AAV virus (AAV5-saCas9-*Fshr* or AAV5-saCas9) was slowly inserted through the anterior pituitary (six injections with 0.5 μ l per injection) until it penetrated to a depth of 5.8-6 mm (coordinates were -2.55 mm, -2.7 mm and -2.95 mm antero-posterior, \pm 0.6 mm lateral to the midline, 300 μ m above the sella turca). Using a syringe pump (Harvard Apparatus), the virus (2 μ l per brain injection site) was delivered at 100 nl min⁻¹ through a Hamilton syringe. Before being slowly removed, the needle was kept for another 10 minutes in place to allow diffusion of the virus. The hole was closed with dental cement and the skin was sutured after the AAV injection. Mice were given time to heal on a heating pad before being returned to their home cage. For post-operative analgesia, all mice received a subcutaneous injection of Carprofen (5 mg kg⁻¹). Sterotaxic injections were performed by Dr. Sen Qiao and myself.

2.2.7.6 CRISPR efficiency verification

8 weeks after AAV injection, pituitaries were dissected. DNA was extracted from pituitaries and then targeted amplification was performed via PCR with the primers against *Fshr* (primers used in PCR are described in table 5). Amplicons were generated using region-specific primers with the Illumina universal adaptor sequences. PCR products were purified with Agencourt AmpureBeads and indexed in a second PCR using Illumina Truseq adapters. After final AmpureBead purification, amplicons were pooled in an equimolar ratio and sequenced on a Miseq (Illumina) using the Miseq Reagent Kit v2 (500-cycles) in paired-end mode, aiming at 10,000 reads per amplicon. The sequence was then analyzed by CRISPResso2 (Clement *et al.*, 2019).

2.2.8 Microcomputed tomography (μ CT)

Using desktop microcomputed tomography (μ CT), a subset of whole bone samples (whole femur) was assessed (Skyscan 1176, Bruker MicroCT, Kontisch, Belgium). Femora were stored at -80°C . A microfocus X-ray tube with a focal spot of $>9\ \mu\text{m}$ size at 4W was used as a source. The scanner was set at a voltage of 50 kV, a current of 200 μA . The CT images were reconstructed in 4032 x 2688 pixels' matrices using a typical convolution back projection approach with a 0.5 mm aluminum filter. The bone was positioned on a turn table that could be automatically shifted 180° plus half the fan angle on either side in the axial direction to perform the measurement. A total of 2500-2600 microtomographic slices were obtained for each sample, with a slice increment of 9 μm . In order to analyze the parameters of the distal femoral metaphyseal trabecular bone, we used the image reconstruction software (NRecon {version 1.6.10.6}), data analysis software (CTAn {version 1.16.4.1}), orientation software (DataViewer {version 1.5.1.2}) and three-dimensional model visualization software (CTVox {version 3.2.0r 1294}) at the end of the acquisition process. Trabecular bone was analyzed over 200 slices, starting with 50 slices distal from the growth plate. The trabecular bone volume fraction (BV/TV), trabecular thickness (Tb.Th) and trabecular number (Tb.N) were analyzed for trabecular bone. Calcium hydroxyapatite (CaHA) phantoms of known densities were used to evaluate BMD.

2.2.9 Quantification and data analysis

2.2.9.1 Software and data analysis

Zeiss Zen 2 and Image J were used for image processing and analysis of Oil Red O staining. Statistical analysis was performed using GraphPadPrism 5. NRecon 1.6.9.8 was used for bone reconstruction after scanning. DataViewer 1.5.1.2 64-bit enabled us to turn the bone in an identical orientation. CTAn 1.16.4.1 + (64-bit) to define the cortical and trabecular regions for analysis. Figures were generated using the ImageJ plugin "FigureJ" and Adobe Illustrator.

2.2.9.2 Statistics

GraphPad Prism 5 software was used to analyze the data. All data are presented as the mean \pm standard error mean. Statistical significance was determined using unpaired two tailed Student's t-tests for single comparisons (unless otherwise stated). A two-way ANOVA was performed for multiple comparisons followed by Bonferroni's multiple comparison test was used (unless otherwise stated).

Results

3.1 Diphtheria toxin injection efficiently ablates gonadotropes

Gonadotropes integrate different hormonal signals and adapt gonadotropin expression and release depending on the hormonal milieu. Moreover, gonadotropins have been reported to have extra-gonadal functions. To systemically dissect the extra-gonadal gonadotropin actions and uncover potential communication between distinct endocrine cell networks within the pituitary, we acutely ablated gonadotropes in adult mice. To do this, we capitalized on a mouse strain bearing a gonadotrope Cre recombinase and Cre-dependent iDTR (Buch *et al.*, 2005; Wen *et al.*, 2008) and GFP alleles (Wen *et al.*, 2011) (GRIC/R26-iDTR/eR26- τ GFP mice) specifically in the gonadotrope cells. This mouse line enables us to selectively ablate gonadotropes upon diphtheria toxin (DT) injection in adulthood. We injected DT in adult mice that had already undergone normal physiology/reproductive development and could therefore focus on the function of gonadotropes in the adult animal. Either DT or vehicle (saline) were injected intraperitoneally into these mice (20 ng/g of DT injected twice with a 3-day interval in between injections) to ablate GnRHR+ cells (Figure 17A). Immunohistochemical analysis confirmed that the number of gonadotropes was indeed dramatically reduced after two-months post-DT injection when compared to vehicle (Figure 17B-C). Using this approach, we first examined expression of LH and FSH after acute gonadotrope ablation. We found that gonadotropin expression no longer colocalized with GFP and that the LH- or FSH-immunoreactive cells were almost completely segregated from the GFP+ population two months after DT injection (Figure 17B-C). Furthermore, the number of GFP+ cells 2 months after ablation was not significantly different to the number of 10 days in adult male pituitaries (Figure 17B), suggesting that the adult male pituitary gland cannot regenerate the gonadotrope cell population. In contrast, we did find a significant difference in the number of GFP+ cells in adult female pituitaries 2 months after DT injection compared to 10 days after ablation (Figure 17C). Further confirming the efficacy of this approach, acute gonadotrope depletion in adult mice lead to severe hypogonadism in both male and female mice (Figure 17D).

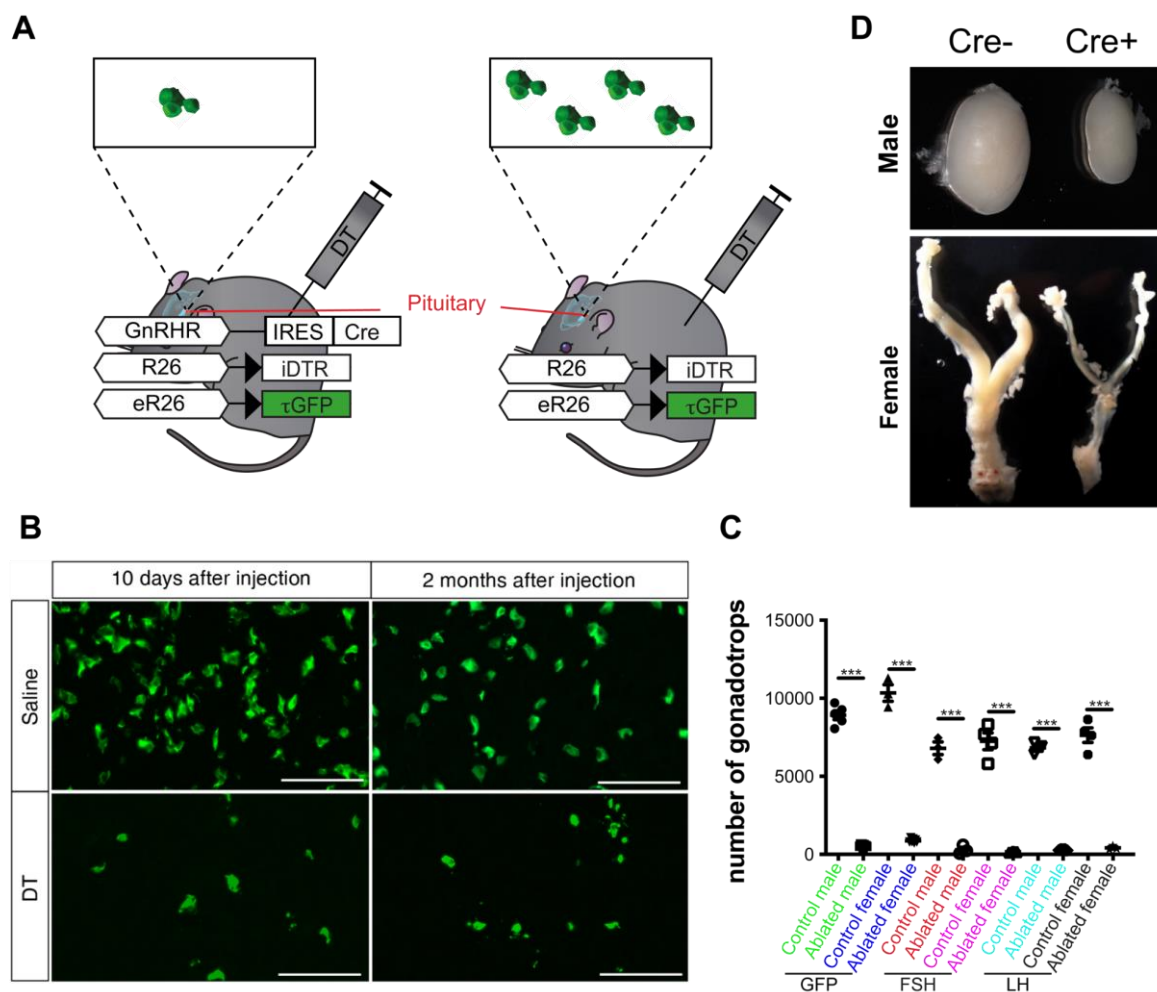


Figure 17: Ablation of gonadotropes results in profound hypogonadism. (A) Illustration depicting the strategy to acutely ablate gonadotropes via the injection of diphtheria toxin (DT) in mice selectively expressing the diphtheria toxin receptor in gonadotropes. (B) GFP-expressing gonadotropes (green) 10 days and 2 months after DT or saline injection of female mice. Scale bars = 100 μ m. (C) Number of GFP+ cells within the pituitaries of DT- or saline-injected GRIC/R26-iDTR/eR26- τ GFP mice and number of follicle-stimulating hormone (FSH) or luteinizing hormone (LH)-positive cells within the pituitaries of DT- or saline injected Cre+ and Cre- (control) GRIC/R26-iDTR/eR26- τ GFP mice. (D) Representative images of testes and female reproductive tracts from Cre+ and Cre- (control) GRIC/R26-iDTR/eR26- τ GFP mice 2 months after DT injection. Error bars represent standard error mean. * = $P < 0.05$, ** = $P < 0.01$ and *** = $P < 0.001$.

3.2 Acute gonadotrope ablation triggers metabolic disorders in a gender-specific manner

Surprisingly, we also found that acute gonadotrope ablation in female mice caused a dramatic increase in body weight (Figure 18A). In particular, some of the female body weights reached 35 g, a weight that normal female mice usually do not attain throughout the entire lifespan. In contrast, in males, the body weight did not show any significant difference compared with controls (Figure 18D-F). Remarkably, acute gonadotrope ablation also triggered impaired glucose tolerance (Figure 18B) and decreased insulin sensitivity (Figure 18C) in female mice, but not in males. This result strongly suggests that gonadotropes regulate metabolic homeostasis in a sex-specific way.

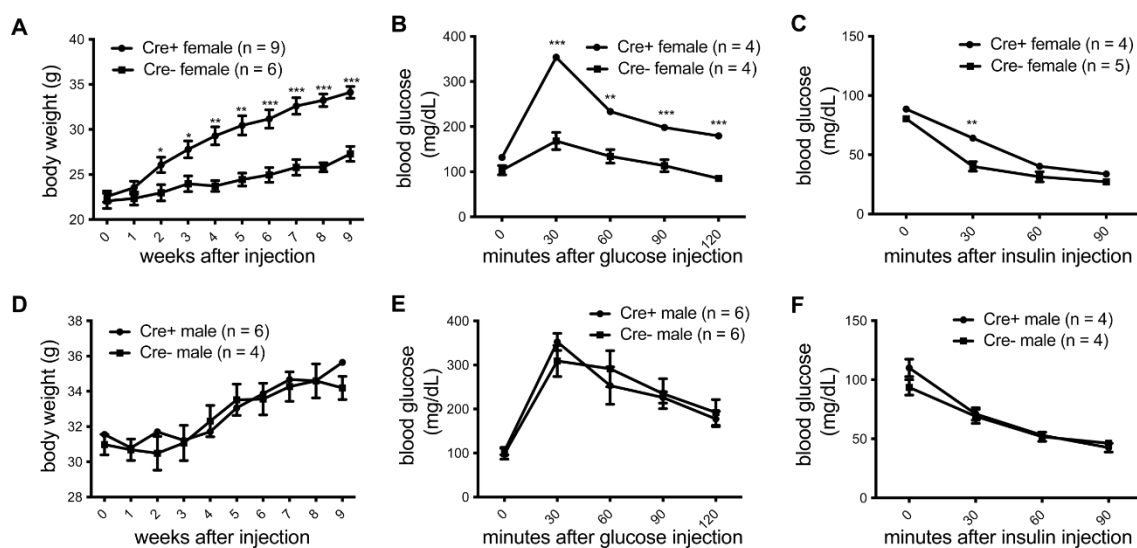


Figure 18: Acute gonadotropes ablation leads to metabolic disorders in female mice. (A, D): Body weight, (B, E): Glucose tolerance test i.p. (GTT) and (C, F): insulin tolerance test i.p. (ITT) from gonadotrope-ablated (Cre+) and control (Cre-) of female and male mice after gonadotrope ablation. Error bars represent standard error mean. * = $P < 0.05$, ** = $P < 0.01$ and *** = $P < 0.001$.

Since NAFLD is a hallmark of the metabolic syndrome (Yki-Jarvinen *et al.*, 2014), we next determined liver histopathology in gonadotrope-ablated mice. We also investigated liver metabolism in these mice by staining the liver sections with Oil Red O (Tata *et al.*, 2018). Surprisingly, both males and females developed fatty liver after gonadotrope ablation (Figure 19A-B). We found hepatic steatosis as early as 10 days after gonadotrope ablation, and this became progressively more severe over time (Figure 19C). There is a clear progression of fatty liver severity when we compared liver histology 10 days and 2 months after ablation (Figure 19C). At 10 days after ablation, female mice developed a steatosis phenotype in the liver and around the liver veins as seen by the accumulation of lipid droplets upon Oil Red O staining. In contrast, 2 months after gonadotrope ablation, the accumulation of lipid droplets had spread throughout the entire liver tissue. Taken together, these data demonstrate that gonadotrope loss recapitulates many of the clinical symptoms of metabolic syndrome in female but only partially in male mice, suggesting sex-specific underlying mechanisms.

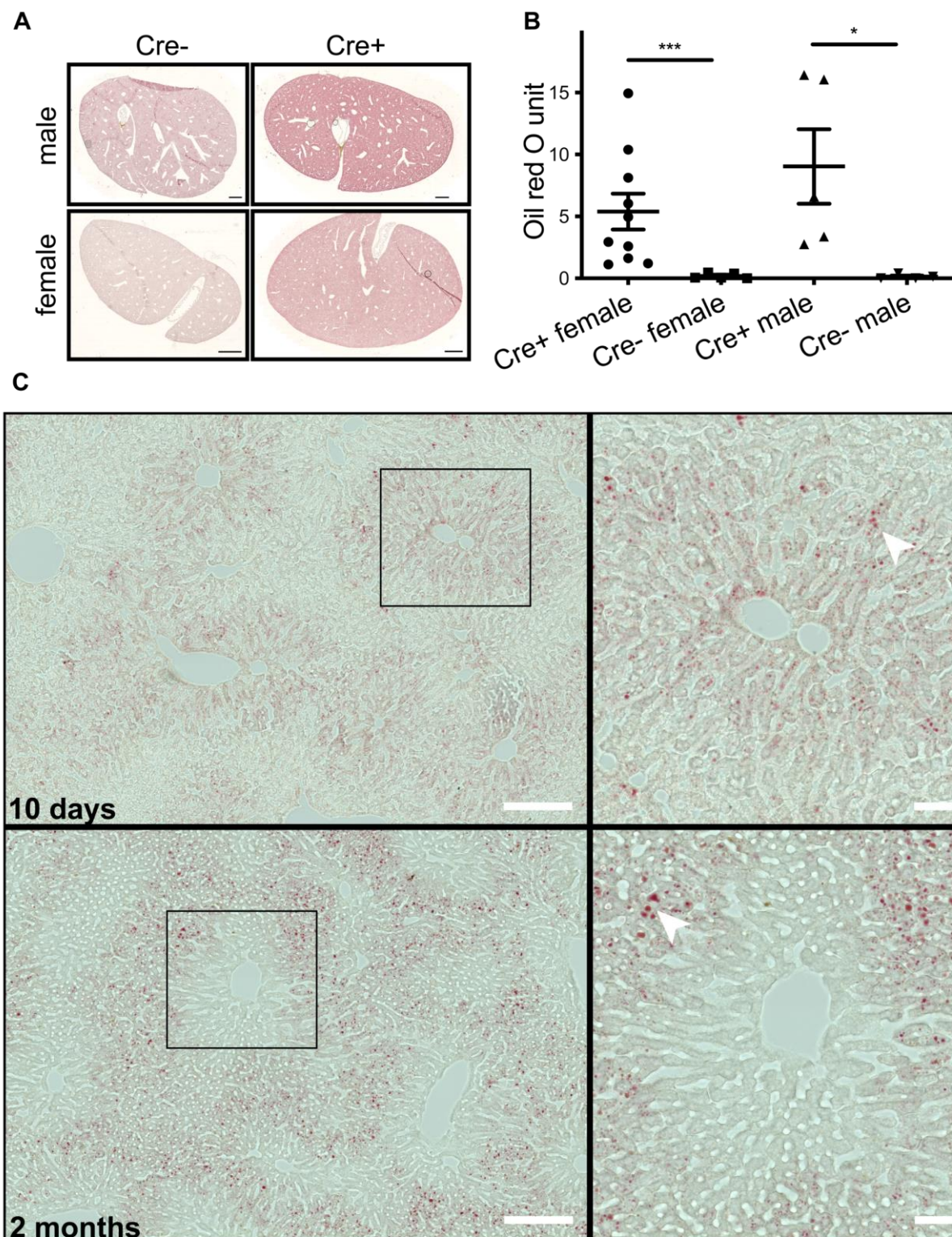


Figure 19: Gonadotrope ablation triggers a fatty liver phenotype in male and female mice. (A) liver oil red O staining, (B) quantification and representative images from gonadotrope-ablated (Cre+) and control (Cre-) female and male mice; (scale bars = 1000 mm). (C) Females develop fatty livers 10 days after acute gonadotrope ablation. Scale bars = 200 μ m in the full-size images and 20 μ m in insets. Error bars represent standard error mean. * = $P < 0.05$, ** = $P < 0.01$ and *** = $P < 0.001$.

3.3 Acute gonadotrope ablation triggers bone loss in both male and female mice

Next, we analyzed bone phenotypes in gonadotrope-ablated mice, as gonadal dysfunction has been associated with bone loss (Mittan *et al.*, 2002) and multiple studies indicated a negative association between metabolic syndrome and bone density (Tegelberg *et al.*, 2019). Strikingly, we found that bone volume, trabecular number, and BMD were significantly reduced (Figure 20A-D), whereas the trabecular separation was significantly increased in femurs of gonadotrope-ablated mice, irrespective of sex.

Taken together, these data demonstrate that acute gonadotrope loss in adults recapitulates major constituents of metabolic syndrome in female and, to a lesser extent, male mice.

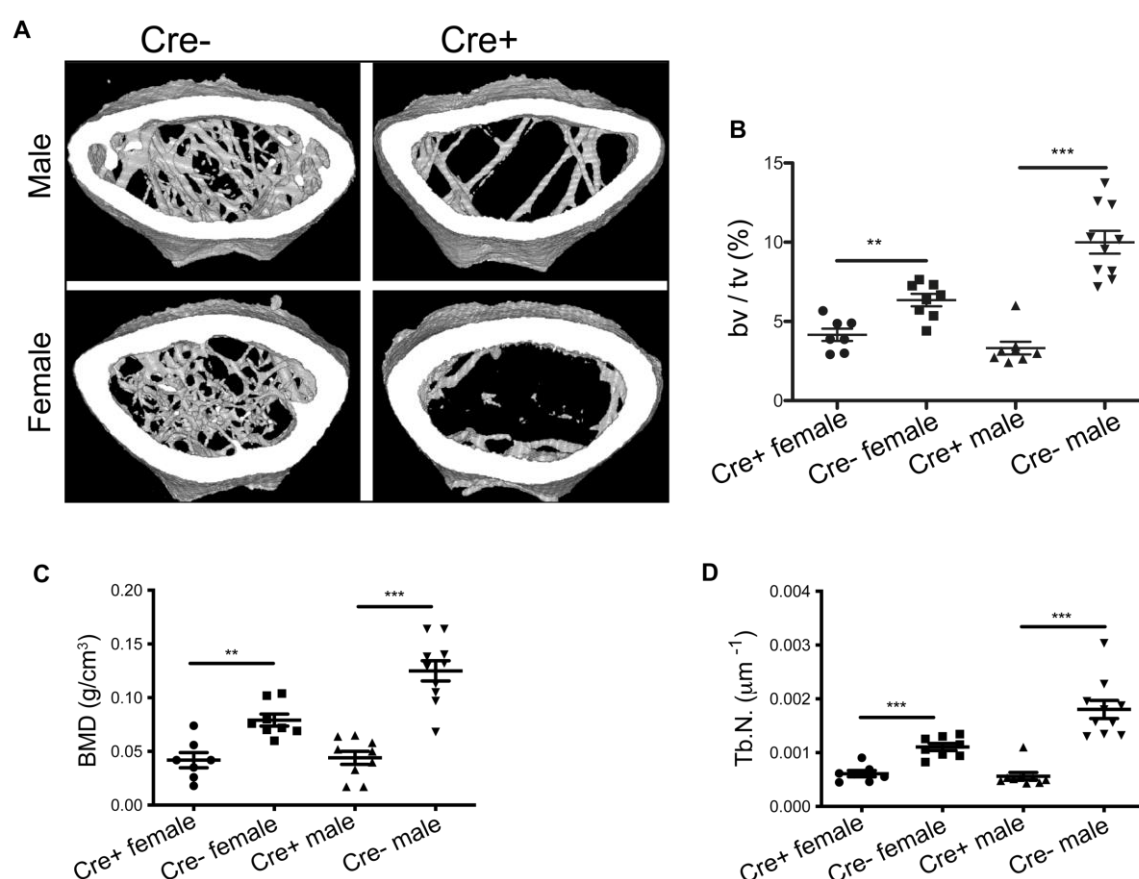


Figure 20: Gonadotrope ablation induces bone loss in male and female mice. (A): Representative microcomputed tomography (μ CT) images of femur GRIC /R26 iDTR mice. (C): Fractional bone volume (BV/TV), (B): Trabecular bone mineral density (BMD). (D): trabecular number of femoral bones from Cre+ and Cre- (control) gonadotrope ablation female and male mice. Error bars represent standard error mean. * = P < 0.05, ** = P < 0.01 and *** = P < 0.001.

3.4 Hepatic steatosis in gonadotrope-ablated females is independent of the gonads, however bone loss is due to gonadal sex steroids

As gonadotropes are classically viewed to regulate the gonads and we showed a profound hypogonadism after gonadotrope ablation, we wondered whether the phenomena that we observed in gonadotrope-

ablated mice could be a direct effect of hypogonadism. To dissect the underlying mechanisms, we sought to determine which phenotypes are mediated through disrupted gonadal function by performing a gonadectomy one week prior to DT injection in Cre⁺ and Cre⁻ mice.

We found that ovariectomy alone was sufficient to trigger weight gain (Figure 21A) and decrease insulin sensitivity (Figure 21C) similar to that of ovariectomized gonadotrope-ablated mice. Conversely, ovariectomized gonadotrope-ablated mice presented with significantly impaired glucose tolerance (Figure 21B) and severe hepatic steatosis in comparison with ovariectomy alone. Most notably, in the absence of gonadotrope ablation (Cre⁻), hepatic steatosis was virtually absent in ovariectomized mice (Figure 22A-B). These data demonstrate that the maintenance of systemic glucose homeostasis and hepatic lipid metabolism depend on the HPG-axis but are independent of ovarian function.

In males, no significant differences were found throughout the metabolic parameters measured including body weight (Figure 21D), insulin sensitivity (Figure 21F) and glucose tolerance (Figure 21E) between the Cre⁺ and Cre⁻ mice after DT injection. However, both gonadectomized and gonadectomized gonadotrope-ablated male mice developed hepatic steatosis (Figure 22A-B) indicating that, in contrast to females, fatty liver in males is triggered by testicular dysfunction and revealing an additional sexually dimorphic effect of gonadotrope ablation on metabolism. With regard to bone loss, gonadectomy alone was sufficient to trigger this phenotype in both sexes (Figure 23A-D), demonstrating that bone loss is mediated by gonadal dysfunction. Taken together, our results suggest that gonadotropes regulate liver steatosis through the classic HPG-axis.

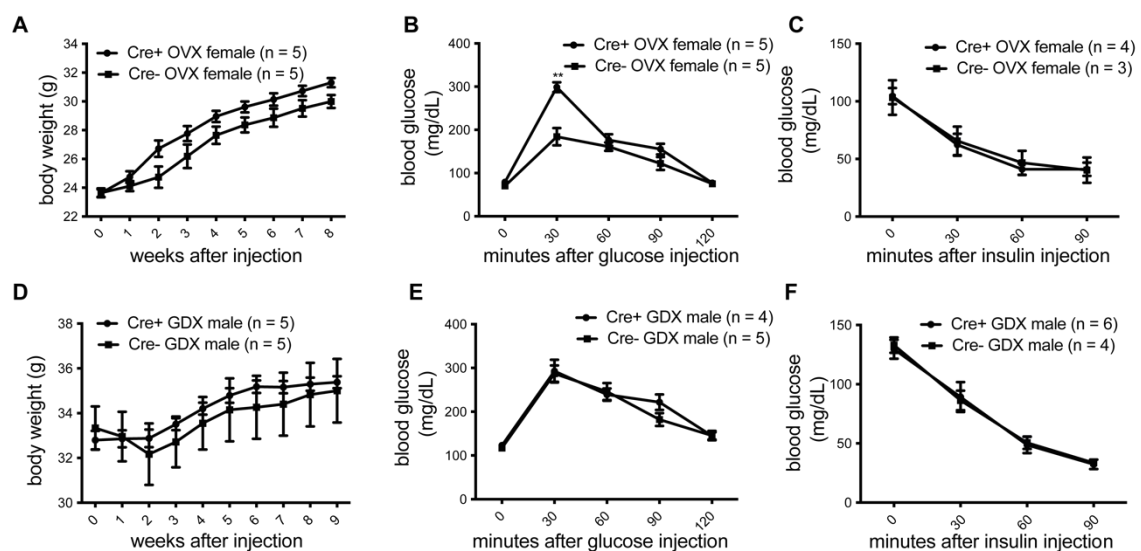


Figure 21: Gonadal loss mimics metabolic syndrome in female mice. (A, D) Body weight, (B, E) glucose tolerance and (C, F) insulin tolerance of Cre⁺ and Cre⁻ (control) gonadectomized female and male mice. Error bars represent standard error mean. * = $P < 0.05$, ** = $P < 0.01$ and *** = $P < 0.001$.

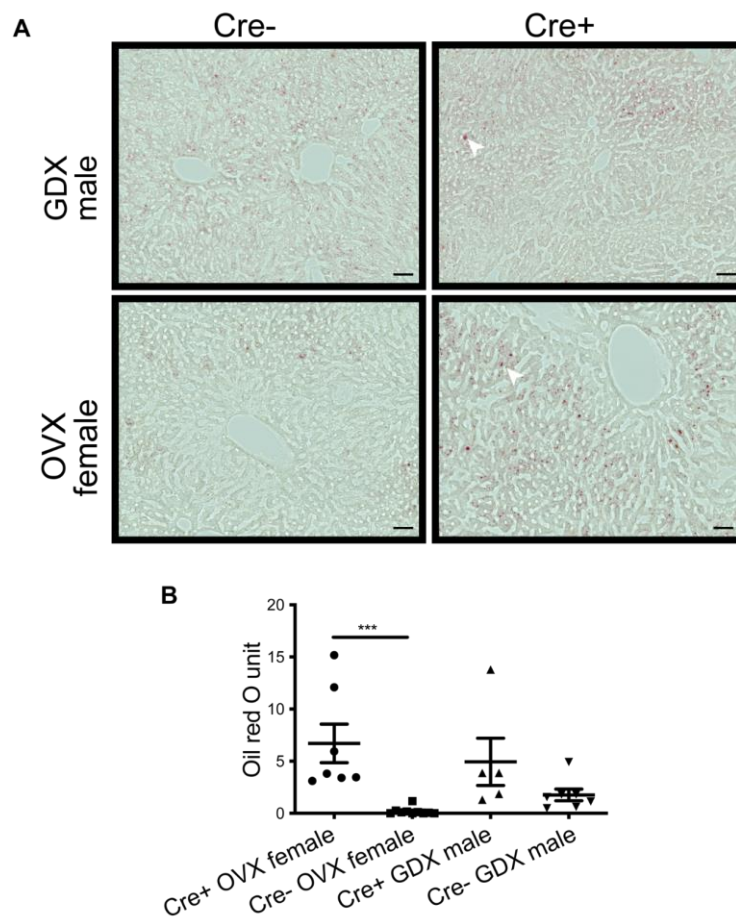


Figure 22: Gonadotrope dysfunction triggers hepatic steatosis independently of the gonads in females. (A) Liver ORO staining quantification and (B) representative images of Cre+ and Cre- (control) in gonadotrope-ablated (Cre+) and control (Cre-) ovariectomized (OVX) female and gonadectomized (GDX) male mice, scale bars = 50 μ m. Error bars represent standard error mean. * = $P < 0.05$, ** = $P < 0.01$ and *** = $P < 0.001$.

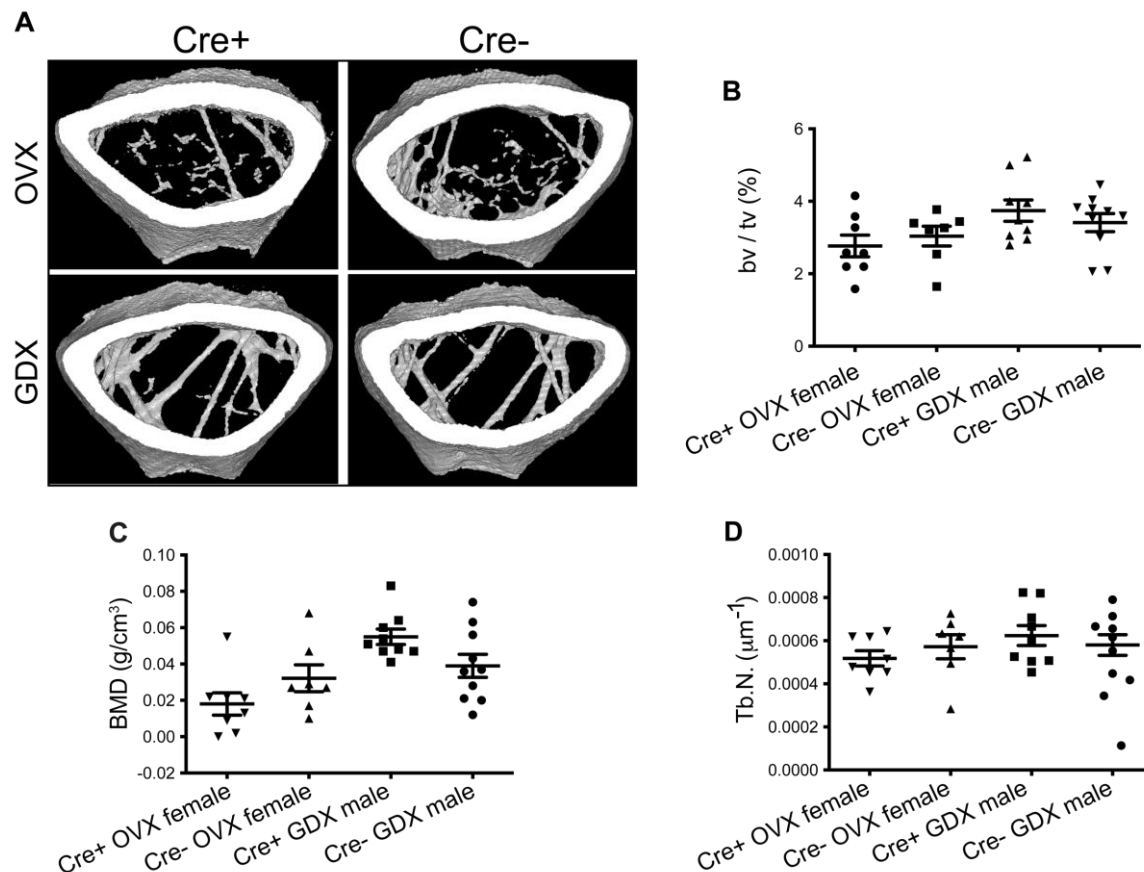


Figure 23: Gonadal loss induces bone loss in male and female mice. (A) Representative microcomputed tomography (μ CT) images of femur of Cre+ and Cre- (control) in gonadotrope-ablated (Cre+) and control (Cre-) ovariectomized (OVX) female and gonadectomized (GDX) male mice. (B) Trabecular fractional bone volume, (C) Bone mineral density and (D) trabecular number of trabecular bones from Cre+ and Cre- (control) gonadectomized female and male mice.

3.5 Sex-steroid replacement abolishes metabolic disorders but does not improve hepatic steatosis

Despite the fact that the gonads are well known for the production of testosterone and estradiol in males and females, respectively, these are not the only hormones and secreted factors produced by them. To determine whether the phenotypes observed in gonadectomized mice were due to the loss of sex steroids or perhaps other substances released by the gonads, we performed gonadectomy together with sex steroid replacement -estradiol for females and testosterone for males- followed by gonadotrope ablation in these mice. The replacement of sex steroids abolished differences in glucose tolerance (Figure 24B, E), insulin sensitivity (Figure 24C, F), weight gain (Figure 24A, D), and bone density (Figure 26A-D) in gonadectomized mice regardless of sex or whether gonadotropes were ablated. Sex steroid replacement also prevented hepatic steatosis in males but contrastingly, had no effect in female mice (Figure 25A, B). These data demonstrate that the majority of cardinal features of metabolic syndrome can be precipitated by the absence of sex steroids originating from the gonads, however liver steatosis

uniquely in females is independent of sex steroids and gonads but rather dependent on pituitary gonadotropes.

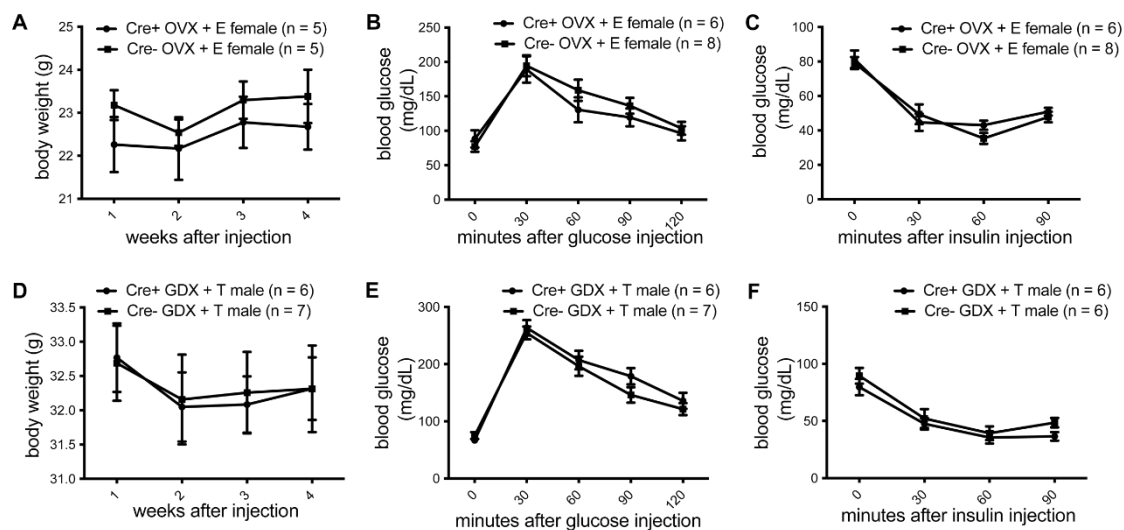


Figure 24: Replacement of sex steroids eliminates metabolic abnormalities. (A, D) Body weight, (B, E) glucose tolerance and (C, F) insulin tolerance of gonadotrope-ablated (Cre+) and control (Cre-) ovariectomized (OVX) female and gonadectomized (GDX) male mice with estrogen (E) or testosterone (T) replacement.

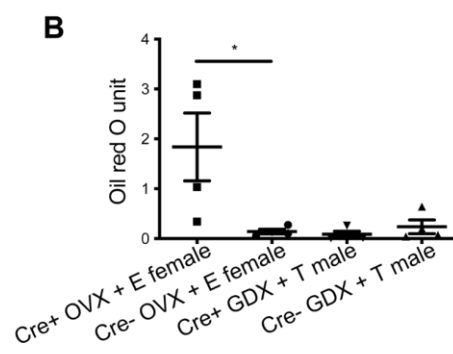
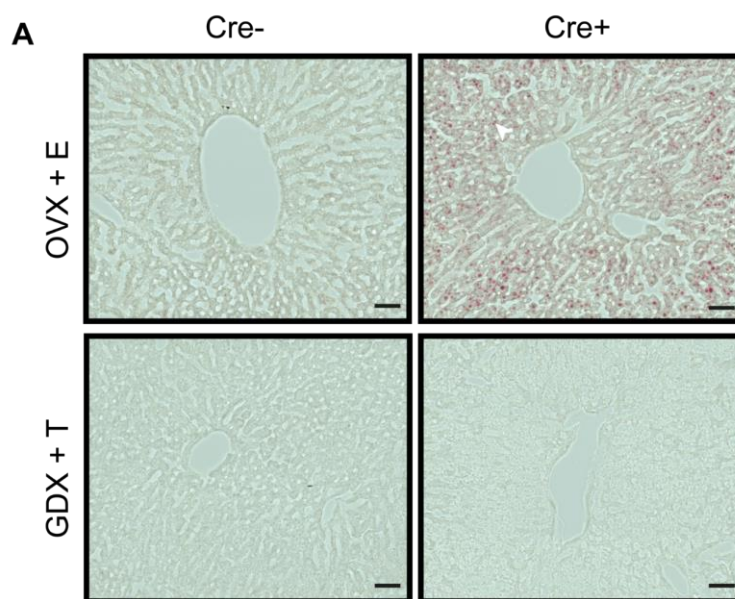


Figure 25: Hepatic steatosis in females is independent of sex steroids. (A) Liver ORO staining quantification and (B) representative images of Cre⁺ and Cre⁻ (control) gonadectomized female and male mice with sex hormone replacement, scale bars = 50 μ m. Error bars represent standard error mean. * = $P < 0.05$.

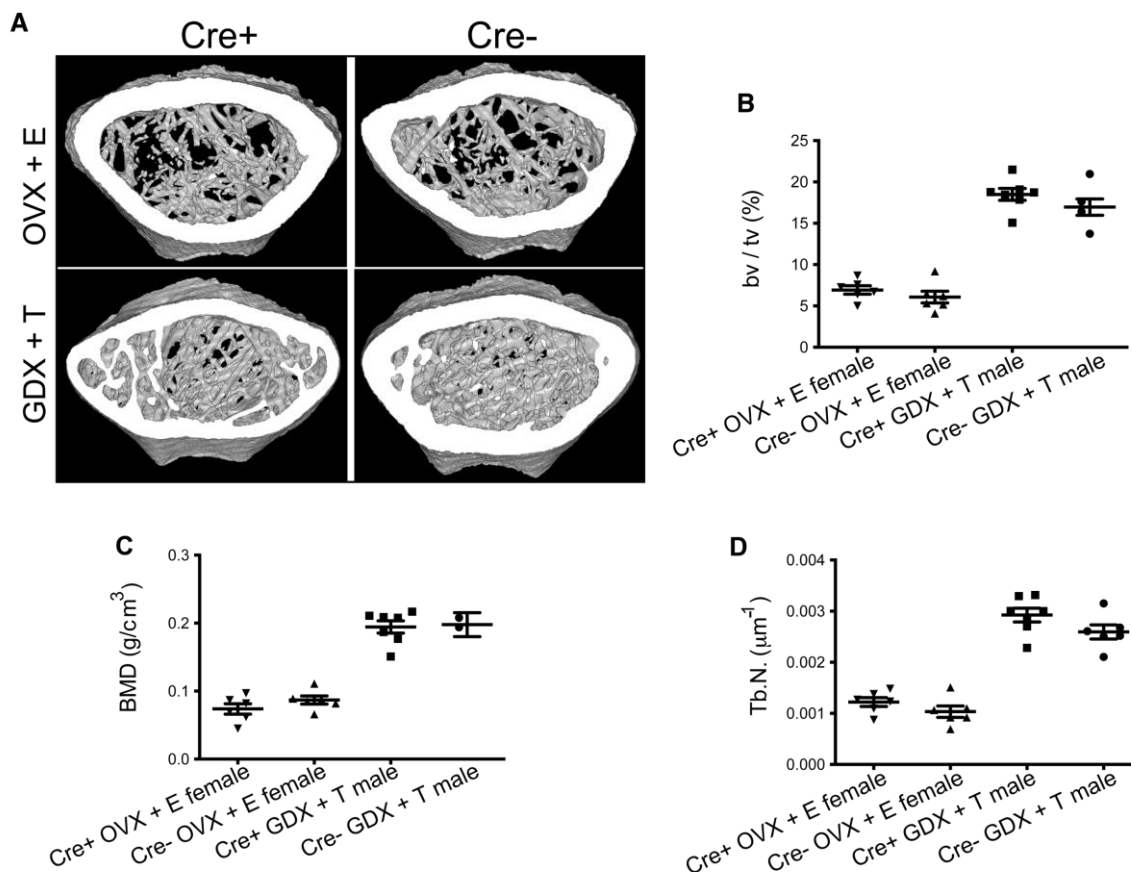


Figure 26: Gonadotropes regulate bone mass through both gonadal and non-gonadal ways in a sex-specific manner. (A) Representative microcomputed tomography (μ CT) images of femur, (B) Trabecular fractional bone volume, (C) bone mineral density and (D) trabecular number of trabecular bones from Cre⁺ and Cre⁻ (control) gonadectomized female and male mice with sex hormone replacement.

3.6 Characterization of the GRIC/eR26- DREADD mouse model

Since we found that acute gonadotropine ablation triggered metabolic disorders, we wondered whether the chronic pharmacogenetic activation of gonadotropes would be beneficial with respect to the symptoms of metabolic disorders. To test this hypothesis, we took advantage of a chemogenetic approach and developed a mouse line GRIC/eR26-DREADD/eR26- τ GFP (Figure 27A), in which a Gq-coupled DREADD (Designer Receptor Exclusively Activated by Designer Drugs) is specifically expressed in gonadotropes. Furthermore, we used a Gq-coupled DREADD since the GnRH receptor is also coupled to Gq. In this model, intraperitoneally injected Clozapine-N-oxide (CNO) in these mice, triggered robust activation of gonadotropes via Gq signaling, as demonstrated by c-FOS expression after CNO administration (Figure 27C).

In order to verify faithful transgene expression of DREADD in gonadotropin-expressing cells, sections from GRIC/eR26-DREADD mice were stained for the HA-tag which is fused to the DREADD. We also

stained for LH and FSH to label gonadotropes. We found that the majority of gonadotropes express HA-tag signals (Figure 27B). This result clearly validates the specificity of this approach. This figure was kindly provided by Debajyoti Das.

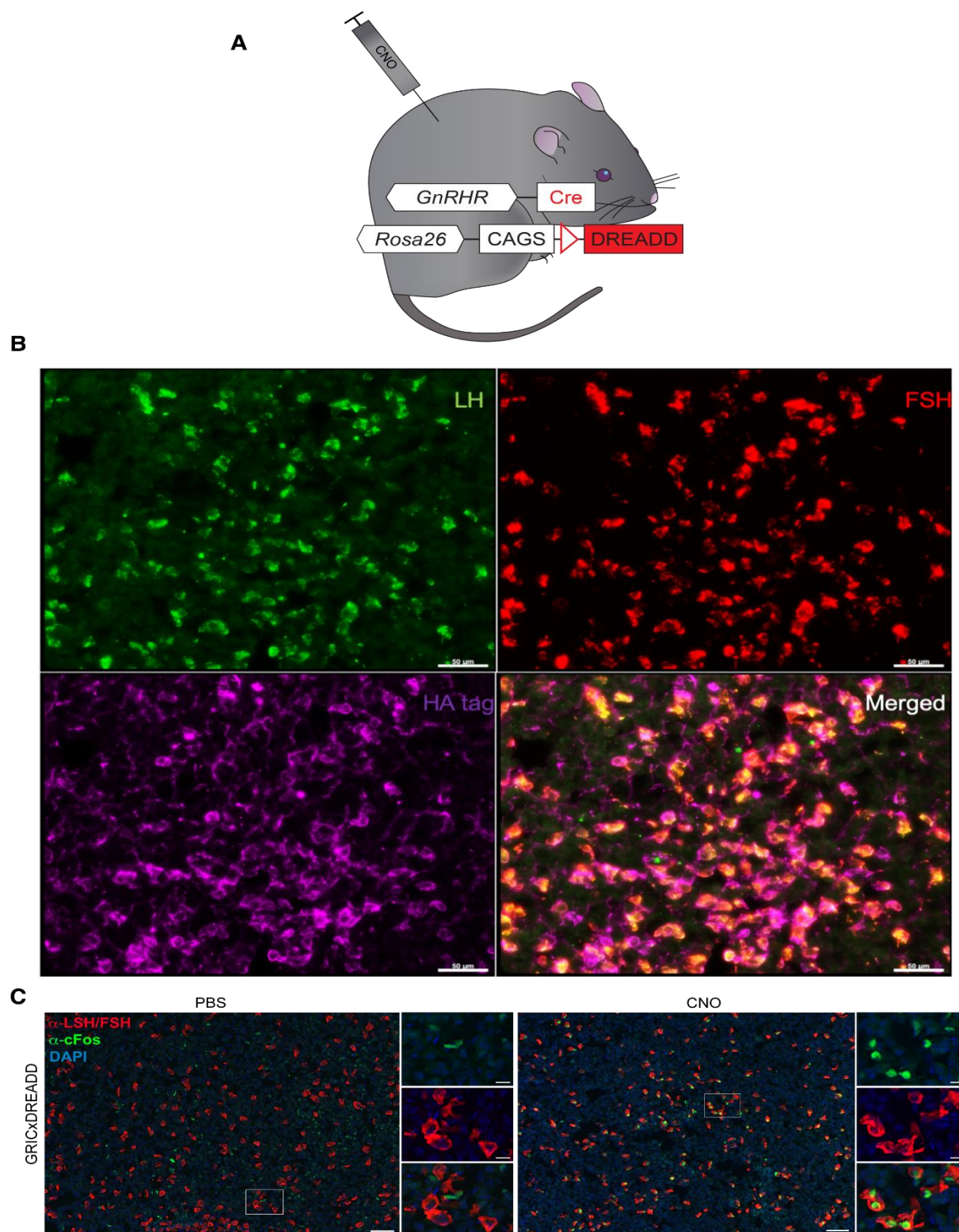


Figure 27: CNO activates gonadotropes in GR1X/eR26-DREADD mice. (A) Illustration depicting the strategy to chronic gonadotrope activation via the injection of Clozapine-N-oxide (CNO) in mice selectively expressing a DREADD in gonadotropes. (B) Representative image of LH and FSH cells in the pituitary expressing HA-tagged

hM3Dq DREADD in the membrane of gonadotrope cells after Cre recombination, scale bars = 50 μ m. (C) Representative images of pituitaries after PBS and CNO i.p. injection in GRIC/eR26-DREADD/eR26- τ GFP mice. The expression of c-Fos (green) was used as a marker for activation. Gonadotropes are shown in red, corresponding to the expression of LH and FSH. DAPI is shown in blue. Scale bars = 50 μ m in the full-size images and 20 μ m in insets.

3.7 Activation of gonadotropes improves metabolic disorders independently of the gonads in a female high fat diet mouse model

To corroborate these results, we first performed a gonadectomy on these mice. One week after gonadectomy, we concomitantly administered CNO in the drinking water and a high fat diet (HFD; a well-established model of metabolic syndrome (Wong, Chin, Suhaimi, Fairus & Ima-Nirwana, 2016)) to induce metabolic disorders. Remarkably, we observed that the body weight in the Cre+ group was significantly lower compared to controls even in the absence of the gonads in females with activated gonadotropes (Figure 28A). Likewise, we found that glucose tolerance (Figure 28B) was significantly improved in the Cre+ group. Most interestingly, liver steatosis was improved upon chronic gonadotrope activation (Figure 28C-D) raising the question as to which gonadotropin might mediate these effects. Meanwhile, we observed no significant difference in body weight or glucose tolerance between Cre+ and Cre- groups in males after chronic gonadotrope activation (Figure 28C). Taken together, these results show that gonadotrope activation improved metabolic disorders independently of the gonads in females. Overall, data from HFD-fed GRIC/eR26-DREADD mice showed an improved development of some of the traditional adverse effects seen with HFD feeding in the development of hepatic steatosis.

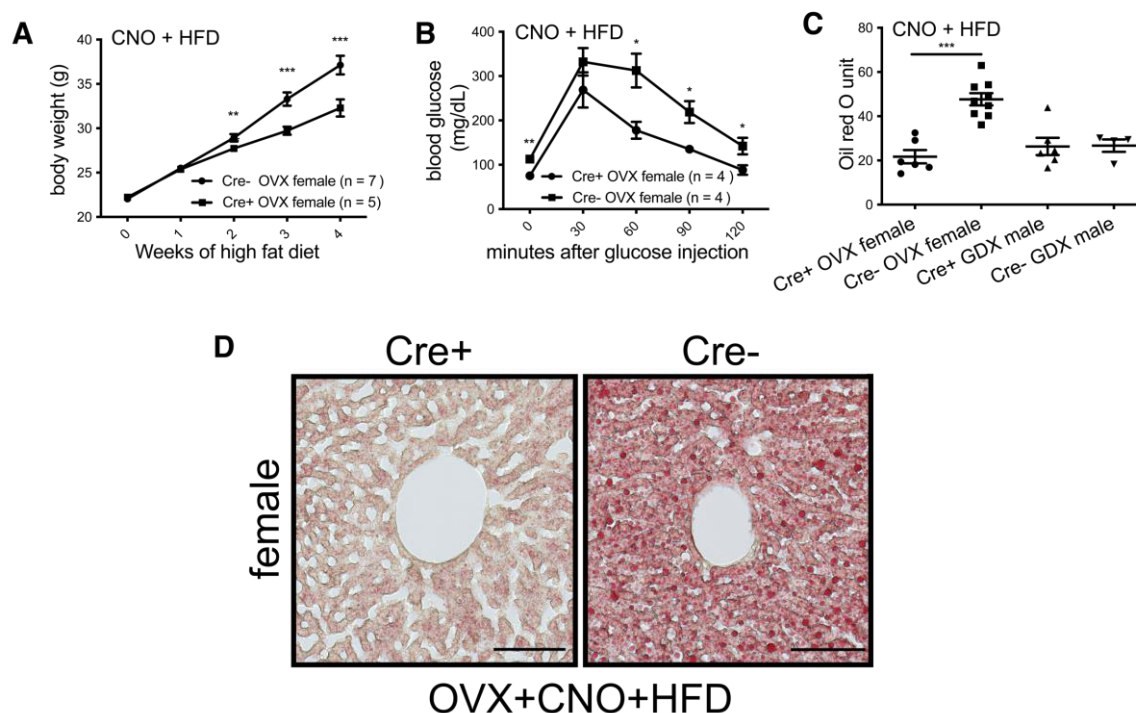


Figure 28: Metabolic phenotype of HFD-fed GRIC/eR26-DREADD mice. (A) Body weight, (B): Glucose tolerance test i.p. (GTT) of Clozapine-N-oxide (CNO) injected Cre+ (chemogenetically-activated) and Cre- (control) gonadectomized female and male mice on high-fat diet (HFD). (C, D): Representative images of liver lipid accumulation by Oil Red O staining and quantification of liver lipid in Cre+ (activation) and Cre- (control)

gonadectomized female and male mice. Data were analyzed by one-way ANOVA or t-test. Data are shown as mean \pm SEM. Asterisks indicate significance, (*) $P < 0.05$, (***) $P < 0.001$, n=4 per genotype (GTT), i.p.= intraperitoneal, Scale bars = 100 μ m.

3.8 FSH administration improves metabolic disorders caused by ovariectomy and high fat diet

Our previous findings demonstrating a dependency on ovarian estradiol for weight gain and glucose metabolism raised the question as to which hormone released by the gonadotropes might mediate these effects. Therefore, we performed multiplexed hormone analysis on OVX/HFD female mice with chronically administered CNO (Figure 29A-F) and found that FSH - but not LH - was significantly increased in response to chemogenetic gonadotrope activation (Figure 29B-F). Intriguingly, we also found that adrenocorticotrophic hormone was significantly reduced after chronic CNO treatment (Figure 29A).

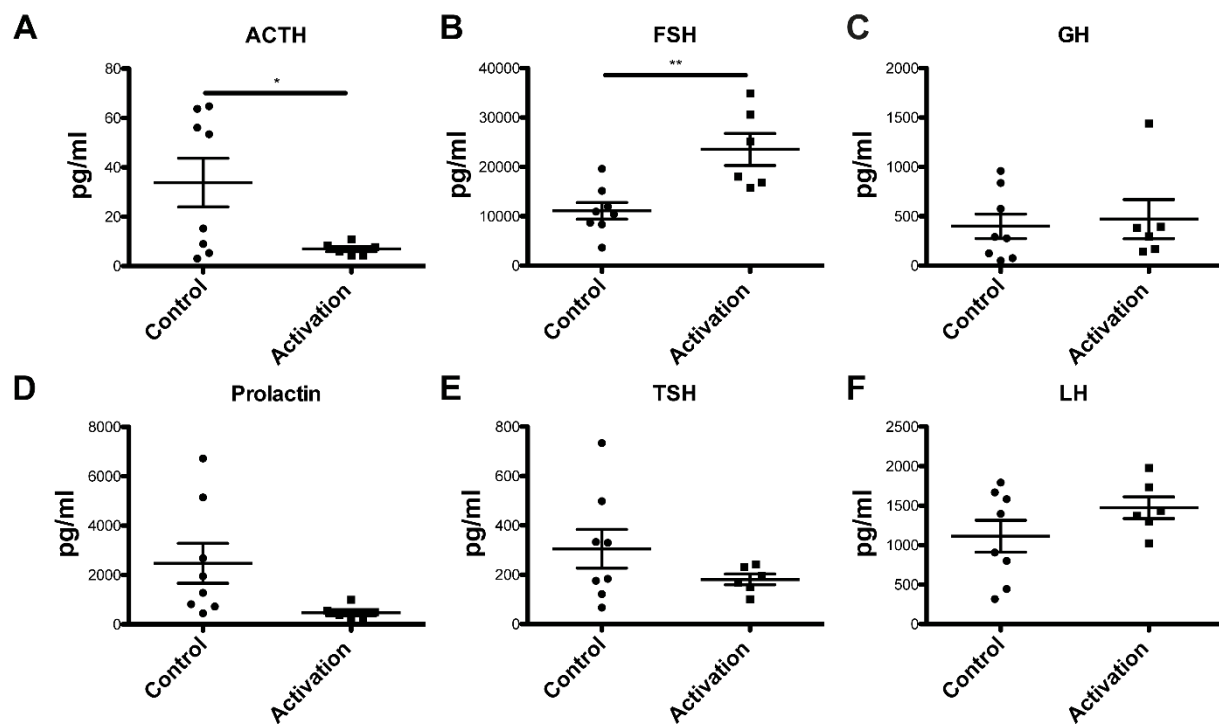


Figure 29: Plasma hormone measurements. (A) Plasma adrenocorticotrophic hormone (ACTH), (B) FSH, (C) growth hormone (GH), (D) prolactin, (E) thyroid stimulating hormone (TSH) and (F) LH of Cre+ (activation) and Cre- (control) gonadectomized female and male mice. Error bars represent standard error mean. * = $P < 0.05$ and ** = $P < 0.01$.

The main hormones produced in gonadotropes in response to GnRH are LH and FSH. Since there are several studies suggesting that FSH plays a role in body homeostasis, we decided to test the function of FSH in metabolic disorders. Considering that NASH is frequently associated with metabolic disorders such as obesity and diabetes, we investigated whether FSH treatment is effective against the symptoms of metabolic syndrome. We performed daily injections of FSH in ovariectomized mice alongside the HFD mouse model. Surprisingly, we found that daily FSH injections were sufficient to reduce weight

gain (Figure 30A), restore glucose tolerance (Figure 30B) and improve hepatic steatosis (Figure 30C-D) compared with the saline-injected groups, demonstrating the potential for FSH treatment to improve the symptoms of metabolic syndrome. These data clearly demonstrate that FSH treatment improves metabolic disorders in female mice.

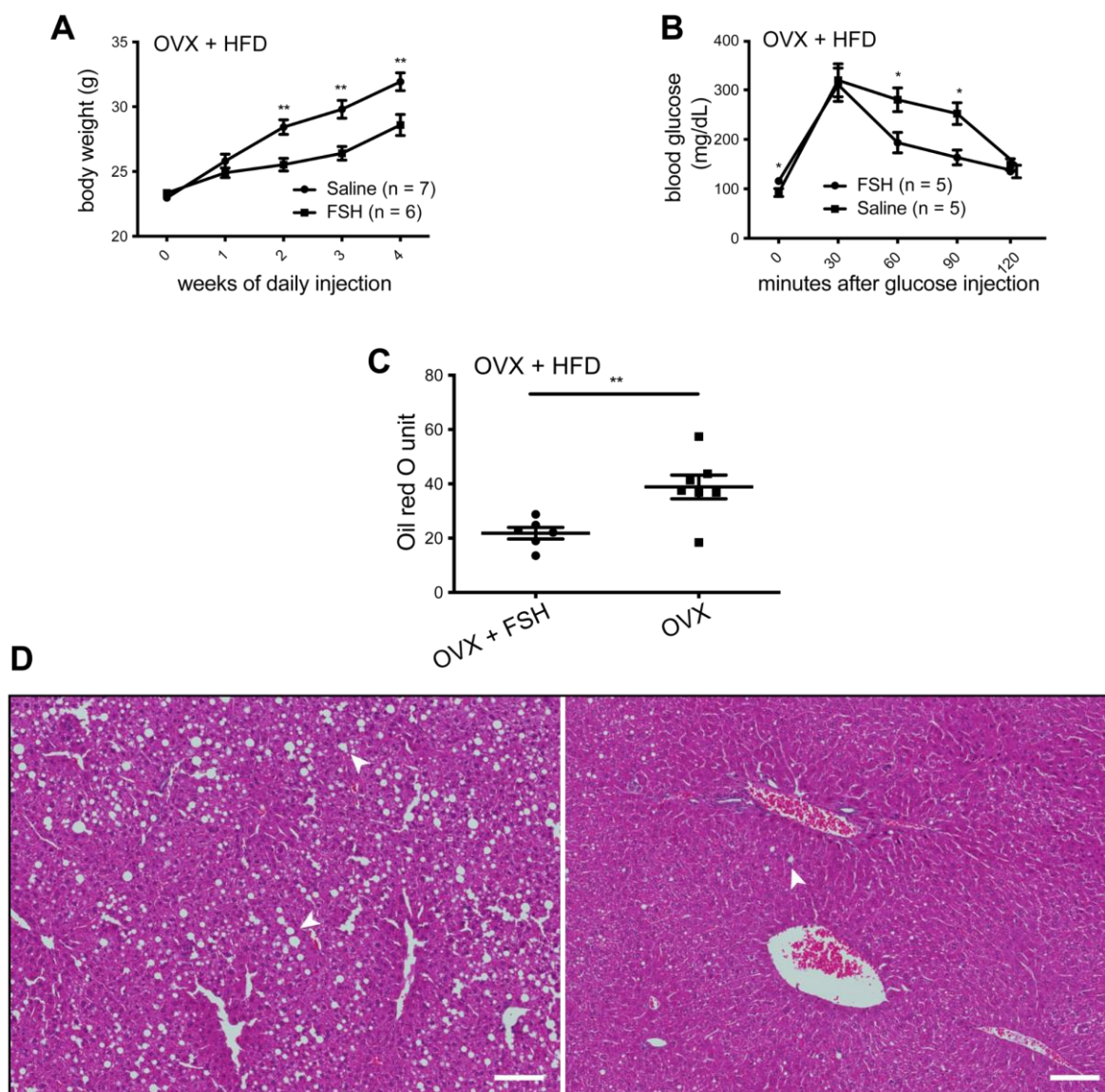


Figure 30: Wildtype mice display improved body weight and glucose tolerance upon FSH treatment after ovariectomy. (A): Body weight and (B): i.p. GTT of FSH treated and saline treated gonadectomized female mice on HFD feeding. (C, E): Liver sections 14 μ m stained with hematoxylin and eosin (H&E) after injection (i.p.) with FSH for 4 weeks. Data were analyzed by one-way ANOVA or t-test. Data are shown as mean \pm SEM. Asterisks indicate significance, (*) $P < 0.05$, (**) $P < 0.01$, (***) $P < 0.001$, $n = 4$ per genotype (GTT), i.p. = intraperitoneal, OVX: ovariectomy. Scale bars = 50 μ m.

3.9 Disrupting FSH signaling in the pituitary induces a fatty liver phenotype

To understand the mechanism underlying the regulatory role of FSH in liver steatosis, we decided to uncover the site of action for FSH in mediating these effects. We performed RT-PCR for the FSH receptor (*Fshr*) on major tissues prepared from female mice. Interestingly, *Fshr* was detected in only

two tissues within the female mouse; the ovary and the pituitary (Figure 31); we further verified this pattern by RT-qPCR (Figure 32A) and RNA-scope (Figure 32B). Moreover, we did not detect FSH receptor gene expression in the liver. This suggests that FSH has an indirect effect on liver tissue.

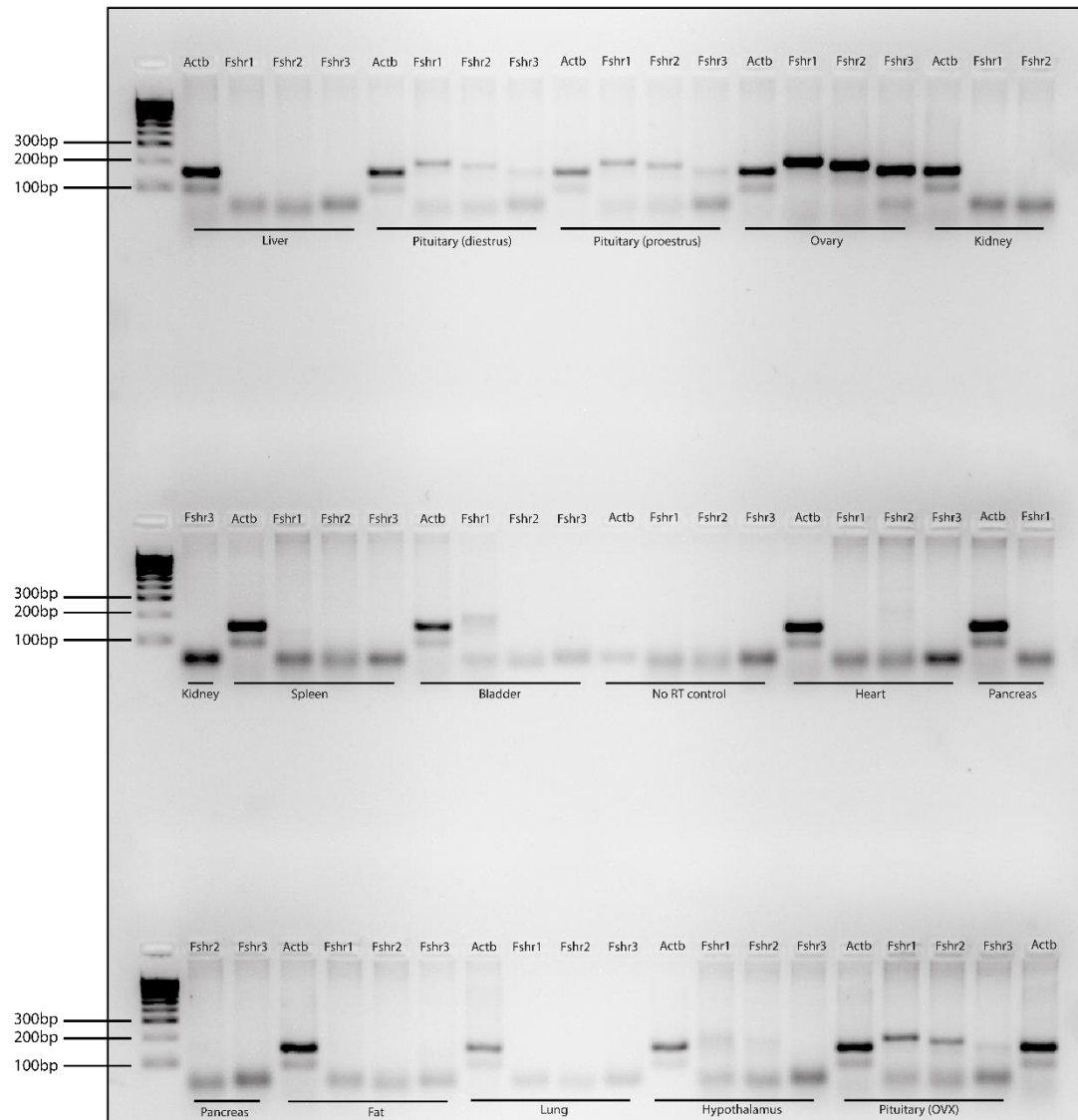


Figure 31: (A) Representative RT-PCR analysis of *Fshr* expression in major organs of adult female mice. (Actb; beta actin. three pairs of primers against *Fshr* were used (*Fshr1*, *Fshr2*, *Fshr3*)).

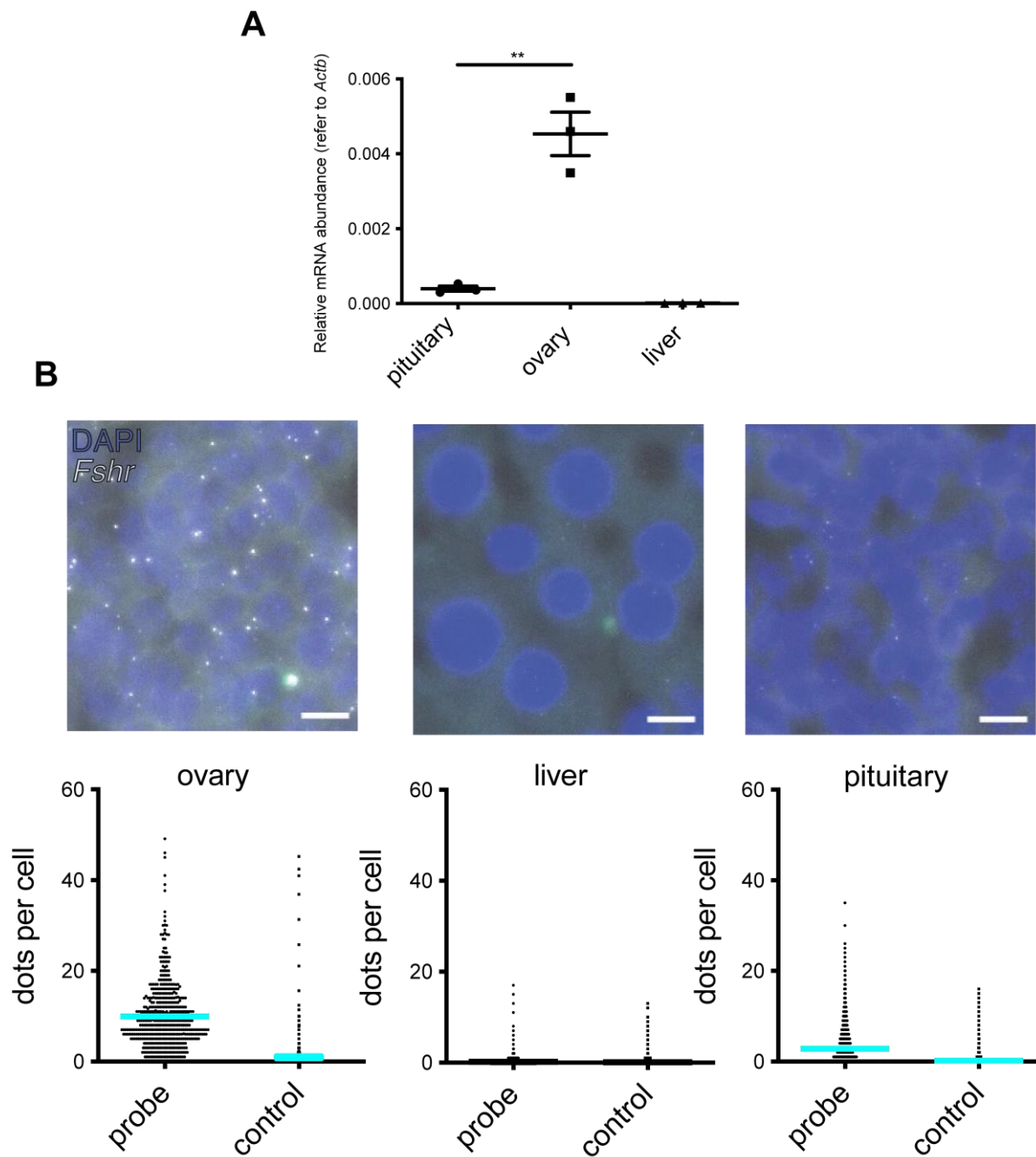


Figure 32: RT-qPCR and RNA-scope analysis of *Fshr* expression levels in the pituitary, ovary, and liver from adult female mice. (A) The expression of FSH receptor in different tissues (pituitary, ovary, and liver) from female mice was measured by RT-qPCR. (B) RNA-scope for FSH- receptor in the ovary, Pituitary, and liver from female mice (b; scale bars = 10 μ m). Data were analyzed by one-way ANOVA or t-test. Data are shown as mean \pm SEM. Asterisks indicate significance, (***) $P < 0.01$.

Therefore, we decided to investigate the function of FSH in the organ where it is produced and released, i.e. the pituitary. We established an *in vitro* whole pituitary assay in which we then blocked the action of FSH by incubating the pituitaries taken from female mice at diestrus (post-ovulation) with a monoclonal antibody against FSH prior to stimulation with GnRH to release the gonadotropins (Figure 33A). Among all the six hormones produced by the anterior pituitary, we found that adrenocorticotropic

hormone (ACTH) exclusively was significantly elevated as a result of FSH sequestration by the monoclonal antibody targeting FSH when compared to the controls (mouse IGG) (Figure 33B-K).

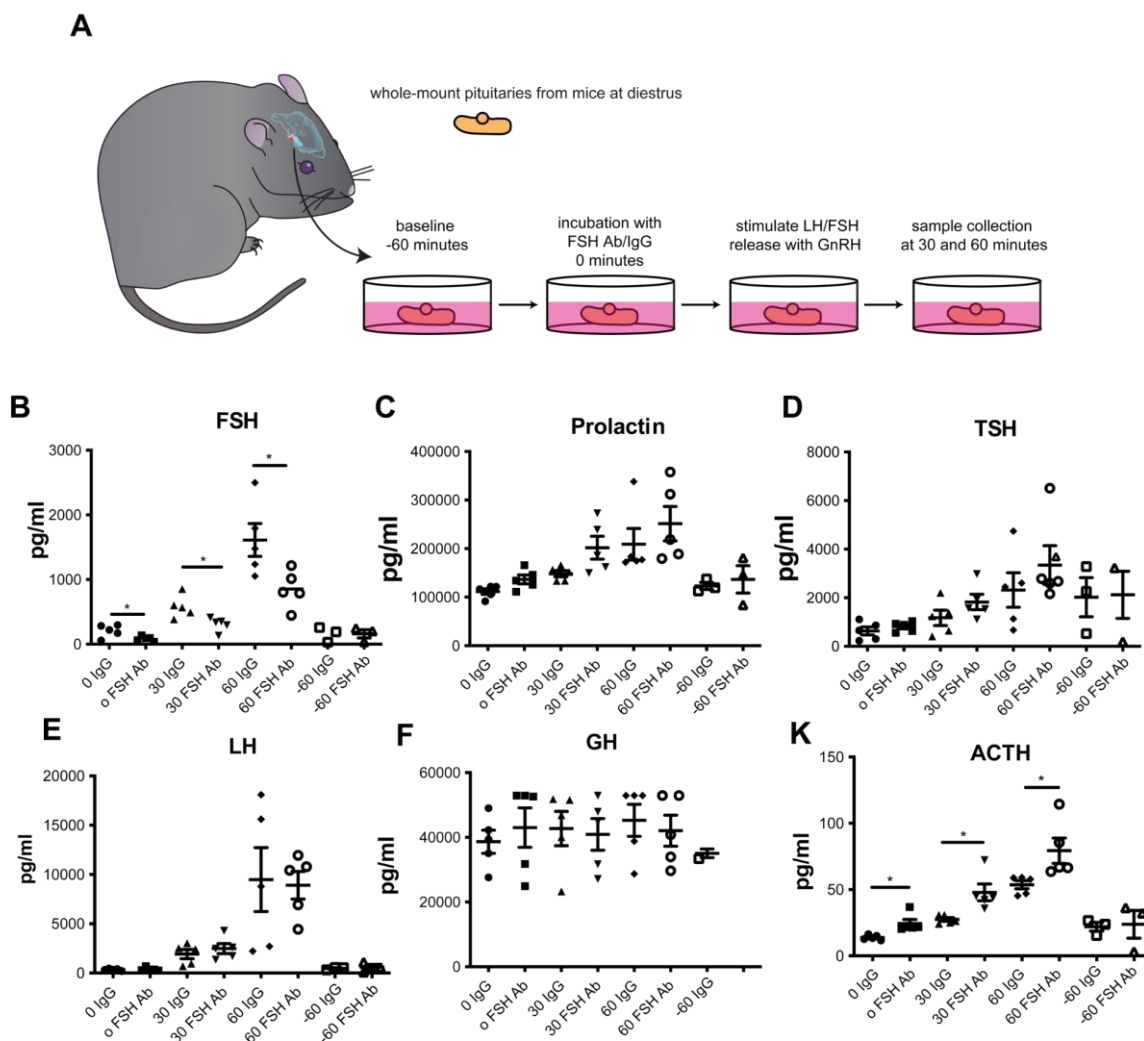


Figure 33: *In vitro* stimulation assay to analyze pituitary hormone secretion. (A) Schematic representation of the *in vitro* stimulation assay used to analyze hormone secretion from intact pituitary. Pituitaries were incubated with a monoclonal anti-FSH antibody or IgG. After that, the pituitary was stimulated with GnRH to release LH/FSH. The samples were collected at 0, 30 and 60 minutes. (B) FSH, (C) prolactin, (D) TSH, (E) LH, (F) GH and (K) ACTH levels of *in vitro* pituitary assay from anti-FSHab-incubated and IGG-incubated GnRH-stimulated pituitaries. Data were analyzed by one-way ANOVA or t-test. Data are shown as mean \pm SEM. Asterisks indicate significance, (*) $P < 0.05$.

This result suggests a potential paracrine FSH action on the release of ACTH. This is consistent with our finding in the RNA-scope experiment in which we found that the FSH receptor is expressed in corticotropes. We wondered if these results were specific for mice. Re-analysis of bulk RNA-seq data confirmed that FSHR is also not expressed in the human liver (Figure 34A) (Brosch *et al.*, 2018). In total, 19 donors were used (6 males, 13 females in that study). In addition, based on recent data, we found that single-cell transcriptional RNA sequencing of human pituitary confirms the expression of FSH receptor in corticotropes as well as in pituitary stem cells and in cycling cells (CC) (Zhang *et al.*, 2020) (Figure 34B).

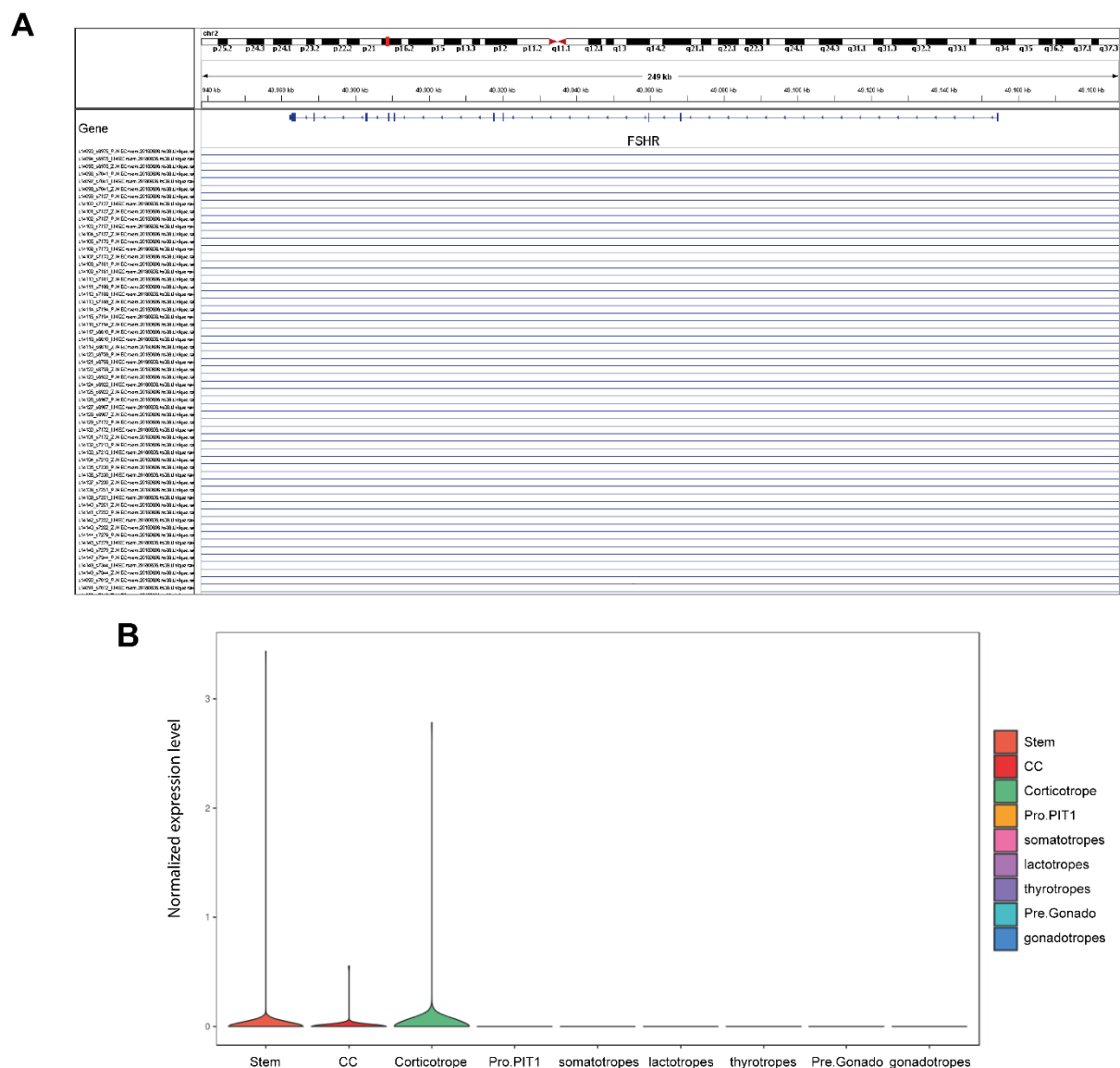


Figure 34: Human corticotropes express the FSH receptor. (A) Detailed genomic view of the *FSHR* locus from RNA-seq data. The IGV browser was used to visualize the genomic loci of *FSHR*. Data were extracted from a published human liver RNA-seq database (Brosch *et al.*, 2018). In total, 19 donors were used (6 males, 13 females). No reads were mapped in this region. (B) *FSHR* expression in human pituitary, cell types are shown as follows: stem cells (Stem), cycling cells (CC), corticotropes, progenitors of the PIT-1 lineage (Pro.PIT1), somatotropes, lactotropes, thyrotropes, precursors of gonadotropes (Pre.Gonado) and gonadotropes. Data were extracted from a published single cell RNA-seq database from the human pituitary (Zhang *et al.*, 2020).

Subsequent hormone analysis revealed that gonadotrope ablation either in intact or ovariectomized females resulted in significantly elevated plasma corticosterone levels, whereas FSH injections were sufficient in both intact and ovariectomized mice on HFD to reduce the plasma corticosterone concentrations (Figure 35A). Corticotropes release ACTH to control the release of GCs in the adrenal gland. GCs have been shown to exert important regulation over steatosis (Quinn *et al.*, 2018). Therefore, we hypothesized that FSH reduces the release of corticosterone through paracrine signaling in the pituitary leading to decreased ACTH release and thus reduced steatosis. To test this hypothesis, the plasma corticosterone levels of the treated mice were determined. Taken together, these findings were

consistent with our RNA-scope experiments in which we observed *Fshr* expression in corticotropes (Figure 35B) and demonstrated that FSH reduced corticosterone release (Figure 35A). Finally, to functionally analyze paracrine FSH action in the pituitary, we used a viral approach to deliver CRISPR-Cas9 system to specifically disrupt FSH receptor expression in the pituitary. We stereotaxically injected an adeno-associated virus (AAV) containing Cas9 in combination with a guide RNA targeting the FSH receptor into the mouse pituitary to knock out *Fshr* expression (Figure 36A). 8 weeks after the stereotaxic injection within the pituitary of intact female mice, we found that these mice developed hepatic steatosis (Figure 36B-D). Taken together, these data demonstrate that paracrine FSH action on corticotropes in the pituitary regulates hepatic lipid metabolism by reducing ACTH and subsequently corticosterone secretion.

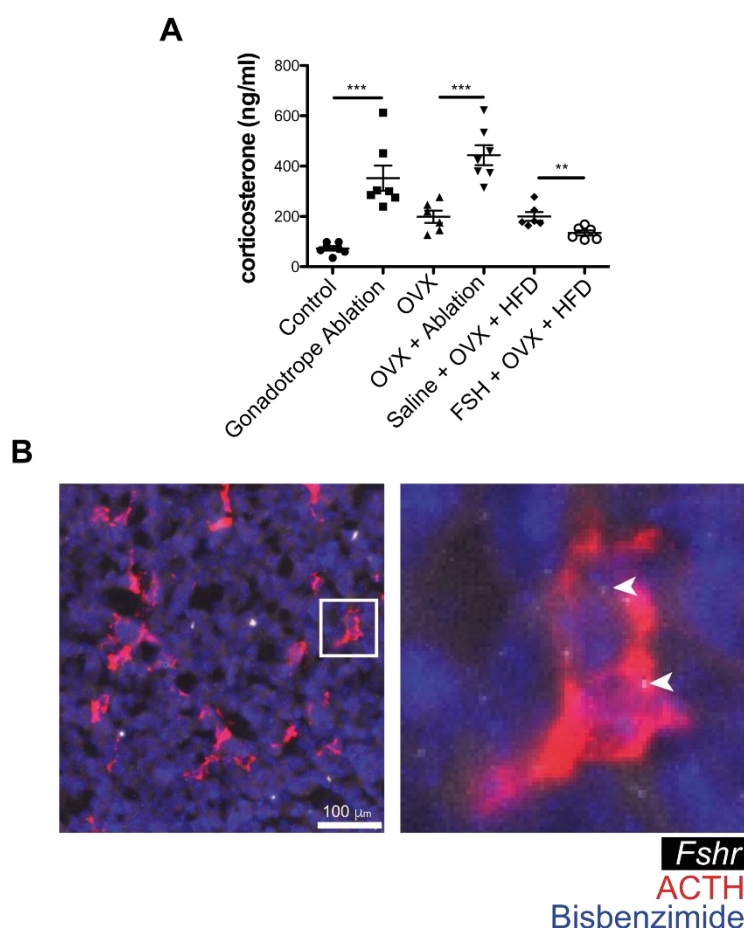


Figure 35: Increased corticosterone plasma levels after acute gonadotrope ablation. (A) Plasma corticosterone levels from control and experimental female mice. (B) Colocalization of *Fshr* mRNA (RNA scope, filled arrowhead) and ACTH; (scale bar = 100 μ m). Error bars represent standard error mean. * = $P < 0.05$, ** = $P < 0.01$ and *** = $P < 0.001$.

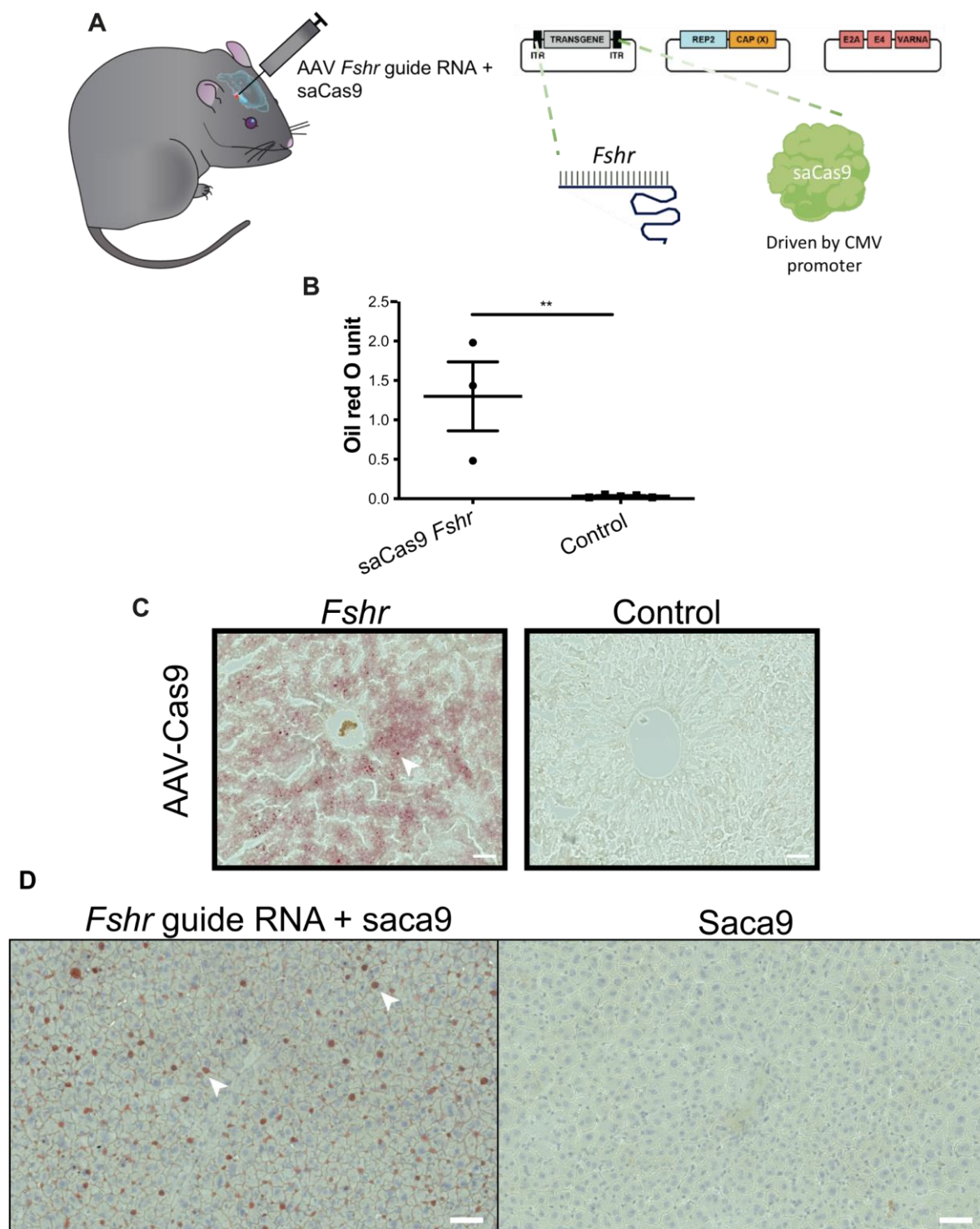


Figure 36: Paracrine FSH actions in the pituitary prevent hepatic steatosis in female mice. (A) Experimental strategy to disrupt *Fshr* expression in the pituitary, AAV-Cas9 with or without guide RNA was injected. (B) Quantification of liver ORO staining (C, D) Representative image of liver section staining with Oil Red O from AAV-Cas9 (with or without guide RNA against follicle-stimulating hormone receptor; *Fshr*) pituitary-injected mice, scale bars = 50 μ m. Error bars represent standard error mean. ** = $P < 0.01$.

Ultimately, these findings highlight the potential clinical benefit of FSH receptor agonism for the treatment of metabolic syndrome and also open up the possibility of drug repurposing for FSH.

Discussion

NAFLD is a complex disease with a rapidly rising global prevalence. Despite numerous attempts, the underlying mechanisms responsible for NAFLD are still not completely understood. Several pathogenic pathways have been described to be involved in the development and progression of NAFLD. Treatments of NAFLD were originally intended to treat diabetes and other metabolic disorders. In the last decades, the most widely used strategy was to block *de novo* lipid synthesis in the liver. Inhibition of lipid transport from adipose tissue to the liver has also been used as another treatment approach (Smeuninx *et al.*, 2020).

Osteoporosis has been a leading public health problem in aging human beings. Patients with osteoporosis are known to have increased osteoclast activity and are at a higher risk of bone fracture and mortality. The tightly regulated linkage of bone production and resorption is essential for skeletal homeostasis and bone remodeling. While the gonadal sex steroid hormones play a key role in bone metabolism, recent studies reported an essential role of other reproductive hormones in bone physiology independent of their role in reproduction.

Moreover, the extragonadal function of FSH has been one of the most strident topics in the last years. Several studies have shown that the action of FSH on the FSHR plays a key role in the metabolism regulation in several organs.

4.1 The HPG-axis controls distinct aspects of the metabolic syndrome

Metabolic disorders such as obesity have been well investigated and shown to play a crucial role in various reproductive disorders including PCOS and infertility. Despite intense research on this topic, the role of HPG-axis dysfunction in metabolic disorders has been difficult to study. The molecular drivers of menopause-induced metabolic dysfunction are not completely known. In the present study, we disrupted the HPG-axis in adult mice by acute ablation of gonadotropes (by injecting DT into mice exclusively expressing DT-receptors on *Gnrhr*-expressing cells) which induced serious metabolic disorders including obesity, glucose intolerance, and insulin intolerance, especially in females. This significant and reproducible effect suggests that gonadotropes regulate metabolic homeostasis in a sex-specific way. Another interesting finding from this experiment was that both sexes developed fatty liver and bone loss. In this thesis, FSH was identified as a new player in the HPA-axis in the regulation of hepatic steatosis. Kisspeptin is the most potent activator of GnRH neurons discovered thus far and has been shown, along with its receptor GPR54, to be an indispensable component of the molecular machinery driving puberty and fertility in mice and man (Seminara *et al.*, 2003). There are several studies which suggest that the *Kiss1* gene responsible for kisspeptin expression is also expressed in several peripheral tissues, including metabolic tissues such as the fat, liver, ovary and testis (Wolfe & Hussain, 2018). This observation suggests that kisspeptin plays a role in metabolism. Tolson *et.al.*

reported in 2014 that female kisspeptin receptor knock-out (*Kiss1r* KO) mice showed dramatically higher leptin levels, body weight, and adiposity (Tolson *et al.*, 2014). In addition, these animals also displayed impaired glucose tolerance. However, kisspeptin receptor knock-out males did not show significant changes in either body weight or glucose tolerance (Tolson *et al.*, 2014). Several studies investigated the contribution of AR deficiency to the development of insulin resistance and its role in inducing fatty liver and osteoporosis in both sexes (Yu, Lin, Sparks, Yeh & Chang, 2014). The underlying mechanism by which androgens regulate metabolic homeostasis is complex. This outcome of testosterone deficiency characterized by obesity, development of diabetes, insulin resistance, and cardiovascular complications has also been observed in prostate cancer patients which received androgen-deprivation therapy (Yu *et al.*, 2014).

In 2018, Quinn *et al.* reported that ovariectomized mice developed increased body weight, steatosis, and insulin resistance (Quinn *et al.*, 2018). The authors showed that the underlying cause driving steatosis in hypogonadal female mice was hepatic GC signaling, and that hepatocyte-specific GR knock-out protected mice from developing ovariectomy-induced steatosis (Quinn *et al.*, 2018). Estradiol could block the development of obesity and insulin resistance following ovariectomy. However, in this study we observed that FSH reduced weight gain and improved glucose tolerance in the absence of either ovarian or supplemented estradiol.

In this study, we decided to dissect the role of the gonadotrope cells independent of sex steroid hormones. We developed an experimental strategy for gonadectomy (ovariectomized or castrated) with sex hormone replacement. By performing this strategy in the GRIC/R26-iDTR mouse model, we have shown that the majority of metabolic disorders caused by gonadotrope ablation are gonad-dependent. However, the fatty liver development seen in females is gonad-independent. Our results indicate that the response of bone metabolism to FSH requires the presence of functional ovaries.

While sex hormones have been well studied to have fundamental contributions to bone loss, whether gonadotropins and in particular FSH have a direct effect on bone tissue is still under debate. Osteoporosis after gonadectomy has been attributed to decreased sex hormone levels. Several studies challenged this view by reporting that gonadotropins, FSH in particular, directly regulate bone metabolism. In 2006, Sun *et al.* demonstrated that globally knocking out either FSH β or FSHR in female mice resulted in hypogonadism without bone loss, suggesting a negative role of FSH on bone (Sun *et al.*, 2006). Combined with *in vitro* studies, the authors speculated that this effect of FSH on bone metabolism is direct and independent of estrogen. Based on these results, Sun *et al.* concluded that “high circulating FSH causes hypogonadal bone loss” (Sun *et al.*, 2006). One caveat we need to consider is that these conclusions were based on global genetic knock-out strategies, i.e. FSH β or FSHR were removed in the germline in these animals. Since FSH signaling is one key regulator of sexual maturation, a global knock-out of FSH β or FSHR could have developmental effects including compensation in these models. However, Khosla *et al.* noted in a later publication that the FSH β and FSHR null mouse model displayed anomalies in essential hormones including testosterone and LH levels which were up to 10

folds increased in female mice (Danilovich *et al.*, 2000; Abel, Huhtaniemi, Pakarinen, Kumar & Charlton, 2003; Khosla *et al.*, 2020).

Likewise, Allan *et al.* generated transgenic female mice over-expressing human FSH (TgFSH) (Allan *et al.*, 2010). They found that this mouse model had a bone mass which was increased, markedly elevated tibial and vertebral trabecular bone volume, in a dose-dependent manner. This effect was also observed in mice lacking GnRH expression and thus endogenous secretion of LH and FSH (Allan *et al.*, 2010), suggesting that FSH-induced bone mass increased occurred independently of background LH or estradiol level.

Furthermore, ovariectomy reversed the increase in bone mass found in TgFSH-HPG mice, suggesting once again the role of ovarian factors (e.g. increased testosterone or other factors) in mediating FSH actions not in lowering, but rather increasing bone mass. It's important to note that the ovary produces both activins and inhibins. Bone resorption is suppressed by inhibins, whereas bone growth is increased by activins (Nicks, Perrien, Akel, Suva & Gaddy, 2009).

A polyclonal antibody targeting the FSH β -subunit enhanced bone mass and, interestingly, reduced fat tissue as reported recently by the Zaidi laboratory. Identical findings using monoclonal antibodies were later reported by the same group (Liu *et al.*, 2017).

In 2021, Zhou *et al.* reported that FSH regulates bone metabolism independent of *Fshr* in osteoclasts. They showed that *Fshr* knock-out in osteoclasts did not protect mice from ovariectomy-induced bone loss. Moreover, *Fshr* expression was low to undetectable in both a murine monocyte cell line which had been differentiated into osteoclasts and in primary murine osteoclasts. Here, by using complementary approaches in mice, we demonstrate unequivocally that gonadotropins influence bone metabolism indirectly via sex steroid production and not by direct action on bone. Consistent with this, *Fshr* and *Lhcgr* expression were low to undetectable in a murine monocyte cell line differentiated into an osteoclast cell line or in primary murine osteoclasts (Figure 37A-D). Moreover, FSH did not significantly affect RANKL-stimulated expression of osteoclast-specific genes in these cells (Figure 37E-L).

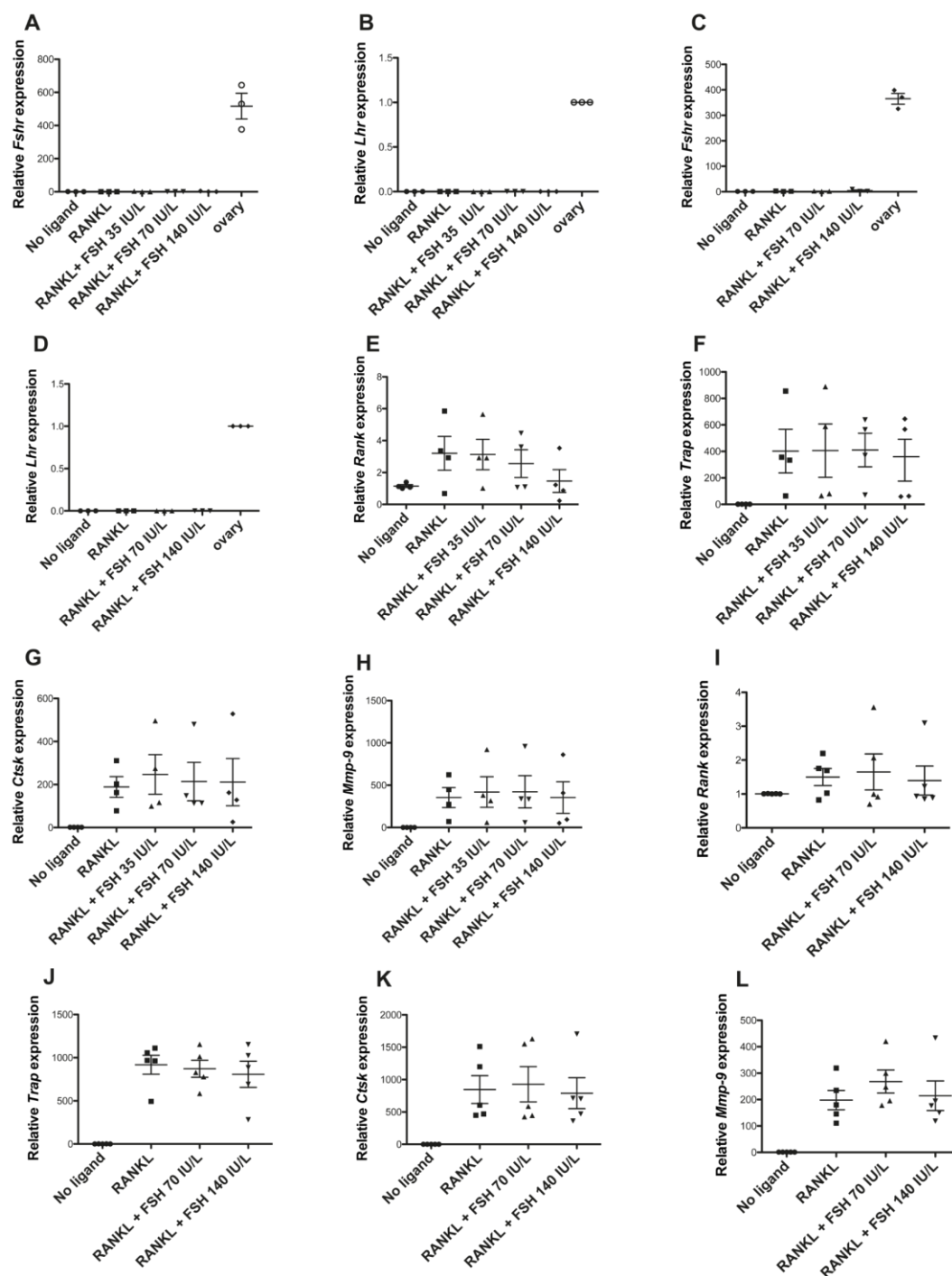


Figure 37: FSH regulates bone metabolism independent of *Fshr* in osteoclasts. (A) *Fshr* and (B) *Lhcgr* expression levels in RAW 264.7 cells in response to the indicated treatments. (C) Expression levels of *Fshr* and (D) *Lhcgr* in primary murine monocytes under different treatment conditions (note that M-CSF was added in all cases). Ovary RNA was included as a positive control. *Fshr* levels are plotted relative to the no-ligand or M-CSF-only treatment conditions. *Lhcgr* expression levels were plotted relative to the ovary as no signal was detected in the cells under any conditions. (E) Expression levels of four osteoclast differentiation markers: receptor activator of nuclear factor κ B (RANK), (F) tartrate-resistant acid phosphatase (Trap), (G) cathepsin k (Ctsk), and (H) matrix metalloproteinase 9 (Mmp-9) in RAW 264.7 cells in response to the indicated treatments. (I) Expression levels of RANK, (J) Trap, (K) Ctsk, and (L) Mmp-9 in primary murine monocytes in response to the different treatments. Adapted from (Zhou 2021, Thesis (MSc) McGill University, Montreal, Canada).

For us as endocrinology researchers, the integration of the clinical results is fundamental. The evaluation of patients not only includes static hormone measurements, but also classical stimulation or suppression tests that usually identify the underlying pathology. For example, a baseline cortisol level alone is definitively not a diagnostic marker of Cushing's syndrome, however, an additional cortisol suppression testing is required for an accurate diagnosis. Stimulation tests, on the other hand, are frequently required to identify adrenal insufficiency. The FSH-bone axis has been studied in both women and men using identical suppression and stimulation techniques. Omodei *et al.* stimulated the FSH level in infertile women undergoing *in vitro* fertilization procedures using recombinant FSH (rFSH) (Omodei *et al.*, 2013). At the same time, Omodei *et al.* used pharmacotherapy (GnRH-analogue) to suppress the production of endogenous gonadotropins and estrogen in 29 premenopausal women. In this clinical model, they evaluated the sequential profile of serum bone turnover markers including osteocalcin and c-telopeptides of type-1 collagen (CTX). They found that the change in the bone resorption marker was proportional to the change in estrogen but not FSH levels in postmenopausal women (Omodei *et al.*, 2013).

To address the same issue in men, Uihlein *et al.* randomized 58 eugonadal men between the ages of 20 and 50, which received monthly GnRH analogue injections (Uihlein, Finkelstein, Lee & Leder, 2014). The intervention group received a topical testosterone gel, while the control group received a placebo, daily for 16 weeks. The authors concluded that FSH does not appear to have a direct effect on bone turnover (Uihlein *et al.*, 2014).

Reproductive dysfunction such as hypogonadism in humans has been reported in clinical studies to be involved in the development of obesity, diabetes, and fatty liver (NAFLD) (Venetsanaki & Polyzos, 2019). However, whether gonadotropins have a direct role in metabolic disorders is still not well analyzed, despite clinical studies suggesting that FSH was negatively associated with NAFLD in aged women. However, preclinical studies using global knock-out mice have reported controversial phenomena (Danilovich *et al.*, 2000; Sun *et al.*, 2006; Allan *et al.*, 2010). Since FSH is the key regulator of gonadal development, these complex phenomena could be a result of the early onset of disrupting the entire reproductive system. By manipulating gonadotropes in adult mice combined with gonadectomy and sex hormone replacement, we dissected the acute gonad-dependent or gonad-independent function of gonadotropes on metabolic disorders without disrupting the development of the reproductive system.

The GRIC/eR26-DREADD mouse model is a powerful tool to delineate FSH function in several tissues including liver and bone. Chemogenetic activation of gonadotropes in these mice resulted in improvements in metabolic function, glucose tolerance, and hepatic steatosis, revealing a potential effect of gonadotropes in liver and bone metabolism. Our subsequent experiments further demonstrated that daily FSH injections in ovariectomized mice on a HFD improved the fatty liver phenotype and hepatic lipid metabolism. Multiple lines of evidence support the idea that FSH signaling has a role beyond that in the reproductive system, as a regulator of metabolism.

In 2018, Quinn *et al.* found that two of the three major GR target genes (PLIN5, LCN2, and LPIN1) were significantly downregulated in the livers of FSH-treated mice. Perilipin-5 (PLIN-5) is a member of the perilipin family that plays a key role in the regulation of triglyceride metabolism (Granneman, Moore, Mottillo, Zhu & Zhou, 2011). The underlying mechanism is still not well understood. Briefly, there are several studies showing that PLIN-5 is highly expressed in tissues which have high triglyceride storage such as the skeletal muscle, heart, and liver (Yamaguchi, Matsushita, Motojima, Hirose & Osumi, 2006). Lipocalin 2 (LCN-2) is a transporter of small lipophilic molecules including steroids and fatty acids in the blood circulation (Asimakopoulou, Weiskirchen & Weiskirchen, 2016). LCN-2 is highly expressed in the liver, kidney and heart (Aigner *et al.*, 2007). Studies have reported that the lack of the LCN-2 gene in mice leads to an increased accumulation of lipids in the liver (Asimakopoulou *et al.*, 2016). Furthermore, Lipin-1 (LPIN1) is suggested to have a function in human triglyceride metabolism (Loos *et al.*, 2007).

In aging women, FSH activity has been proposed to promote obesity and bone loss independently of estradiol deficiency (Sun *et al.*, 2006; Wang *et al.*, 2016). In line with this finding, a recent study (Guo *et al.*, 2019) has demonstrated that FSH increases serum cholesterol levels independent of estrogen, through *de novo* cholesterol biosynthesis via activation of the $Gi2\alpha/\beta$ -arrestin-2/Akt pathway and subsequent inhibition of FoxO1 binding to the *SREBP-2* promoter. FoxO1 is a member of the Forkhead transcription factor superfamily, which has been linked to a variety of human disorders and developmental processes (Hannenhalli & Kaestner, 2009). FOXO1 plays a key role in homeostasis of glucose signaling and is known as a regulator of hepatic gluconeogenesis in response to insulin signaling. Consistent with this, it was also shown that blocking FSH signaling effectively prevents hypercholesteremia induced by FSH intraperitoneal injections or by high-cholesterol diet feeding. This finding was based on blocking FSH signaling by an anti-FSH β antibody, as specific antibodies against the FSHR are not currently available (Chrusciel, Ponikwicka-Tyszko, Wolczynski, Huhtaniemi & Rahman, 2019).

4.2 Extra-gonadal FSH actions

FSH has been reported to have extragonadal actions, most predominantly in liver and bone metabolism, however, the mechanisms underlying this action are still not clear. By screening for FSHR expression, we identified the pituitary as a target organ of FSH. Using *in vitro* pituitary stimulation assays, we could show significantly elevated plasma GC levels as a result of FSH sequestration by a monoclonal antibody targeting FSH. The anterior pituitary gland orchestrates inter-organ communication via the coordinated release of distinct hormones produced by five different cell types (Le Tissier *et al.*, 2017). Recent studies suggest that the individual hormone-secreting cells in the pituitary are organized in networks (Le Tissier *et al.*, 2017). While these experiments had thus far mainly focused on analyzing the activities of cells that secrete the same hormone, some anatomical observations had long fueled speculations about communication between different hormone-secreting cell populations within the pituitary (Budry *et al.*, 2011). Specifically, gonadotropes were found to be invariantly positioned in close proximity to corticotropes, raising the possibility of crosstalk between these two hormone-secreting cell populations. If and how gonadotropes and corticotropes communicate with each other and how this potential interaction might impinge on body homeostasis had remained mysterious. In this study, we revealed that FSH paracrine signaling, most likely in the corticotropes, regulates the liver metabolism and mediates, via gonadal sex steroid hormones, indirect effects on bone physiology (Figure 38).

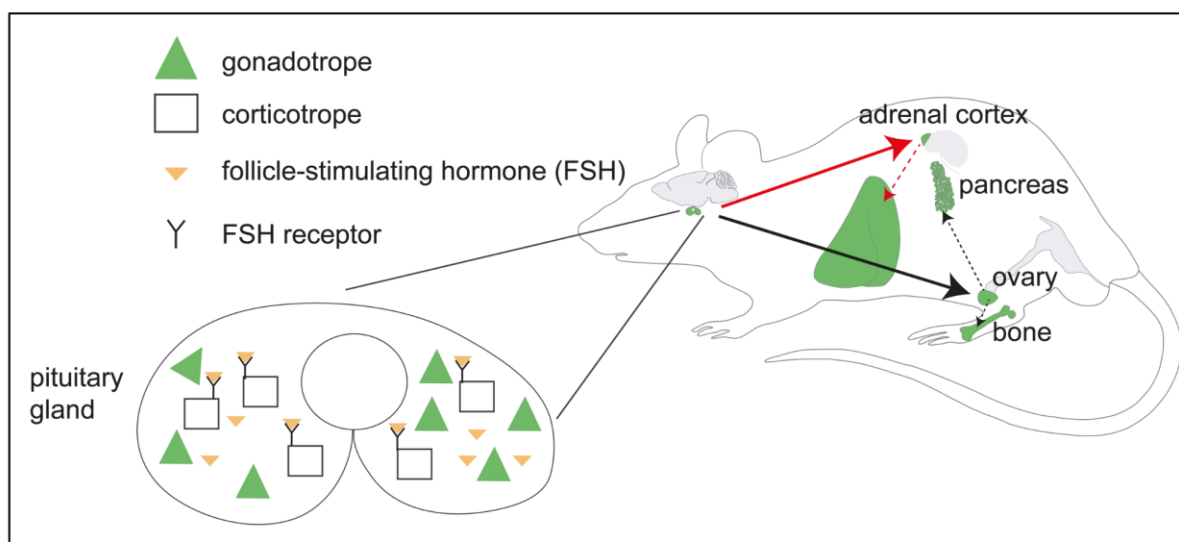


Figure 38: FSH receptor expression in the pituitary. Model of gonadotrope actions on the gonads and the pituitary. The demonstration of paracrine signaling within the pituitary -most likely to corticotropes- is essential to prevent the development of hepatic steatosis. (filled black arrow illustrates gonadotrope actions on the gonads; dashed black arrow indicates indirect gonadotrope effects on pancreas and bone via sex steroids released by the gonads; filled red arrow indicates corticotrope on the adrenal cortex (via paracrine FSH intra-pituitary action); dashed red arrow indicates the effect of elevated corticosterone levels on the liver).

Interestingly, by revisiting a human pituitary single cell RNA-seq database (Zhang *et al.*, 2020), FSHR was indeed expressed in the corticotropes but not in other hormone-producing cells in the pituitary. qPCR analysis revealed significant expression of *Fshr* in the pituitary but not in the liver (Figure 31,

32). The anterior pituitary gland is a key regulator of mammalian body homeostasis and communication between different organs via the coordinated release of distinct hormones (Friesen & Astwood, 1965). Different pituitary cell types produce growth hormone, prolactin, thyroid-stimulating hormone, adrenocorticotrophic hormone, or gonadotropins, which act on distinct target organs. However, communication between the gonadotrope and corticotrope cell networks is bidirectional. While gonadotropes act via paracrine FSH action on corticotropes in adults, the establishment of the corticotrope network controls the anatomical organization of the gonadotrope network during fetal development (Budry *et al.*, 2011). The inverse functional inter-network communication between these two endocrine cell populations may also provide an explanation for why gonadotropes and corticotropes are intermingled and invariantly positioned in close proximity to each other in the gland (Budry *et al.*, 2011) (Figure 34). These findings suggest that FSH might have elicited biological effects through the action in the pituitary. This has revealed a potential mechanism by which the FSH level might regulate lipid metabolism through the corticotropes and hepatic GR signaling.

FSHR has been reported to be expressed in several extragonadal tissues (Chrusciel *et al.*, 2019). In our studies, we found that FSH-receptor was detected only in two tissues, the ovary and the pituitary (Figure 31,32). These data provide the first clear evidence in the pituitary *in vivo* for an emerging endocrine paradigm; the structural and functional organization of one endocrine cell type can impinge on the functioning of other endocrine cells within the same gland. Other important examples include pancreatic islets in which alpha glucagon cells act on beta cells (Gromada, Chabosseau & Rutter, 2018). Several studies have provided evidence that insulin suppresses glucagon secretion (Kawamori *et al.*, 2009). This effect could be mediated directly via insulin receptors on the alpha cells or indirectly via increased somatostatin secretion from neighboring delta cells (Gromada, Chabosseau & Rutter, 2018).

Throughout these experiments, we have investigated the function of one of the gonadotropins, FSH, extensively in the development of metabolic syndrome. Until now, we have not yet studied the functional role of the other gonadotropin, LH, in this syndrome. To investigate this further, our lab has generated a new Cre driver mouse line, LHRT465I-IRES-CRE, in which Cre expression is driven by the LHR promoter, giving us genetic access to major cell types of the reproductive axis. This mouse line also carries a mutation in the LHR gene, which was identified in infertile patients. By crossing this mouse line with the reporter mouse line τ GFP, we will be able to map LHR expression in different genders, tissues, and developmental stages of mice. Furthermore, by comparing the homozygous genotype with wild type littermates, we can extensively study the function of LH in the development of metabolic syndrome.

Our findings demonstrating functional crosstalk between gonadotropes and corticotropes now set the stage to look at additional means of communication between different hormonal cell types in the anterior pituitary gland. Progress should be facilitated by the technical advances presented here using stereotactic injections of Cre-dependent AAVs carrying specific guide RNAs into the pituitary to achieve gene

conditional knock-outs in this tissue representing a major temporal advantage over classical gene targeting techniques (Candlish, De Angelis, Götz & Boehm, 2015). Furthermore, adaptation of this technique to include several guide RNAs should allow to knock out multiple genes simultaneously, providing an additional temporal and spatial advantage and also allowing to reduce the number of animals needed for multiple gene knock-outs.

Finally, these results highlight the potential clinical utility of FSH receptor agonism for the treatment of metabolic syndrome and also open the possibility of drug repurposing for FSH.

4.3 FSH: a new therapeutic avenue?

The excessive accumulation of fat in the liver causes NAFLD. Moreover, steatosis can progress to NASH. NASH is frequently associated with metabolic disorders including dyslipidemia, obesity, and diabetes (Eckel, Grundy & Zimmet, 2005). Despite the fact that >25% of the world's population suffer from NAFLD, there is until now no effective treatment for NASH or NAFLD (Estes *et al.*, 2018). In our study, we found that FSH plays a key role in body homeostasis and symptoms of metabolic disorders.

Reproductive axis dysfunction has previously been implicated in the development of metabolic disorders. For example, estrogens have been reported to have a protective role in postmenopausal women against NAFLD and osteoporosis but also have strong adverse effects leading to breast cancer and other undesirable side effects (Hart-Unger *et al.*, 2017). This has led us to develop another targeting strategy against NAFLD based on our findings of the essential role of FSH in body homeostasis. Several publications suggest that estrogen signaling modulates the risk of NAFLD. Additionally, women with congenital estrogen deficiency as a result of Turners syndrome are at high risk for developing NAFLD. Similarly, men with congenital testosterone deficiency as a result of Klinefelter syndrome (47, XXY) are four times more likely to develop the metabolic syndrome (Ishikawa, Yamaguchi, Kondo, Takenaka & Fujisawa, 2008). Moreover, the suppression of the reproductive axis in men using GnRH analogs, as for the treatment of prostate cancer, triggers weight gain, bone loss, and insulin resistance (M. R. Smith *et al.*, 2001; S. M. Smith & Vale, 2006). In my thesis, we found that both chronic chemogenetic activation of gonadotropes and FSH administration improves the symptoms of metabolic syndrome in hypogonadal female mice. This supports our hypothesis that FSH acting via its receptor (FSHR) activates paracrine trophic effects in the pituitary on corticotrope cells.

Gonadotropins are known to be essential regulators of reproductive organs. However, some studies have demonstrated that the interaction between FSH and its receptors plays physiological roles in fat and bone tissues. Our data do not support the previous model of FSH action in bone. Instead, by using complementary approaches in mice, we demonstrate unequivocally that gonadotropins influence bone metabolism indirectly via sex steroid production and not by direct action on bone. Loss of sex hormones was previously described to contribute to bone loss; however, direct FSH effects on bone were debated (Baron *et al.*, 2006; Seibel, Dunstan, Zhou, Allan & Handelsman, 2006). While osteoporosis after

gonadectomy had been attributed to decreased sex hormone levels (Riggs *et al.*, 2002), several studies challenged this view by reporting that FSH directly regulated bone metabolism. Global FSH β or FSHR knock-out in female mice resulted in hypogonadism without bone loss, consistent with a protective role for FSH on bone (L. Sun *et al.*, 2006). Combined with *in vitro* studies, the authors speculated that this effect of FSH on bone metabolism is direct and independent of estrogen. One caveat we need to consider is that FSH β or FSHR were removed in the germline in these animals. Since FSH signaling is one key regulator of sexual maturation, a global knock-out of FSH β or FSHR could have developmental effects including compensation in these models. Therefore, the reported bone phenotype could for example result from elevated LH and/or testosterone levels as reported (Danilovich *et al.*, 2000).

Our findings, that FSH injection reduces weight gain and improved glucose tolerance in the absence of either ovarian or supplemented estradiol, highlight the potential clinical benefit of FSH receptor agonism. Therapeutics that target FSH signaling in the pituitary, when combined, may offer new therapy options for postmenopausal steatosis and osteoporosis. Immunoglobulins, doubly active chimeric gonadotropins, and allosteric ligands bound to FSH could be promising candidates for future tailored pharmaceutical treatments for these individuals.

Conclusions

Our data reveal a crucial role for the reproductive system in preventing metabolic syndrome-like symptoms in female mice. The ablation of gonadotropes or ovariectomy were both sufficient to trigger weight gain, decrease insulin sensitivity and cause hepatic steatosis in female mice however ovariectomy alone was insufficient to cause hepatic steatosis, pointing to the role of the gonadotropes independent of the gonads. By knocking out the *Fshr* within the pituitary using a viral CRISPR/Cas9 approach we were able to demonstrate that paracrine signaling within the pituitary – most likely to corticotropes – is essential to prevent the development of hepatic steatosis. Consistent with this, FSH injections or chemogenetic gonadotrope activation (which drives FSH secretion) improved liver pathology. Despite demonstrating a clear role for estradiol in preventing the development of obesity and decreased insulin sensitivity, FSH injection and gonadotrope activation both reduced weight gain and improved glucose tolerance. This occurred in the absence of either ovarian or supplemented estradiol. Sex hormones have been well studied to have fundamental contributions to bone loss. However, whether gonadotropins - especially FSH - have direct effects on bone tissue is still under debate. In our study, by using complementary approaches of genetic mouse models, we demonstrate unequivocally that gonadotropins prevent bone loss via gonadal sex steroid production in both males and females.

The extra-gonadal actions of gonadotropins, especially FSH, were not previously reported. However, the mechanism underlying these actions is still not clear. By screening for the FSH receptor expression, we identified the pituitary as a target organ of FSH. By *in vitro* pituitary stimulation assay, plasma GC level measurement, and especially disruption of FSHR in the pituitary, we revealed an FSH paracrine signaling mechanism, most likely in the corticotropes, regulating the liver metabolism. Interestingly, by re-analysis of a human pituitary single cell RNA-seq database, we confirmed that FSHR is indeed expressed in the corticotropes but not in other hormone-producing cells in the pituitary, indicating potential translation of our preclinical observations to patients. These findings revealed a potential mechanism through which FSH might regulate lipid metabolism through the corticotropes and hepatic GR signaling, which make FSH a potential therapeutic option for steatosis.

Bibliography

- Abel, M. H., Huhtaniemi, I., Pakarinen, P., Kumar, T. R., & Charlton, H. M. (2003). Age-related uterine and ovarian hypertrophy in FSH receptor knock-out and FSHbeta subunit knock-out mice. *Reproduction*, *125*(2), 165-173. doi:10.1530/rep.0.1250165
- Aigner, F., Maier, H. T., Schwelberger, H. G., Wallnofer, E. A., Amberger, A., Obrist, P., Troppmair, J. (2007). Lipocalin-2 regulates the inflammatory response during ischemia and reperfusion of the transplanted heart. *Am J Transplant*, *7*(4), 779-788. doi:10.1111/j.1600-6143.2006.01723.x
- Allan, C. M., Kalak, R., Dunstan, C. R., McTavish, K. J., Zhou, H., Handelsman, D. J., & Seibel, M. J. (2010). Follicle-stimulating hormone increases bone mass in female mice. *Proc Natl Acad Sci U S A*, *107*(52), 22629-22634. doi:10.1073/pnas.1012141108
- Angulo, P. (2002). Nonalcoholic fatty liver disease. *N Engl J Med*, *346*(16), 1221-1231. doi:10.1056/NEJMra011775
- Angulo, P., Keach, J. C., Batts, K. P., & Lindor, K. D. (1999). Independent predictors of liver fibrosis in patients with nonalcoholic steatohepatitis. *Hepatology*, *30*(6), 1356-1362. doi:10.1002/hep.510300604
- Aoki, M., Wartenberg, P., Grunewald, R., Phillipps, H. R., Wyatt, A., Grattan, D. R., & Boehm, U. (2019). Widespread Cell-Specific Prolactin Receptor Expression in Multiple Murine Organs. *Endocrinology*, *160*(11), 2587-2599. doi:10.1210/en.2019-00234
- Arshad, T., Golabi, P., Paik, J., Mishra, A., & Younossi, Z. M. (2019). Prevalence of Nonalcoholic Fatty Liver Disease in the Female Population. *Hepatol Commun*, *3*(1), 74-83. doi:10.1002/hep4.1285
- Asimakopoulou, A., Weiskirchen, S., & Weiskirchen, R. (2016). Lipocalin 2 (LCN2) Expression in Hepatic Malfunction and Therapy. *Front Physiol*, *7*, 430. doi:10.3389/fphys.2016.00430
- Astuti, D., Latif, F., Dallol, A., Dahia, P. L., Douglas, F., George, E., Maher, E. R. (2001). Gene mutations in the succinate dehydrogenase subunit SDHB cause susceptibility to familial pheochromocytoma and to familial paraganglioma. *Am J Hum Genet*, *69*(1), 49-54. doi:10.1086/321282
- Ayonrinde, O. T., Olynyk, J. K., Beilin, L. J., Mori, T. A., Pennell, C. E., de Klerk, N., Adams, L. A. (2011). Gender-specific differences in adipose distribution and adipocytokines influence adolescent nonalcoholic fatty liver disease. *Hepatology*, *53*(3), 800-809. doi:10.1002/hep.24097
- Azziz, R., Carmina, E., Dewailly, D., Diamanti-Kandarakis, E., Escobar-Morreale, H. F., Futterweit, W., Androgen Excess, S. (2006). Positions statement: criteria for defining polycystic ovary syndrome as a predominantly hyperandrogenic syndrome: an Androgen Excess Society guideline. *J Clin Endocrinol Metab*, *91*(11), 4237-4245. doi:10.1210/jc.2006-0178

- Bae, S., Park, J., & Kim, J. S. (2014). Cas-OFFinder: a fast and versatile algorithm that searches for potential off-target sites of Cas9 RNA-guided endonucleases. *Bioinformatics*, *30*(10), 1473-1475. doi:10.1093/bioinformatics/btu048
- Baig, M. A., & Bacha, D. (2021). Histology, Bone. In *StatPearls*. Treasure Island (FL).
- Baron, R. (2006). FSH versus estrogen: who's guilty of breaking bones? *Cell Metab*, *3*(5), 302-305. doi:10.1016/j.cmet.2006.04.007
- Bentley-Lewis, R., Koruda, K., & Seely, E. W. (2007). The metabolic syndrome in women. *Nat Clin Pract Endocrinol Metab*, *3*(10), 696-704. doi:10.1038/ncpendmet0616
- Bone cells, sclerostin, and FGF23: what's bred in the bone will come out in the flesh. (2015). *Kidney Int*, *88*(1), 203. doi:10.1038/ki.2015.154
- Brosch, M., Kattler, K., Herrmann, A., von Schonfels, W., Nordstrom, K., Seehofer, D., Hampe, J. (2018). Epigenomic map of human liver reveals principles of zonated morphogenic and metabolic control. *Nat Commun*, *9*(1), 4150. doi:10.1038/s41467-018-06611-5
- Buch, T., Heppner, F. L., Tertilt, C., Heinen, T. J., Kremer, M., Wunderlich, F. T., Waisman, A. (2005). A Cre-inducible diphtheria toxin receptor mediates cell lineage ablation after toxin administration. *Nat Methods*, *2*(6), 419-426. doi:10.1038/nmeth762
- Buckley, L., & Humphrey, M. B. (2018). Glucocorticoid-Induced Osteoporosis. *N Engl J Med*, *379*(26), 2547-2556. doi:10.1056/NEJMcp1800214
- Budry, L., Lafont, C., El Yandouzi, T., Chauvet, N., Conejero, G., Drouin, J., & Mollard, P. (2011). Related pituitary cell lineages develop into interdigitated 3D cell networks. *Proc Natl Acad Sci U S A*, *108*(30), 12515-12520. doi:10.1073/pnas.1105929108
- Bugianesi, E., McCullough, A. J., & Marchesini, G. (2005). Insulin resistance: a metabolic pathway to chronic liver disease. *Hepatology*, *42*(5), 987-1000. doi:10.1002/hep.20920
- Candlish, M., De Angelis, R., Gotz, V., & Boehm, U. (2015). Gene Targeting in Neuroendocrinology. *Compr Physiol*, *5*(4), 1645-1676. doi:10.1002/cphy.c140079
- Casarini, L., & Crepieux, P. (2019). Molecular Mechanisms of Action of FSH. *Front Endocrinol (Lausanne)*, *10*, 305. doi:10.3389/fendo.2019.00305
- Chen, J. F., Lin, P. W., Tsai, Y. R., Yang, Y. C., & Kang, H. Y. (2019). Androgens and Androgen Receptor Actions on Bone Health and Disease: From Androgen Deficiency to Androgen Therapy. *Cells*, *8*(11). doi:10.3390/cells8111318
- Chrusciel, M., Ponikwicka-Tyszko, D., Wolczynski, S., Huhtaniemi, I., & Rahman, N. A. (2019). Extragonadal FSHR Expression and Function-Is It Real? *Front Endocrinol (Lausanne)*, *10*, 32. doi:10.3389/fendo.2019.00032
- Clement, K., Rees, H., Canver, M. C., Gehrke, J. M., Farouni, R., Hsu, J. Y., Pinello, L. (2019). CRISPResso2 provides accurate and rapid genome editing sequence analysis. *Nat Biotechnol*, *37*(3), 224-226. doi:10.1038/s41587-019-0032-3

- Concordet, J. P., & Haeussler, M. (2018). CRISPOR: intuitive guide selection for CRISPR/Cas9 genome editing experiments and screens. *Nucleic Acids Res*, *46*(W1), W242-W245. doi:10.1093/nar/gky354
- Couillard, C., Gagnon, J., Bergeron, J., Leon, A. S., Rao, D. C., Skinner, J. S., Bouchard, C. (2000). Contribution of body fatness and adipose tissue distribution to the age variation in plasma steroid hormone concentrations in men: the HERITAGE Family Study. *J Clin Endocrinol Metab*, *85*(3), 1026-1031. doi:10.1210/jcem.85.3.6427
- Danilovich, N., Babu, P. S., Xing, W., Gerdes, M., Krishnamurthy, H., & Sairam, M. R. (2000). Estrogen deficiency, obesity, and skeletal abnormalities in follicle-stimulating hormone receptor knock-out (FORKO) female mice. *Endocrinology*, *141*(11), 4295-4308. doi:10.1210/endo.141.11.7765
- Dietrich, P., & Hellerbrand, C. (2014). Non-alcoholic fatty liver disease, obesity and the metabolic syndrome. *Best Pract Res Clin Gastroenterol*, *28*(4), 637-653. doi:10.1016/j.bpg.2014.07.008
- Eckel, R. H., Grundy, S. M., & Zimmet, P. Z. (2005). The metabolic syndrome. *Lancet*, *365*(9468), 1415-1428. doi:10.1016/S0140-6736(05)66378-7
- Edwardson, C. L., Gorely, T., Davies, M. J., Gray, L. J., Khunti, K., Wilmot, E. G., Biddle, S. J. (2012). Association of sedentary behaviour with metabolic syndrome: a meta-analysis. *PLoS One*, *7*(4), e34916. doi:10.1371/journal.pone.0034916
- Estes, C., Anstee, Q. M., Arias-Loste, M. T., Bantel, H., Bellentani, S., Caballeria, J., Razavi, H. (2018). Modeling NAFLD disease burden in China, France, Germany, Italy, Japan, Spain, United Kingdom, and United States for the period 2016-2030. *J Hepatol*, *69*(4), 896-904. doi:10.1016/j.jhep.2018.05.036
- Filippou, P., & Homburg, R. (2017). Is foetal hyperexposure to androgens a cause of PCOS? *Hum Reprod Update*, *23*(4), 421-432. doi:10.1093/humupd/dmx013
- Frenkel, B., White, W., & Tuckermann, J. (2015). Glucocorticoid-Induced Osteoporosis. *Adv Exp Med Biol*, *872*, 179-215. doi:10.1007/978-1-4939-2895-8_8
- Friedrich, G., & Soriano, P. (1991). Promoter traps in embryonic stem cells: a genetic screen to identify and mutate developmental genes in mice. *Genes Dev*, *5*(9), 1513-1523. doi:10.1101/gad.5.9.1513
- Gathercole, L. L., Morgan, S. A., Bujalska, I. J., Hauton, D., Stewart, P. M., & Tomlinson, J. W. (2011). Regulation of lipogenesis by glucocorticoids and insulin in human adipose tissue. *PLoS One*, *6*(10), e26223. doi:10.1371/journal.pone.0026223
- Geer, E. B., Islam, J., & Buettner, C. (2014). Mechanisms of glucocorticoid-induced insulin resistance: focus on adipose tissue function and lipid metabolism. *Endocrinol Metab Clin North Am*, *43*(1), 75-102. doi:10.1016/j.ecl.2013.10.005
- Golds, G., Houdek, D., & Arnason, T. (2017). Male Hypogonadism and Osteoporosis: The Effects, Clinical Consequences, and Treatment of Testosterone Deficiency in Bone Health. *Int J Endocrinol*, *2017*, 4602129. doi:10.1155/2017/4602129

- Gore, A. C. (2002). GnRH: The master molecule of reproduction. Norwell, Massachusetts: Kluwer Academic Publishers.
- Götz, V., Qiao, S., Beck, A., & Boehm, U. (2017). Transient receptor potential (TRP) channel function in the reproductive axis. *Cell Calcium*, *67*, 138-147. doi:10.1016/j.ceca.2017.04.004
- Granneman, J. G., Moore, H. P., Mottillo, E. P., Zhu, Z., & Zhou, L. (2011). Interactions of perilipin-5 (Plin5) with adipose triglyceride lipase. *J Biol Chem*, *286*(7), 5126-5135. doi:10.1074/jbc.M110.180711
- Gromada, J., Chabosseau, P., & Rutter, G. A. (2018). The alpha-cell in diabetes mellitus. *Nat Rev Endocrinol*, *14*(12), 694-704. doi:10.1038/s41574-018-0097-y
- Gu, H., Marth, J. D., Orban, P. C., Mossmann, H., & Rajewsky, K. (1994). Deletion of a DNA polymerase beta gene segment in T cells using cell type-specific gene targeting. *Science*, *265*(5168), 103-106. doi:10.1126/science.8016642
- Guo, Y., Zhao, M., Bo, T., Ma, S., Yuan, Z., Chen, W., Zhao, J. (2019). Blocking FSH inhibits hepatic cholesterol biosynthesis and reduces serum cholesterol. *Cell Res*, *29*(2), 151-166. doi:10.1038/s41422-018-0123-6
- Haider, A., Gooren, L. J., Padungtod, P., & Saad, F. (2010). Improvement of the metabolic syndrome and of non-alcoholic liver steatosis upon treatment of hypogonadal elderly men with parenteral testosterone undecanoate. *Exp Clin Endocrinol Diabetes*, *118*(3), 167-171. doi:10.1055/s-0029-1202774
- Han, S. K., Gottsch, M. L., Lee, K. J., Popa, S. M., Smith, J. T., Jakawich, S. K., Herbison, A. E. (2005). Activation of gonadotropin-releasing hormone neurons by kisspeptin as a neuroendocrine switch for the onset of puberty. *J Neurosci*, *25*(49), 11349-11356. doi:10.1523/JNEUROSCI.3328-05.2005
- Hannenhalli, S., & Kaestner, K. H. (2009). The evolution of Fox genes and their role in development and disease. *Nat Rev Genet*, *10*(4), 233-240. doi:10.1038/nrg2523
- Hart-Unger, S., Arao, Y., Hamilton, K. J., Lierz, S. L., Malarkey, D. E., Hewitt, S. C., Korach, K. S. (2017). Hormone signaling and fatty liver in females: analysis of estrogen receptor alpha mutant mice. *Int J Obes (Lond)*, *41*(6), 945-954. doi:10.1038/ijo.2017.50
- Harter, C. J. L., Kavanagh, G. S., & Smith, J. T. (2018). The role of kisspeptin neurons in reproduction and metabolism. *J Endocrinol*, *238*(3), R173-R183. doi:10.1530/JOE-18-0108
- Hashimoto, E., & Tokushige, K. (2011). Prevalence, gender, ethnic variations, and prognosis of NASH. *J Gastroenterol*, *46 Suppl 1*, 63-69. doi:10.1007/s00535-010-0311-8
- Hellier, V., Brock, O., Candlish, M., Desroziers, E., Aoki, M., Mayer, C., Bakker, J. (2018). Female sexual behavior in mice is controlled by kisspeptin neurons. *Nat Commun*, *9*(1), 400. doi:10.1038/s41467-017-02797-2
- Herbison, A. E. (2016). Control of puberty onset and fertility by gonadotropin-releasing hormone neurons. *Nat Rev Endocrinol*, *12*(8), 452-466. doi:10.1038/nrendo.2016.70

- Hernlund, E., Svedbom, A., Ivergard, M., Compston, J., Cooper, C., Stenmark, J., Kanis, J. A. (2013). Osteoporosis in the European Union: medical management, epidemiology and economic burden. A report prepared in collaboration with the International Osteoporosis Foundation (IOF) and the European Federation of Pharmaceutical Industry Associations (EFPIA). *Arch Osteoporos*, 8, 136. doi:10.1007/s11657-013-0136-1
- Hirdes, W., Dinu, C., Bauer, C. K., Boehm, U., & Schwarz, J. R. (2010). Gonadotropin-releasing hormone inhibits ether-a-go-go-related gene K⁺ currents in mouse gonadotropes. *Endocrinology*, 151(3), 1079-1088. doi:10.1210/en.2009-0718
- Hirode, G., & Wong, R. J. (2020). Trends in the Prevalence of Metabolic Syndrome in the United States, 2011-2016. *JAMA*, 323(24), 2526-2528. doi:10.1001/jama.2020.4501
- Hoess, R., Abremski, K., & Sternberg, N. (1984). The nature of the interaction of the P1 recombinase Cre with the recombining site loxP. *Cold Spring Harb Symp Quant Biol*, 49, 761-768. doi:10.1101/sqb.1984.049.01.086
- Hughes, D. E., Dai, A., Tiffie, J. C., Li, H. H., Mundy, G. R., & Boyce, B. F. (1996). Estrogen promotes apoptosis of murine osteoclasts mediated by TGF-beta. *Nat Med*, 2(10), 1132-1136. doi:10.1038/nm1096-1132
- Ingberg, E., Theodorsson, A., Theodorsson, E., & Strom, J. O. (2012). Methods for long-term 17beta-estradiol administration to mice. *Gen Comp Endocrinol*, 175(1), 188-193. doi:10.1016/j.ygcen.2011.11.014
- Ishikawa, T., Yamaguchi, K., Kondo, Y., Takenaka, A., & Fujisawa, M. (2008). Metabolic syndrome in men with Klinefelter's syndrome. *Urology*, 71(6), 1109-1113. doi:10.1016/j.urology.2008.01.051
- Jeon, U. S. (2008). Kidney and calcium homeostasis. *Electrolyte Blood Press*, 6(2), 68-76. doi:10.5049/EBP.2008.6.2.68
- Juszczak, A., Morris, D., & Grossman, A. (2000). Cushing's Syndrome. In K. R. Feingold, B. Anawalt, A. Boyce, G. Chrousos, W. W. de Herder, K. Dhatariya, K. Dungan, J. M. Hershman, J. Hofland, S. Kalra, G. Kaltsas, C. Koch, P. Kopp, M. Korbonits, C. S. Kovacs, W. Kuohung, B. Laferrere, M. Levy, E. A. McGee, R. McLachlan, J. E. Morley, M. New, J. Purnell, R. Sahay, F. Singer, M. A. Sperling, C. A. Stratakis, D. L. Trencce, & D. P. Wilson (Eds.), *Endotext*. South Dartmouth (MA).
- Kalra, A., Yetiskul, E., Wehrle, C. J., & Tuma, F. (2021). Physiology, Liver. In *StatPearls*. Treasure Island (FL).
- Kanis, J. A. (1994). Assessment of fracture risk and its application to screening for postmenopausal osteoporosis: synopsis of a WHO report. WHO Study Group. *Osteoporos Int*, 4(6), 368-381. doi:10.1007/BF01622200

- Kawamori, D., Kurpad, A. J., Hu, J., Liew, C. W., Shih, J. L., Ford, E. L., . . . Kulkarni, R. N. (2009). Insulin signaling in alpha cells modulates glucagon secretion *in vivo*. *Cell Metab*, 9(4), 350-361. doi:10.1016/j.cmet.2009.02.007
- Khosla, S. (2020). Estrogen Versus FSH Effects on Bone Metabolism: Evidence From Interventional Human Studies. *Endocrinology*, 161(8). doi:10.1210/endocr/bqaa111
- Kiela, P. R., & Ghishan, F. K. (2009). Recent advances in the renal-skeletal-gut axis that controls phosphate homeostasis. *Lab Invest*, 89(1), 7-14. doi:10.1038/labinvest.2008.114
- Kumar, T. R. (2014). Extragonadal FSH receptor: is it real? *Biol Reprod*, 91(4), 99. doi:10.1095/biolreprod.114.124222
- Kupelian, V., Page, S. T., Araujo, A. B., Travison, T. G., Bremner, W. J., & McKinlay, J. B. (2006). Low sex hormone-binding globulin, total testosterone, and symptomatic androgen deficiency are associated with development of the metabolic syndrome in nonobese men. *J Clin Endocrinol Metab*, 91(3), 843-850. doi:10.1210/jc.2005-1326
- Labun, K., Montague, T. G., Krause, M., Torres Cleuren, Y. N., Tjeldnes, H., & Valen, E. (2019). CHOPCHOP v3: expanding the CRISPR web toolbox beyond genome editing. *Nucleic Acids Res*, 47(W1), W171-W174. doi:10.1093/nar/gkz365
- Le Tissier, P., Campos, P., Lafont, C., Romano, N., Hodson, D. J., & Mollard, P. (2017). An updated view of hypothalamic-vascular-pituitary unit function and plasticity. *Nat Rev Endocrinol*, 13(5), 257-267. doi:10.1038/nrendo.2016.193
- Lenders, J. W., Pacak, K., Walther, M. M., Linehan, W. M., Mannelli, M., Friberg, P., Eisenhofer, G. (2002). Biochemical diagnosis of pheochromocytoma: which test is best? *JAMA*, 287(11), 1427-1434. doi:10.1001/jama.287.11.1427
- Lin, H. Y., Yu, I. C., Wang, R. S., Chen, Y. T., Liu, N. C., Altuwaijri, S., Chang, C. S. (2008). Increased hepatic steatosis and insulin resistance in mice lacking hepatic androgen receptor. *Hepatology*, 47(6), 1924-1935. doi:10.1002/hep.22252
- Liu, P., Ji, Y., Yuen, T., Rendina-Ruedy, E., DeMambro, V. E., Dhawan, S., Zaidi, M. (2017). Blocking FSH induces thermogenic adipose tissue and reduces body fat. *Nature*, 546(7656), 107-112. doi:10.1038/nature22342
- Livak, K. J., & Schmittgen, T. D. (2001). Analysis of relative gene expression data using real-time quantitative PCR and the 2(-Delta Delta C(T)) Method. *Methods*, 25(4), 402-408. doi:10.1006/meth.2001.1262
- Livingstone, D. E., Barat, P., Di Rollo, E. M., Rees, G. A., Weldin, B. A., Rog-Zielinska, E. A., Andrew, R. (2015). 5 α -Reductase type 1 deficiency or inhibition predisposes to insulin resistance, hepatic steatosis, and liver fibrosis in rodents. *Diabetes*, 64(2), 447-458. doi:10.2337/db14-0249
- Llovet, J. M., Bustamante, J., Castells, A., Vilana, R., Ayuso Mdel, C., Sala, M., Bruix, J. (1999). Natural history of untreated nonsurgical hepatocellular carcinoma: rationale for the design and evaluation of therapeutic trials. *Hepatology*, 29(1), 62-67. doi:10.1002/hep.510290145

- Loos, R. J., Rankinen, T., Perusse, L., Tremblay, A., Despres, J. P., & Bouchard, C. (2007). Association of lipin 1 gene polymorphisms with measures of energy and glucose metabolism. *Obesity (Silver Spring)*, *15*(11), 2723-2732. doi:10.1038/oby.2007.324
- Lunenfeld, B., Saad, F., & Hoesl, C. E. (2005). ISA, ISSAM and EAU recommendations for the investigation, treatment and monitoring of late-onset hypogonadism in males: scientific background and rationale. *Aging Male*, *8*(2), 59-74. doi:10.1080/13685530500163416
- Makarova, K. S., Wolf, Y. I., Alkhnbashi, O. S., Costa, F., Shah, S. A., Saunders, S. J., Koonin, E. V. (2015). An updated evolutionary classification of CRISPR-Cas systems. *Nat Rev Microbiol*, *13*(11), 722-736. doi:10.1038/nrmicro3569
- Malik, S., Wong, N. D., Franklin, S. S., Kamath, T. V., L'Italien, G. J., Pio, J. R., & Williams, G. R. (2004). Impact of the metabolic syndrome on mortality from coronary heart disease, cardiovascular disease, and all causes in United States adults. *Circulation*, *110*(10), 1245-1250. doi:10.1161/01.CIR.0000140677.20606.0E
- Manolagas, S. C., O'Brien, C. A., & Almeida, M. (2013). The role of estrogen and androgen receptors in bone health and disease. *Nat Rev Endocrinol*, *9*(12), 699-712. doi:10.1038/nrendo.2013.179
- Marschensini M.D. (2003). Nonalcoholic fatty liver, steatohepatitis, and the metabolic syndrome <https://doi.org/10.1053/jhep.2003.50161>.
- Mato, J. M., Alonso, C., Nouredin, M., & Lu, S. C. (2019). Biomarkers and subtypes of deranged lipid metabolism in non-alcoholic fatty liver disease. *World J Gastroenterol*, *25*(24), 3009-3020. doi:10.3748/wjg.v25.i24.3009
- Mehlem, A., Hagberg, C. E., Muhl, L., Eriksson, U., & Falkevall, A. (2013). Imaging of neutral lipids by oil red O for analyzing the metabolic status in health and disease. *Nat Protoc*, *8*(6), 1149-1154. doi:10.1038/nprot.2013.055
- Mills, E. G., Yang, L., Nielsen, M. F., Kassem, M., Dhillon, W. S., & Cominos, A. N. (2021). The Relationship Between Bone and Reproductive Hormones Beyond Estrogens and Androgens. *Endocr Rev*, *42*(6), 691-719. doi:10.1210/endrev/bnab015
- Mittan, D., Lee, S., Miller, E., Perez, R. C., Basler, J. W., & Bruder, J. M. (2002). Bone loss following hypogonadism in men with prostate cancer treated with GnRH analogs. *J Clin Endocrinol Metab*, *87*(8), 3656-3661. doi:10.1210/jcem.87.8.8782
- Moe, K. E. (2005). Menopause. *Karen E. Moe, in Principles and Practice of Sleep Medicine (Fourth Edition)*. doi:10.1016/j.cnur.2003.11.006
- Nakamura, T., Imai, Y., Matsumoto, T., Sato, S., Takeuchi, K., Igarashi, K., Kato, S. (2007). Estrogen prevents bone loss via estrogen receptor alpha and induction of Fas ligand in osteoclasts. *Cell*, *130*(5), 811-823. doi:10.1016/j.cell.2007.07.025
- Nicks, K. M., Perrien, D. S., Akel, N. S., Suva, L. J., & Gaddy, D. (2009). Regulation of osteoblastogenesis and osteoclastogenesis by the other reproductive hormones, Activin and Inhibin. *Mol Cell Endocrinol*, *310*(1-2), 11-20. doi:10.1016/j.mce.2009.07.001

- Oftadeh, R., Perez-Viloria, M., Villa-Camacho, J. C., Vaziri, A., & Nazarian, A. (2015). Biomechanics and mechanobiology of trabecular bone: a review. *J Biomech Eng*, *137*(1). doi:10.1115/1.4029176
- Omodei, U., Mazziotti, G., Donarini, G., Gola, M., Guella, V., Pagani, F., Giustina, A. (2013). Effects of recombinant follicle-stimulating hormone on bone turnover markers in infertile women undergoing *in vitro* fertilization procedure. *J Clin Endocrinol Metab*, *98*(1), 330-336. doi:10.1210/jc.2012-2778
- Ott, Susan M. (2015). Bone cells, sclerostin, and FGF23: what's bred in the bone will come out in the flesh. *Kidney Int*, *88*(1), 203. doi:10.1038/ki.2015.154
- Patel, R., Williams-Dautovich, J., & Cummins, C. L. (2014). Minireview: new molecular mediators of glucocorticoid receptor activity in metabolic tissues. *Mol Endocrinol*, *28*(7), 999-1011. doi:10.1210/me.2014-1062
- Perumpail, B. J., Khan, M. A., Yoo, E. R., Cholankeril, G., Kim, D., & Ahmed, A. (2017). Clinical epidemiology and disease burden of nonalcoholic fatty liver disease. *World J Gastroenterol*, *23*(47), 8263-8276. doi:10.3748/wjg.v23.i47.8263
- Pivonello, R., De Leo, M., Vitale, P., Cozzolino, A., Simeoli, C., De Martino, M. C., Colao, A. (2010). Pathophysiology of diabetes mellitus in Cushing's syndrome. *Neuroendocrinology*, *92 Suppl 1*, 77-81. doi:10.1159/000314319
- Pratley, R. E., Coon, P. J., Rogus, E. M., & Goldberg, A. P. (1995). Effects of weight loss on norepinephrine and insulin levels in obese older men. *Metabolism*, *44*(4), 438-444. doi:10.1016/0026-0495(95)90049-7
- Qiao, S., Nordstrom, K., Muijs, L., Gasparoni, G., Tierling, S., Krause, E., Boehm, U. (2016). Molecular Plasticity of Male and Female Murine Gonadotropes Revealed by mRNA Sequencing. *Endocrinology*, *157*(3), 1082-1093. doi:10.1210/en.2015-1836
- Quinn, M. A., Xu, X., Ronfani, M., & Cidlowski, J. A. (2018). Estrogen Deficiency Promotes Hepatic Steatosis via a Glucocorticoid Receptor-Dependent Mechanism in Mice. *Cell Rep*, *22*(10), 2690-2701. doi:10.1016/j.celrep.2018.02.041
- Quirk, M., Kim, Y. H., Saab, S., & Lee, E. W. (2015). Management of hepatocellular carcinoma with portal vein thrombosis. *World J Gastroenterol*, *21*(12), 3462-3471. doi:10.3748/wjg.v21.i12.3462
- Rafacho, A., Ortsater, H., Nadal, A., & Quesada, I. (2014). Glucocorticoid treatment and endocrine pancreas function: implications for glucose homeostasis, insulin resistance and diabetes. *J Endocrinol*, *223*(3), R49-62. doi:10.1530/JOE-14-0373
- Rebar, R., Judd, H. L., Yen, S. S., Rakoff, J., Vandenberg, G., & Naftolin, F. (1976). Characterization of the inappropriate gonadotropin secretion in polycystic ovary syndrome. *J Clin Invest*, *57*(5), 1320-1329. doi:10.1172/JCI108400

- Riggs, B. L., Khosla, S., & Melton, L. J., 3rd. (2002). Sex steroids and the construction and conservation of the adult skeleton. *Endocr Rev*, *23*(3), 279-302. doi:10.1210/edrv.23.3.0465
- Rockall, A. G., Sohaib, S. A., Evans, D., Kaltsas, G., Isidori, A. M., Monson, J. P., Reznick, R. H. (2003). Hepatic steatosis in Cushing's syndrome: a radiological assessment using computed tomography. *Eur J Endocrinol*, *149*(6), 543-548. doi:10.1530/eje.0.1490543
- Sapolsky, R. M., Romero, L. M., & Munck, A. U. (2000). How Do Glucocorticoids Influence Stress Responses? Integrating Permissive, Suppressive, Stimulatory, and Preparative Actions. *Endocrine Reviews*, *21*(1), 55-89. doi:10.1210/edrv.21.1.0389
- Sauer, B., & Henderson, N. (1988). The cyclization of linear DNA in Escherichia coli by site-specific recombination. *Gene*, *70*(2), 331-341. doi:10.1016/0378-1119(88)90205-3
- Schacke, H., Docke, W. D., & Asadullah, K. (2002). Mechanisms involved in the side effects of glucocorticoids. *Pharmacol Ther*, *96*(1), 23-43. doi:10.1016/s0163-7258(02)00297-8
- Seminara, S. B., Messager, S., Chatzidaki, E. E., Thresher, R. R., Acierno, J. S., Jr., Shagoury, J. K., Colledge, W. H. (2003). The GPR54 gene as a regulator of puberty. *N Engl J Med*, *349*(17), 1614-1627. doi:10.1056/NEJMoa035322
- Shieh, A., Greendale, G. A., Cauley, J. A., Karvonen-Gutierrez, C., Crandall, C. J., & Karlamangla, A. S. (2019). Estradiol and Follicle-Stimulating Hormone as Predictors of Onset of Menopause Transition-Related Bone Loss in Pre- and Perimenopausal Women. *J Bone Miner Res*, *34*(12), 2246-2253. doi:10.1002/jbmr.3856
- Smith, M. R., McGovern, F. J., Zietman, A. L., Fallon, M. A., Hayden, D. L., Schoenfeld, D. A., Finkelstein, J. S. (2001). Pamidronate to prevent bone loss during androgen-deprivation therapy for prostate cancer. *N Engl J Med*, *345*(13), 948-955. doi:10.1056/NEJMoa010845
- Smith, S. M., & Vale, W. W. (2006). The role of the hypothalamic-pituitary-adrenal axis in neuroendocrine responses to stress. *Dialogues Clin Neurosci*, *8*(4), 383-395.
- Soriano, P. (1999). Generalized lacZ expression with the ROSA26 Cre reporter strain. *Nat Genet*, *21*(1), 70-71. doi:10.1038/5007
- Sun, L., Peng, Y., Sharrow, A. C., Iqbal, J., Zhang, Z., Papachristou, D. J., Zaidi, M. (2006). FSH directly regulates bone mass. *Cell*, *125*(2), 247-260. doi:10.1016/j.cell.2006.01.051
- Sun, M., Wu, X., Yu, Y., Wang, L., Xie, D., Zhang, Z., Li, F. (2020). Disorders of Calcium and Phosphorus Metabolism and the Proteomics/Metabolomics-Based Research. *Front Cell Dev Biol*, *8*, 576110. doi:10.3389/fcell.2020.576110
- Tata, B., Mimouni, N. E. H., Barbotin, A. L., Malone, S. A., Loyens, A., Pigny, P., Giacobini, P. (2018). Elevated prenatal anti-Mullerian hormone reprograms the fetus and induces polycystic ovary syndrome in adulthood. *Nat Med*, *24*(6), 834-846. doi:10.1038/s41591-018-0035-5
- Tegelberg, P., Tervonen, T., Knuutila, M., Jokelainen, J., Keinanen-Kiukaanniemi, S., Auvinen, J., & Ylostalo, P. (2019). Long-term metabolic syndrome is associated with periodontal pockets and alveolar bone loss. *J Clin Periodontol*, *46*(8), 799-808. doi:10.1111/jcpe.13154

- Thomas, K. R., & Capecchi, M. R. (1987). Site-directed mutagenesis by gene targeting in mouse embryo-derived stem cells. *Cell*, *51*(3), 503-512. doi:10.1016/0092-8674(87)90646-5
- Tolson, K. P., Garcia, C., Yen, S., Simonds, S., Stefanidis, A., Lawrence, A., Kauffman, A. S. (2014). Impaired kisspeptin signaling decreases metabolism and promotes glucose intolerance and obesity. *J Clin Invest*, *124*(7), 3075-3079. doi:10.1172/JCI71075
- Torchen, L. C. (2017). Cardiometabolic Risk in PCOS: More than a Reproductive Disorder. *Curr Diab Rep*, *17*(12), 137. doi:10.1007/s11892-017-0956-2
- Torre, L. A., Bray, F., Siegel, R. L., Ferlay, J., Lortet-Tieulent, J., & Jemal, A. (2015). Global cancer statistics, 2012. *CA Cancer J Clin*, *65*(2), 87-108. doi:10.3322/caac.21262
- Tsutsumi, R., & Webster, N. J. (2009). GnRH pulsatility, the pituitary response and reproductive dysfunction. *Endocr J*, *56*(6), 729-737. doi:10.1507/endocrj.k09e-185
- Turchinovich, A., Baranova, A., Drapkina, O., & Tonevitsky, A. (2018). Cell-Free Circulating Nucleic Acids as Early Biomarkers for NAFLD and NAFLD-Associated Disorders. *Front Physiol*, *9*, 1256. doi:10.3389/fphys.2018.01256
- Uihlein, A. V., Finkelstein, J. S., Lee, H., & Leder, B. Z. (2014). FSH suppression does not affect bone turnover in eugonadal men. *J Clin Endocrinol Metab*, *99*(7), 2510-2515. doi:10.1210/jc.2013-3246
- Ulloa-Aguirre, A., Reiter, E., & Crepieux, P. (2018). FSH Receptor Signaling: Complexity of Interactions and Signal Diversity. *Endocrinology*, *159*(8), 3020-3035. doi:10.1210/en.2018-00452
- Unal, M., Cingoz, F., Bagcioglu, C., Sozer, Y., & Akkus, O. (2018). Interrelationships between electrical, mechanical and hydration properties of cortical bone. *J Mech Behav Biomed Mater*, *77*, 12-23. doi:10.1016/j.jmbbm.2017.08.033
- Vaananen, H. K., & Harkonen, P. L. (1996). Estrogen and bone metabolism. *Maturitas*, *23 Suppl*, S65-69. doi:10.1016/0378-5122(96)01015-8
- van Santbrink, E. J., Hop, W. C., & Fauser, B. C. (1997). Classification of normogonadotropic infertility: polycystic ovaries diagnosed by ultrasound versus endocrine characteristics of polycystic ovary syndrome. *Fertil Steril*, *67*(3), 452-458. doi:10.1016/s0015-0282(97)80068-4
- Venetsanaki, V., & Polyzos, S. A. (2019). Menopause and Non-Alcoholic Fatty Liver Disease: A Review Focusing on Therapeutic Perspectives. *Curr Vasc Pharmacol*, *17*(6), 546-555. doi:10.2174/1570161116666180711121949
- Wang, N., Kuang, L., Han, B., Li, Q., Chen, Y., Zhu, C., Lu, Y. (2016). Follicle-stimulating hormone associates with prediabetes and diabetes in postmenopausal women. *Acta Diabetol*, *53*(2), 227-236. doi:10.1007/s00592-015-0769-1
- Wang, N., Li, Q., Han, B., Chen, Y., Zhu, C., Chen, Y., Lu, Y. (2016). Follicle-stimulating hormone is associated with non-alcoholic fatty liver disease in Chinese women over 55 years old. *J Gastroenterol Hepatol*, *31*(6), 1196-1202. doi:10.1111/jgh.13271

- Weiss, J., Rau, M., & Geier, A. (2014). Non-alcoholic fatty liver disease: epidemiology, clinical course, investigation, and treatment. *Dtsch Arztebl Int*, *111*(26), 447-452. doi:10.3238/arztebl.2014.0447
- Weitzmann, M. N., & Ofotokun, I. (2016). Physiological and pathophysiological bone turnover - role of the immune system. *Nat Rev Endocrinol*, *12*(9), 518-532. doi:10.1038/nrendo.2016.91
- Wen, S., Ai, W., Alim, Z., & Boehm, U. (2010). Embryonic gonadotropin-releasing hormone signaling is necessary for maturation of the male reproductive axis. *Proc Natl Acad Sci U S A*, *107*(37), 16372-16377. doi:10.1073/pnas.1000423107
- Wen, S., Gotze, I. N., Mai, O., Schauer, C., Leinders-Zufall, T., & Boehm, U. (2011). Genetic identification of GnRH receptor neurons: a new model for studying neural circuits underlying reproductive physiology in the mouse brain. *Endocrinology*, *152*(4), 1515-1526. doi:10.1210/en.2010-1208
- Wen, S., Schwarz, J. R., Niculescu, D., Dinu, C., Bauer, C. K., Hirdes, W., & Boehm, U. (2008). Functional characterization of genetically labeled gonadotropes. *Endocrinology*, *149*(6), 2701-2711. doi:10.1210/en.2007-1502
- Wildt, L., Hausler, A., Marshall, G., Hutchison, J. S., Plant, T. M., Belchetz, P. E., & Knobil, E. (1981). Frequency and amplitude of gonadotropin-releasing hormone stimulation and gonadotropin secretion in the rhesus monkey. *Endocrinology*, *109*(2), 376-385. doi:10.1210/endo-109-2-376
- Wintermantel, T. M., Campbell, R. E., Porteous, R., Bock, D., Grone, H. J., Todman, M. G., Herbison, A. E. (2006). Definition of estrogen receptor pathway critical for estrogen positive feedback to gonadotropin-releasing hormone neurons and fertility. *Neuron*, *52*(2), 271-280. doi:10.1016/j.neuron.2006.07.023
- Wolfe, A., & Hussain, M. A. (2018). The Emerging Role(s) for Kisspeptin in Metabolism in Mammals. *Front Endocrinol (Lausanne)*, *9*, 184. doi:10.3389/fendo.2018.00184
- Wong, S. K., Chin, K. Y., Suhaimi, F. H., Fairus, A., & Ima-Nirwana, S. (2016). Animal models of metabolic syndrome: a review. *Nutr Metab (Lond)*, *13*, 65. doi:10.1186/s12986-016-0123-9
- Wu, S., Chen, Y., Fajobi, T., DiVall, S. A., Chang, C., Yeh, S., & Wolfe, A. (2014). Conditional knock-out of the androgen receptor in gonadotropes reveals crucial roles for androgen in gonadotropin synthesis and surge in female mice. *Mol Endocrinol*, *28*(10), 1670-1681. doi:10.1210/me.2014-1154
- Yamaguchi, T., Matsushita, S., Motojima, K., Hirose, F., & Osumi, T. (2006). MLDP, a novel PAT family protein localized to lipid droplets and enriched in the heart, is regulated by peroxisome proliferator-activated receptor alpha. *J Biol Chem*, *281*(20), 14232-14240. doi:10.1074/jbc.M601682200
- Yki-Jarvinen, H. (2014). Non-alcoholic fatty liver disease as a cause and a consequence of metabolic syndrome. *Lancet Diabetes Endocrinol*, *2*(11), 901-910. doi:10.1016/S2213-8587(14)70032-4

- Yu, I. C., Lin, H. Y., Sparks, J. D., Yeh, S., & Chang, C. (2014). Androgen receptor roles in insulin resistance and obesity in males: the linkage of androgen-deprivation therapy to metabolic syndrome. *Diabetes*, *63*(10), 3180-3188. doi:10.2337/db13-1505
- Zhang, S., Cui, Y., Ma, X., Yong, J., Yan, L., Yang, M., Qiao, J. (2020). Single-cell transcriptomics identifies divergent developmental lineage trajectories during human pituitary development. *Nat Commun*, *11*(1), 5275. doi:10.1038/s41467-020-19012-4
- Zitzmann, M. (2009). Testosterone deficiency, insulin resistance and the metabolic syndrome. *Nat Rev Endocrinol*, *5*(12), 673-681. doi:10.1038/nrendo.2009.212

Publications

Qiao S, Alasmi S, Wyatt A, Wang H, Candlish M, Grünewald R, Aoki M, Das D, Tian Q, Wartenberg P, Yu Q, Belkacemi A, Raza A, Kattler K, Gasparoni G, Karatayli E, Karatayli SC, Walter J, Mollard P, Lammert F & Boehm U (2022). **Intra-pituitary follicle-stimulating hormone signaling regulates hepatic lipid metabolism.** *Manuscript resubmitted to Nature Communications after revision, under review.*

Götz V, Qiao S, Wartenberg P, Wyatt A, Wahl V, Gamayun I, Alasmi S, Rad R, Kaltenbacher T, Kattler K, Lipp P, Becherer U, Mollard P, Candlish M & Boehm U (2022). **Ovulation is triggered by a cyclical transformation of gonadotropes into a hyperexcitable state.** *Manuscript resubmitted to Cell Reports after revision, under review.*

Posters and oral presentations

Qiao S, Alasmi S, ... & Boehm U (2022). **Intra-pituitary follicle-stimulating hormone signaling regulates hepatic lipid metabolism.** *Presented by Sen Qiao and Samer Alasmi at the "SFB 894 Symposium" June 15-18, 2022, Homburg, Germany.*

Alasmi S, Qiao S, ... & Boehm U (2022). **Intra-pituitary follicle-stimulating hormone signaling regulates hepatic lipid metabolism.** *Poster and talk presented by Samer Alasmi at the "European Centre for Reproductive Endocrinology (EUCRE)" September 25-28, 2022, Mopani Camp Kruger National Park, South Africa.*

Acknowledgements

I would like to thank Prof. Ulrich Boehm for giving me the opportunity to work in his research group and also thank all the members of A.G. Boehm. Coming to a foreign country where one does not speak much (if any) of the language is challenging but being lucky enough to join such a great group of people really made things so much easier. With regard to the research, everyone was more than happy to help and teach me what they knew and share new ideas. This makes not only a substantial input to one's own personal learning and the development of new ideas, but also to the environment within the laboratory and for that, I am very grateful.

I would like to thank all the members of A.G. Weißgerber for taking care of the mice for us and special thanks to Amanda Wyatt for performing genotyping for both genotyping and producing cryosections. I would especially like to thank Dr. Sen Qiao for helping me to learn every technique in our lab and for good research advices. I wish him and his family all the best.

I would also like to thank all of my friends, who supported me during my studies.

My special thanks go to Nadia Alawar, who has always supported me throughout my doctoral studies as a critical researcher and reliable friend.

I would like to thank my german family for their never-ending support in all aspects of life. None of this would have been accomplished without them.

Curriculum Vitae

Aus datenschutzrechtlichen Gründen wird der Lebenslauf in der elektronischen Fassung der Dissertation nicht veröffentlicht.

